

**DOCTORATE PROGRAMME IN ENERGY AND SUSTAINABLE
ENGINEERING**

**NEW AND IMPROVED SOLUTIONS FOR THE
CONFIGURATION, MANAGEMENT AND OPERATION OF
LARGE-SCALE PHOTOVOLTAIC POWER PLANTS USING
HYBRID ENERGY STORAGE SYSTEM**

**SOLUCIONES NUEVAS Y MEJORADAS PARA LA
CONFIGURACIÓN, GESTIÓN Y OPERACIÓN DE PLANTAS DE
ENERGÍA FOTOVOLTAICA A GRAN ESCALA UTILIZANDO
SISTEMAS HÍBRIDOS DE ALMACENAMIENTO DE ENERGÍA**

University of Cádiz

**ESCUELA TÉCNICA SUPERIOR DE INGENIERÍA DE
ALGECIRAS**

AUTORA/AUTHOR: LAÍS DE OLIVEIRA ASSIS

**DIRECTORES/SUPERVISORS: LUIS M. FERNÁNDEZ RAMÍREZ
RAÚL SARRIAS MENA**

December 2021

**DOCTORATE PROGRAMME IN ENERGY AND SUSTAINABLE
ENGINEERING**

**NEW AND IMPROVED SOLUTIONS FOR THE
CONFIGURATION, MANAGEMENT AND OPERATION OF
LARGE-SCALE PHOTOVOLTAIC POWER PLANTS USING
HYBRID ENERGY STORAGE SYSTEM**

**SOLUCIONES NUEVAS Y MEJORADAS PARA LA
CONFIGURACIÓN, GESTIÓN Y OPERACIÓN DE PLANTAS DE
ENERGÍA FOTOVOLTAICA A GRAN ESCALA UTILIZANDO
SISTEMAS HÍBRIDOS DE ALMACENAMIENTO DE ENERGÍA**

Laís de Oliveira Assis

Vº. Bº de los Directores de la Tesis

Fdo: Luis M. Fernández Ramírez

Fdo: Raúl Sarrias Mena

Trabajo presentado para optar al grado de Doctor por la Universidad de Cádiz.

A thesis submitted for the degree of Doctor at the University of Cádiz.

Doctor of Philosophy

Doctorate Programme in Energy and Sustainable Engineering

University of Cádiz

December 2021

“The greatest enemy of knowledge is not
ignorance, is the illusion of knowledge”
Stephen Hawking

Acknowledgments

My special thanks to my tutors Luis and Raúl, for their valuable contribution not only to this work, but also to obtaining this title. My thanks are extensible to their families, specially Pili, Tracy, Alejandra and Zoe, who adopted us as part of their families.

To my husband Emanuel for all his company, dedication, patience and support, which were essential for the conclusion of this work, giving me joy in difficult moments and sharing my happiness in good moments.

To my mother Celeste, my dear family and friends, for their support even at a distance, giving me the necessary motivation to contribute for this achievement to be possible.

To all the TESYR lab members, especially Pablo, for sharing their knowledge and great moments of laughs and uncountable coffees. It was an honor for me to have worked with everyone.

This thesis was supported by the National Council for Scientific and Technological Development (CNPq), to which I am grateful.

Abstract

This thesis is presented in the context of multiple efforts being made by research groups in order to disseminate and evolve the technological knowledge in the renewable energy (RE) field. The motivation of this study is based on the main disadvantages of photovoltaic (PV) solar power generation compared to conventional energy sources, such as intermittency, non-dispatchability, and unreliability. From those drawbacks, the aim is to find creative solutions to mitigate these issues with a power plant combining PV and hybrid energy storage systems (HESS). In doing so, hybrid power plants represent a very interesting option for power generation and grid integration of PV systems, since they allow increased efficiency in the energy generation, as well as storing and supporting RE generation when needed.

The storage systems are particularly important to deal with the intermittent nature of solar radiation. A wide variety of storage systems exists nowadays, all of them based on different operating principles and target applications. A thorough review of the literature has exposed that, depending on the application, a certain type of storage could be preferred above others. Besides, two or more different technologies working together can present complementary features. In this sense, the HESS can accomplish higher efficiencies and improved systems for grid connection.

The objective is to develop new solutions to improve the configuration, management, and operation of PV plants with energy storage, designing the necessary control techniques and validating them through real-time simulations. In this context, this thesis presents a large-scale PV power plant with HESS, through a DC/DC impedance source converter (DC/DC-ZSC), and a new simplified model (SM) of the quasi Z-source inverter with battery energy storage (qZSI-BES) attached directly to the Z-network without an extra DC/DC converter. The HESS consists of battery arrays (BES) and ultracapacitors (UC). The newly designed SM is implemented, assessed, and validated experimentally in laboratory through a TYPHOON HIL system and a dSPACE MicroLabBox control board. Three different energy management strategies are implemented, using two of them advanced control techniques based on fuzzy logic. The

control loops of the active, reactive, BES, and UC power have been conveniently deployed. The results obtained are coherent with the expected responses, observing an appropriate power balance and grid energy dispatch.

This thesis aims for a relevant contribution in the development of low polluting energy sources that can fulfill the growing electricity demand. Following the global trends, and recognizing the importance of this knowledge for the scientific community and for society, this thesis will provide new solutions in the field of solar PV generation. In view of the fact that research has mainly focused on small-scale hybrid power plants so far, further studies are required regarding the configuration, design, control, energy management, operation, and problems associated with large PV power plants with hybrid storage.

Resumen

Esta tesis se presenta en el contexto de múltiples esfuerzos que están realizando numerosos grupos de investigación con el fin de avanzar en el conocimiento tecnológico en el campo de las energías renovables (RE). La motivación de este estudio se basa en las principales desventajas de la generación de energía solar fotovoltaica (PV) en comparación con las fuentes de energía convencionales, como son su intermitencia, o la falta de disponibilidad y fiabilidad. A partir de esos inconvenientes, el objetivo es encontrar soluciones creativas para mitigar estos problemas con una planta de energía que combine sistemas fotovoltaicos y sistemas de almacenamiento de energía híbridos (HESS). De este modo, las centrales híbridas representan una opción muy interesante para la generación de energía y la integración de sistemas fotovoltaicos en la red, ya que permiten una mayor eficiencia en la generación de energía, así como el almacenamiento y el apoyo a la generación de energía renovable cuando sea necesario.

Los sistemas de almacenamiento son particularmente importantes para hacer frente a la naturaleza intermitente de la radiación solar. Actualmente existe una amplia variedad de sistemas de almacenamiento, todos ellos basados en diferentes principios operativos y potenciales aplicaciones. Una revisión exhaustiva de la literatura ha revelado que, dependiendo de la aplicación, un cierto tipo de almacenamiento será preferible sobre otros. Además, dos o más tecnologías diferentes trabajando juntas pueden presentar características complementarias. En este sentido, el HESS puede lograr una mayor eficiencia y otras mejoras en los sistemas conectados a la red.

El objetivo es desarrollar nuevas soluciones para mejorar la configuración, gestión y operación de plantas fotovoltaicas con almacenamiento de energía, diseñando las técnicas de control necesarias y validándolas mediante simulaciones en tiempo real. En este contexto, esta tesis presenta una planta fotovoltaica a gran escala con HESS, a través de un convertidor CC/CC en fuente de impedancia (CC/CC-ZSC), y un nuevo modelo simplificado (SM) del inversor cuasi-fuente de impedancia con batería (qZSI-BES) conectado directamente a la red de impedancia sin necesidad de un convertidor CC/CC adicional. El HESS consta de bancos de baterías (BES) y ultracondensadores (UC). El

nuevo SM se implementa, evalúa y valida experimentalmente en laboratorio a través de un sistema TYPHOON HIL y una tarjeta de control dSPACE MicroLabBox. Se implementan tres estrategias diferentes de gestión de la energía, utilizando dos de ellas técnicas de control avanzado basadas en lógica difusa. Se han implementado los lazos de control de la potencia activa, reactiva, del BES y del UC. Los resultados obtenidos son coherentes con las respuestas esperadas, observando un adecuado balance de potencia e inyección de energía a la red.

Esta tesis tiene como objetivo realizar una contribución relevante en el desarrollo de fuentes de energía poco contaminantes que puedan satisfacer la creciente demanda de energía eléctrica. Siguiendo las tendencias globales, y reconociendo la importancia de este conocimiento para la comunidad científica y para la sociedad en general, esta tesis aportará nuevas soluciones en el campo de la generación solar fotovoltaica. Dado que, hasta el momento, la investigación se ha centrado principalmente en plantas de energía híbrida a pequeña escala, se requieren más estudios sobre la configuración, diseño, control, gestión de energía, operación y problemas asociados con las plantas de producción de energía fotovoltaica a gran escala con HESS.

Table of contents

<i>Abstract</i>	<i>i</i>
<i>Resumen</i>	<i>iii</i>
<i>List of Figures</i>	<i>ix</i>
<i>List of Tables</i>	<i>xii</i>
<i>PART I. CONTEXTUALIZATION</i>	<i>1</i>
<i>Chapter 1. Introduction</i>	<i>3</i>
<i>Chapter 2. Hypotheses and Objectives</i>	<i>6</i>
2.1. Hypotheses	6
2.2. Objectives	7
<i>Chapter 3. Literature Review</i>	<i>8</i>
3.1. PV panels technologies	8
3.1.1. Crystalline Silicon	9
3.1.2. Thin-film	9
3.1.3. Other technologies	10
3.1.4. Comparison and considerations of PV panel technologies	11
3.2. Energy storage systems technologies	15
3.2.1. Flywheel	16
3.2.2. Electrochemical batteries	17
3.2.3. Ultracapacitors	20
3.2.4. Hydrogen	21
3.2.5. ESS comparison	21
3.3. Converter technologies	26
3.4. PV power plants with energy storage system	29
3.4.1. Small-scale PV power plants	29
3.4.2. Large-scale PV power plants	30

3.4.3.	Energy storage systems	35
3.4.4.	Control techniques	39
Chapter 4. Methodology		44
 PART II. MODELING AND CONTROL SYSTEMS		47
Chapter 5. Configuration and Modeling		49
5.1.	PV Panels	49
5.2.	Detailed model of the Quasi Z-source inverter	51
5.3.	Simplified model of the Quasi Z-source inverter	52
5.4.	DC / DC Converter based on Z-Source	55
5.5.	Battery	56
5.6.	Ultra-capacitor	57
5.7.	LCL Filter	59
5.8.	System parameters considered in the simulation cases	61
Chapter 6. Control Strategy		63
6.1.	MPPT	64
6.2.	Z-Space Vector Modulation	64
6.3.	Battery and Ultra-Capacitor	68
6.4.	Active and Reactive Power	68
Chapter 7. Energy Management System		71
7.1.	Strategy considering one storage system (EMS 1)	71
7.2.	Strategy considering one storage system applying fuzzy logic control (EMS 2)	73
7.3.	Strategy considering two storage systems and fuzzy logic control (EMS 3)	77
 PART III. RESULTS AND DISCUSSIONS		83

Chapter 8. Simulation Results	85
8.1. Case 1	85
8.1.1. Comparison of the detailed and simplified models	85
8.1.2. Comparison of the computational efforts of the models	91
8.1.3. Experimental HIL validation	92
8.2. Case 2	96
8.3. Case 3	98
8.4. Case 4	101
PART IV. FUTURE RESEARCH AND CONCLUSIONS	111
Chapter 9. Conclusions	113
Chapter 10. Future Works	117
Bibliography	119
List of publications	133
Curriculum Vitae	135

List of Figures

Fig. 3.1. PV materials	9
Fig. 3.2. Average monthly prices of PV modules by technology and country of manufacture	11
Fig. 3.3. Price curve by technology (cumulative production)	12
Fig. 3.4. PV cells efficiency by technology	13
Fig. 3.5. PV production by technology in percentage of global annual production	14
Fig. 3.6. Examples of energy storage systems	16
Fig. 3.7. Performance index for nine storage technologies for the four application categories.....	22
Fig. 3.8. Distribution of storage techniques according to the application.....	23
Fig. 3.9. Distribution of storage techniques based on energy efficiency and lifetime	24
Fig. 3.10. Distribution of storage technologies as a function of investment costs per unit of power	25
Fig. 3.11. General structure of a ZSC	27
Fig. 3.12. (a) General structure of a qZSI converter, (b) shoot-through state; and (c) non-shoot-through state of the qZSI	28
Fig. 3.13. Trends for installed PV power systems by countries / continents	31
Fig. 3.14. qZSI with battery (a) in parallel with C_2 , (b) in parallel with C_1	33
Fig. 3.15. Configuration considered in [1] with PV plant and HESS.	40
Fig. 5.1. General configuration of the plant under study	49
Fig. 5.2. Proposed qZSI simplified model	53
Fig. 5.3. Averaged model of the DC/DC ZSC	55
Fig. 6.1. Overall control system	63
Fig. 6.2. Comparison between SPWM and ZSVM	65
Fig. 6.3. (a) Switching time sequences in ZSVM6. (b) Complete switching states in the six sectors for ZSVM6	67
Fig. 7.1. Control scheme for the EMS 1.....	71
Fig. 7.2. EMS 2 inputs and outputs	74

Fig. 7.3. Membership functions of the EMS 2 based on fuzzy logic for: (a) PV power (input), (b) SOC (input), (c) Price (input), and (d) Battery reference power (output)	75
Fig. 7.4. Input of fuzzy logic (price)	75
Fig. 7.5. UC power compensation to BES slow response.....	77
Fig. 7.6. EMS 3 inputs and outputs	79
Fig. 7.7. Membership functions of the EMS 3 based on fuzzy logic control for: (a) Battery and UC state of charge (input); (b) Primary battery power (input); (c) Primary UC power (input); (d) Power complementary (output).....	80
Fig. 8.1. Irradiation profile for case 1.....	86
Fig. 8.2. Case 1: (a) PV power (b) Battery power (c) Grid power (d) SOC.....	88
Fig. 8.3. Case 1: (a) Grid active power (b) Grid reactive power.....	90
Fig. 8.4. Case 2: (a) Phase-A grid voltage; and (b) Phase-A grid current during the voltage sag	91
Fig. 8.5. HIL experimental setup.....	93
Fig. 8.6. Experimental results with power variation and battery current control for: (a) Detailed model. (b) Simplified model	94
Fig. 8.7. Experimental results including a voltage sag for: (a) Detailed model. (b) Simplified model	95
Fig. 8.8. Case 2: (a) PV power, battery power, grid power, SO demand, and maximum available power. (b) Battery SOC and trading in electricity market	97
Fig. 8.9. Case 3: (a) Irradiation profile. (b) Power balance between PV panels, battery and grid. (c) Battery SOC.....	99
Fig. 8.10. Case 3: Battery current control	100
Fig. 8.11. Case 3: PV voltage, MVDC voltage and voltage boost achieved from PV panels to DC side of the qZSI.....	100
Fig. 8.12. Case 3: Duty cycle (D) and modulation index (M).....	101
Fig. 8.13. Case 4: Hybrid system power balance (a) Power balance between PV, HESS, SO and grid. (b) BES and UC power.....	102
Fig. 8.14. Case 4: Battery demanded power and battery response.....	103
Fig. 8.15. Case 4: State of charge (a) BES. (b) UC.....	104
Fig. 8.16. Case 4: Current control (a) BES. (b) UC	105
Fig. 8.17. Case 4: Hybrid system power balance with high initial SOC (a) Power balance between PV, HESS, SO and grid. (b) BES and UC power	106
Fig. 8.18. Case 4: State of charge for (a) BES starting with high SOC (b) UC	107

Fig. 8.19. Case 4: Hybrid system power balance with low initial SOC (a) Power balance between PV, HESS, SO and grid. (b) BES and UC power BES and UC power for high initial SOC 108

Fig. 8.20. Case 4: State of charge for (a) BES starting with low SOC. (b) UC 109

List of Tables

Table 3.1. DETAILS OF SOME OPERATIONAL LARGE-SCALE PV SOLAR PLANTS	14
Table 3.2. THE TEN LARGEST ESS (BY POWER CAPACITY) UNDER COMMISSION OR IN OPERATION FOR THE ELECTRICITY GRID AS OF 2016	37
Table 5.1. SYSTEM PARAMETERS FOR CASES 1 AND 2	61
Table 5.2. SYSTEM PARAMETERS FOR CASES 3 AND 4	62
Table 7.1. RULE LIST OF THE FUZZY LOGIC CONTROLLER FOR EMS 2.....	76
Table 7.2. RULES OF THE FUZZY LOGIC CONTROLLER FOR EMS 3.....	81
Table 8.1. COMPARISON OF THE COMPUTATIONAL EFFORT OF THE DM AND SM MODELS	92

I

Contextualization

In this first part, an overview of the main topics covered in this thesis is presented with contextualization purposes. An introduction will set up the study, then the hypotheses and objectives will be presented. Subsequently, a literature review showing previous studies in the field will be shown; and finally, the methodology will be described in order to obtain the results.

Chapter 1

Introduction

Due to growing environmental concerns, renewable energy sources are an alternative in constant development. Among these sources, photovoltaic (PV) systems have an important role to meet the increase in electricity requirements. Nowadays, most PV systems are small-scale and distributed. The large-scale PV power plants (LS-PVPP) are beginning to increase their participation, starting to reach a significant share in the PV market. This growing penetration of renewables in the energy mix brings some challenges that are important to overcome. In this context, energy storage, power electronic converters, and advanced control techniques are relevant aspects to be taken into account in order to alleviate the existing issues.

One of these issues is the intermittent nature of solar radiation. The energy generated by the PV modules is directly proportional to the amount of sunlight that reaches their surface. There are many factors that interpose solar radiation. Shading due to clouds, vegetation, dust, buildings, etc. could be mentioned as examples. Therefore, the output power is strongly dependent on these external factors. To reduce the effects of this intermittence and maximize the conversion efficiency, several methods can be applied, such as sun trackers, maximum power point tracking (MPPT), and energy storage systems (ESS). Considering that the sun trackers require energy consumption, they are not recommended for operation under partially shaded conditions. However, the application of the MPPT technique and ESS can be suitable options.

The ESS can mitigate the intermittent nature of solar generation and make the PV installation able to operate even during the absence of sunlight for a certain period. Also, the ESS can smooth the PV power output and contribute to voltage and frequency regulation. The use of hybrid ESS (HESS), combining different storage technologies, could have advantages for large PV penetration, covering a wide range of power and energy requirements.

The use of ESS requires controlling their charge/discharge, and a suitable supervisory control of the energy sources. From a broad perspective, studying the control systems for

PV generation is important to achieve an efficient power conversion with energy storage and satisfy the power quality requirements. There are numerous control techniques. Among them, PI/PID controller is extensively found in the literature, but the need for more robust control systems leads to the use of intelligent control techniques. In this work, the aim is to design a control system based on advanced control techniques for different control variables, such as the state of charge (SOC) of the ESS, voltage, or reactive power, among others, in order to improve the efficiency and operation of the energy sources.

The converter is a crucial component for the connection of a PV power plant. This element is responsible for converting the direct current (DC) produced into alternate current (AC), maintaining the voltage and frequency levels required by the grid. Moreover, the converter can boost the DC voltage to reach the desired value to operate at the MPPT of the PV panels. The most commonly used power electronic converter for high power applications is the voltage sourced converter (VSC). Nevertheless, this converter has some technical limitations. The presence of switching dead times, which implies distortion on the output waveform; the need for a subsequent voltage boost stage in many applications; and the necessary use of an impedance filter to obtain a sinusoidal signal of acceptable quality at the output, thereby increasing the losses in the system, can be cited as examples. In contrast, the converters based on impedance sources, also called Z-source converters (ZSC), have interesting characteristics that make them suitable for PV applications. These converters can implement voltage buck/boost, perform an inversion on a single stage, provide integration of ESS without an additional converter, etc. Due to the interest of scientists in recent years, and for its capacity to overcome the limitations of VSC, the converter based on impedance source was selected as an attractive option to integrate the PV power plant and ESS under study.

The topic covered in this thesis is worth of greater research efforts, since there are few works published that address the study of LS-PVPP with HESS connected to the impedance-based converter. The main objective of this thesis is to find the most suitable configuration for a LS-PVPP with HESS connected to a ZSC, and design new control systems to achieve an efficient energy management in the proposed plant.

With this research, it is expected to achieve more efficient and reliable hybrid plants based on LS-PV and ESS, which will support the development and implementation of this

type of power plant. The proposed solutions mean a breakthrough in the search for improved systems, particularly targeted at large-scale applications.

This thesis is part of the research project titled “MVDC grids integrating renewable energy technologies, energy storage systems and DC/AC impedance-source converters” (Ref. RTI2018-095720-B-C32) funded by the Spanish Ministry of Science, Innovation and Universities in the competitive call for projects “Retos de Investigación 2018”.

Chapter 2

Hypotheses and Objectives

Due to the increasing importance of power systems based on renewable sources over the last decades, PV systems play an important role in the energy mix nowadays. However, for this system to become widespread, an increase in its efficiency is required. In this context, different configurations, new supervisory control strategies, and the use of two types of ESS either combined or independent, will be investigated in this thesis. The proposed solutions will mean a breakthrough in the search for improved systems, particularly targeted at large-scale applications.

2.1. Hypotheses

The combination of LS-PVPP with ESS is expected to yield more efficient and reliable systems, which will support the development and implementation of this kind of hybrid power plant. The main hypotheses of this thesis are presented below:

- The incorporation of an ESS in a LS-PVPP (hybrid power plant) will improve its response against variations in weather conditions (solar radiation) and disturbances in the electricity grid.
- The study and evaluation of different configurations regarding the connection of the energy sources within the hybrid plant will allow a critical comparison from an operational point of view, stating their advantages and disadvantages, and choosing the appropriate configuration for the plant, based on objective criteria.
- The control design based on advanced control techniques to be developed will allow achieving an adequate and efficient plant operation, being able to satisfy the requirements of the electric grid, and find improved solutions for the control and energy management between the PV power plant and the ESS.
- The evaluation of the advantages of the coordinated or independent use, as well as different ESS technologies in a PV plant, such as ultra-capacitor (UC)

and batteries, will allow enhancing the positive aspects of the hybridization of the power sources.

2.2. Objectives

The fundamental objective of this thesis is the study of the configuration, energy management and operation of a hybrid power plant based on solar PV and ESS, generating new knowledge in the topic, and proposing innovative solutions that favor its viability and contribute to its development. Taking this into account, the specific objectives of this thesis are:

- Definition of the parameters and characteristics of the plant under study.
- Study and evaluation of different configurations for the hybrid PV plant with ESS.
- Development of models and controllers for the elements of the plant, and evaluation of their operation.
- Design and implementation of a supervisory control system for the hybrid PV plant with ESS.
- Evaluation and comparison of the different solutions proposed in order to establish the main conclusions.

Chapter 3

Literature Review

The last decade has witnessed a great growth of PV systems all over the world as well as a significant cost reduction. With the technical improvements and lower costs, PV technology will be increasingly used in the future [2]. Among the advantages of PV sources, vast fuel resources, no moving parts, high reliability, and no emissions can be highlighted [3].

On the other hand, due to the intermittency and fluctuation of the PV power generation, it is important to pay attention to the integration of these systems in the electric grid. If this integration is not dealt properly, excessive PV generation may lead to voltage instability, power fluctuation, or malfunctioning of the voltage regulation equipment, among other issues. Therefore, it is necessary to find solutions by developing advanced control and operation techniques to maximize PV power utilization while keeping the system reliable and stable [2]. The use of energy storage technologies (ESS) is regarded as one of the plausible solutions to this problem.

Considering the above-mentioned, the background in the field of PV plants with ESS is described along this section, in terms of available technologies and their respective applications. Furthermore, a comparison of technical features is also depicted.

3.1. PV panels technologies

The technology used in the manufacture of PV cells is an important parameter to be taken into account in any PV project, since efficiency is a factor that influences the performance and the costs of the plant.

Currently, various technologies are used to manufacture PV panels, as shown in Fig. 3.1. The most relevant characteristics of the main PV materials are presented below.

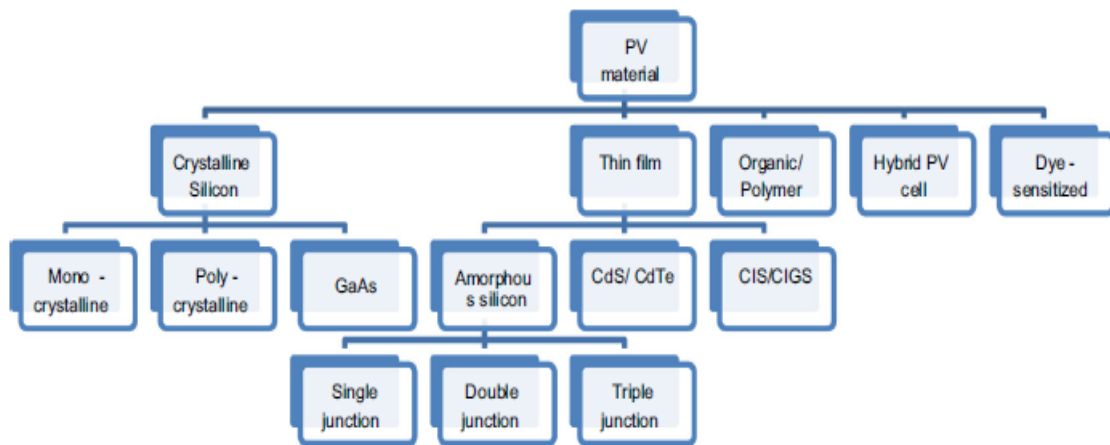


Fig. 3.1. PV materials [4]

3.1.1. Crystalline Silicon

The most used technology is silicon, due to its high efficiency and maturity [5]. Silicon supply is readily available as it is the second most abundant raw material on earth [6]. Crystalline semiconductors of mono-crystalline silicon and GaAs have a better performance. However, GaAs manufacturing and raw materials are expensive and are used mainly in PV concentrators and in space technology, as they have greater resistance to high temperatures and are lighter [8]. Examples of silicon-based but less pure materials, are the poly-crystalline or amorphous organic and inorganic materials, being these cell categories cheaper when compared to mono-crystalline and GaAs [2]. An alternative to the high cost of mono-crystalline silicon is poly-crystalline, being both the most commercialized modules [7].

3.1.2. Thin-film

Due to its low weight, high flexibility, and low cost, thin-film technology has excellent potential despite its low efficiency [3]. Amorphous silicon is the most popular technology compared to other materials like CIS, CIGS and CdS, CdTe, and despite being the most common and occupying the first position in the market among thin-film technology, it is more prone to degradation [5]. In 2013, the highest efficiency of a cell reached 18.8%.

However, the maximum commercial efficiency is 15%, and the most frequently found values are in a range between 9% and 12% [9].

3.1.3. Other technologies

Other less popular PV technologies are organic/polymeric, hybrid, and dye-sensitized solar cells.

Polymer PV cells are a relatively new technology studied in laboratories by groups of companies and by universities around the world. Still largely in the experimental phase, they offer interesting prospects. They are based on organic macromolecules derived from petrochemicals, whose manufacturing processes use much less energy than those used for cells based on mineral semiconductors. Their cost is much lower and they are lighter and less fragile. Their flexible nature makes them very suitable for integration into flexible materials or organic polymers or silicones, even textile fibers. Its main weakness lays in its limited lifetime due to the degradation of polymers when exposed to sunlight [6]–[8].

A hybrid solar cell is generally the result of the combination of crystalline and non-crystalline silicon, which makes the manufacturing process even more complex [9]. High performance was obtained with the union of amorphous silicon with crystalline silicon. In Japan, Sanyo developed a cell with an efficiency of 21% [10].

The Graetzel solar cell, also known as a dye-sensitized solar cell, is a relatively new technology that is being studied as an alternative to problems of efficiency, cost, and environmental issues [11]. They are considered in the initial stage of development. They are low-cost cells belonging to thin-film solar cells. This cell has quite attractive properties, since, in addition to being low-cost, it is very easy to create, semi-flexible, semi-transparent, or even totally transparent in those recently designed. In practice, the use of this cell shows certain drawbacks such as the wear of the electrolyte or the anode in use at certain environmental conditions [11]. However, although its energy conversion efficiency is lower than that of silicon-based solar panels, they present an improvement in terms of manufacturing price, making it a suitable candidate for future distribution.

3.1.4. Comparison and considerations of PV panel technologies

Comparing the different PV materials mentioned above in economic terms, Fig. 3.2 shows a downward trend in the price of the most commercialized PV technologies, from 2009 to 2014. It is also possible to observe that the cheapest technology is amorphous silicon, and the most expensive is crystalline silicon.

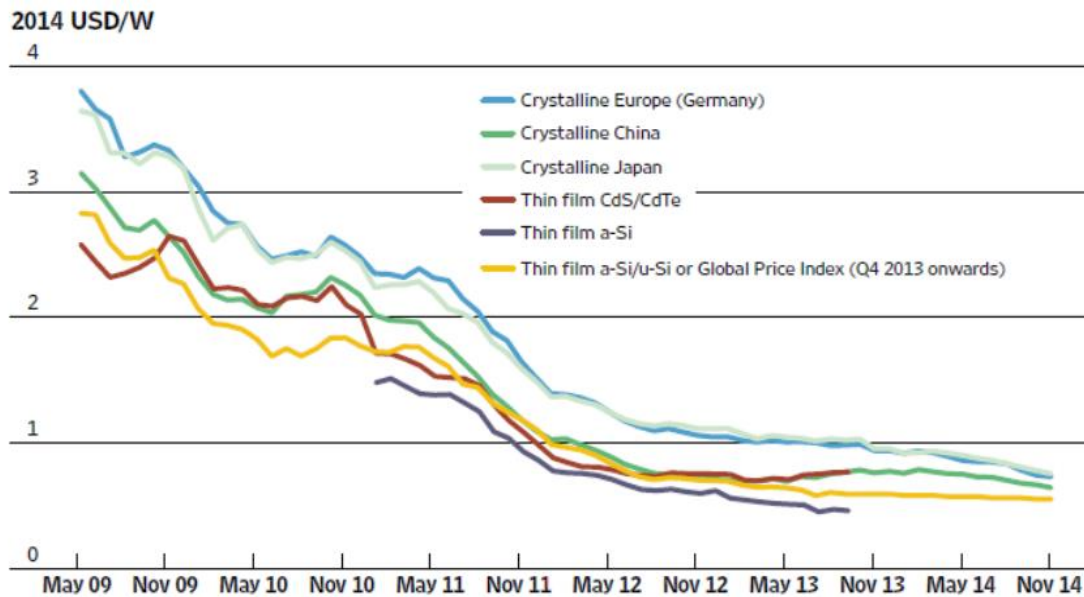


Fig. 3.2. Average monthly prices of PV modules by technology and country of manufacture [12]

The price of the modules depend on the production volume of the PV panels, as it is possible to observe in Fig. 3.3 for thin-film and crystalline silicon technologies. In this figure, Q1 refers to the first three months of the year, Q2 to the subsequent three months, and so on, until Q4.

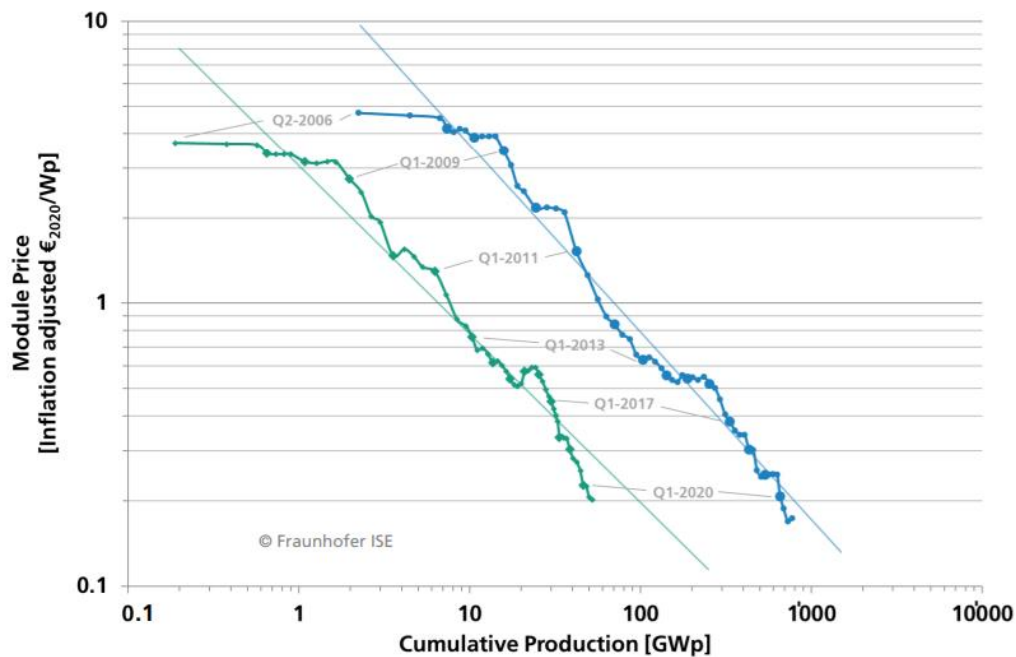


Fig. 3.3. Price curve by technology (cumulative production) [13]

The efficiency of the solar cell is an important parameter for better use of the available solar resources and, also, to establish a certain technology in the market. The available technologies in the market and their respective efficiencies are presented in Fig. 3.4.

From Fig. 3.4 and other additional references, it is possible to make the following considerations:

- The efficiency of monocrystalline silicon cells has shown a considerable improvement over the years. In 1975 the efficiency was around 13%, reaching 27% today. However, whereas the best mono-crystalline panels slightly exceed 20% [14], most panels have an efficiency of around 14,5%, as stated in [15].

- The polycrystalline cells reached the efficiency of 23% in 2020, but the efficiency of commercial PV is around 13% ~ 16%, according to [16].

- Multijunction cells have the highest efficiency among all the technologies mentioned, with 47% in 2019, confirmed by the Fraunhofer Institute for Solar Energy Systems laboratory.

Regarding the most commercialized technologies, it can be mentioned that the production of PV cells/panels has been increasing over the years [5], and due to the efficiency and maturity of the technology, silicon-based cells lead the market, as shown in Fig. 3.5.

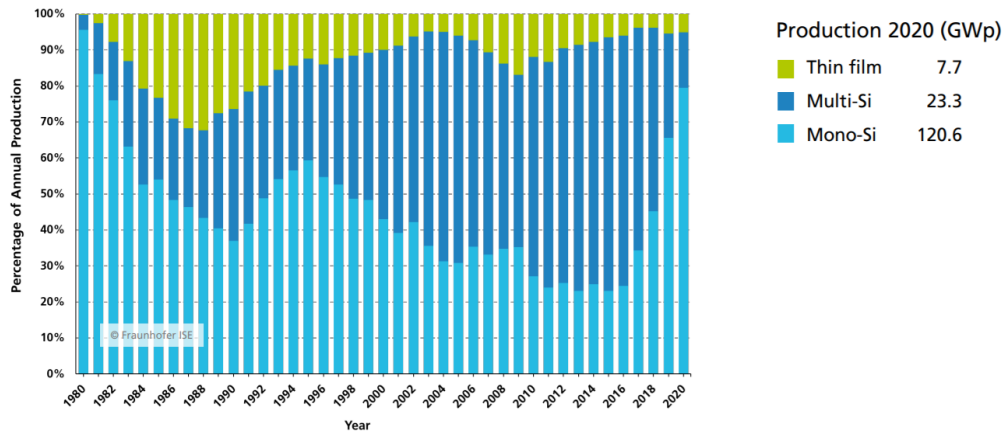


Fig. 3.5. PV production by technology in percentage of global annual production [17]

For a better comprehension of the importance of the PV panel technology, Table 3.1 brings data from real PV plants. The data detailed in Table 3.1 show that the materials mostly used in PV panels are polycrystalline Si and thin-film. In high-power PV plants, thin-film solar panels occupy twice the area of those using polycrystalline Si. Only three plants in Table 3.1 use Si monocrystalline, and these show a fewer number of PV panels and less occupied area, due to their higher efficiency.

TABLE 3.1. DETAILS OF SOME OPERATIONAL LARGE-SCALE PV SOLAR PLANTS [18]

Photovoltaic power plant	Power (MWp)	Area (km ²)	Panels (×10 ³)	Panel type	Inverters number	Topology
Korat I	6.0	0.13	29	m-Si	540	M
Narbonne	7.0	0.23	95	Thin film	19	C
Rapale	7.7	0.49	100	Thin film	900	M
Airport, Athens	8.1	0.16	29	m-Si	12	C
Saint Amadou	8.5	0.24	113	Thin film	16	C
Volkswagen Chattanooga	9.5	0.13	33	m-Si	10	C
Masdar	10	0.22	87	m-Si, Thin film	16	C
Adelanto	10.4	0.16	46	m-Si	13	C
Taan	14	0.30	70	m-Si	28	C
Jacksonville	15	0.40	200	Thin film	20	C
San Antonio	16.0	0.45	214	Thin film	22	C
Cotton Center	18.0	0.58	93	m-Si	36	C
Almaraz	22.1	1.2	126	m-Si	6697	M
Veprek	35.1	0.83	185	c-Si	3069	M
Long Island	37.0	0.80	164	m-Si	50	C
Reckahn	37.8	0.98	487	Thin film	43	C
Ban Pa-In	44.0	0.80	160	m-Si	61	C
Lieberose	71.0	2.2	900	Thin Film	38	C
Kalkbult	75.0	1.05	312	m-Si	84	C
Eggebek	80.0	1.29	76	m-Si	3200	M
Montalto di Castro	85.0	2.83	280	c-Si	124	C
Templin	128	2.14	1500	Thin Film	114	C
California Valley Ranch	250	6.01	749	c-Si	500	C
Agua Caliente	290	9.71	5200	Thin Film	400	C

In the cases of the Veprek and Long Island solar plants with a power of 35 MW and 37 MW, respectively, the occupied area is similar. Long Island (monocrystalline) uses twenty thousand less PV panels than Veprek solar plant (polycrystalline), although the power is higher in the former. From the table, the relationship between the occupied area and the type of material used in the panel is clear. If thin-film solar cells are chosen, as in Reckahn, the occupied area increases by 20%, and the number of panels is almost three times more than in the case of the Long Island PV plant.

For the future, opinions differ among the authors. However, the most broadly established opinion is that materials that allow increasing efficiency and reducing costs are necessary.

For Frankl et al. [19], crystalline silicon, which is the predominant material today, will continue for many years. However, in the long term (2030 and beyond) silicon will be progressively reduced. For the authors, many technologies will coexist, and the efficiencies will be slightly different from today's values. Moreover, it is mentioned that these technologies can be divided into two types: (i) Cells with ultra-low-cost, with efficiencies varying from medium to low, highlighting the concept of dye-sensitized cells; and (ii) cells with ultra-high efficiency, highlighting the third generation in PV cells (such as the multijunction made of amorphous Silicon or Gallium Arsenide).

Razykov et al. [20] expect thin-film photovoltaic technologies to play an important role in the future global PV market. It is stated that further research and development will be conducted to increase the effectiveness of Copper Indium Gallium Selenide (CIGS) thin films, CdTe, Si, and multijunction cells and nano PV devices.

3.2. Energy storage systems technologies

Energy storage integrated into photovoltaic plants allows the excess energy generated to be stored for a later use when necessary. Energy storage can help power grids withstand peak demand, allowing transmission and distribution grids to function efficiently. In shorter periods, storage can be effective in smoothing short peaks and distortion in voltage [21].

Energy storage technologies can be classified as electrical, electrochemical, chemical, thermal, and mechanical, as presented in Fig. 3.6.

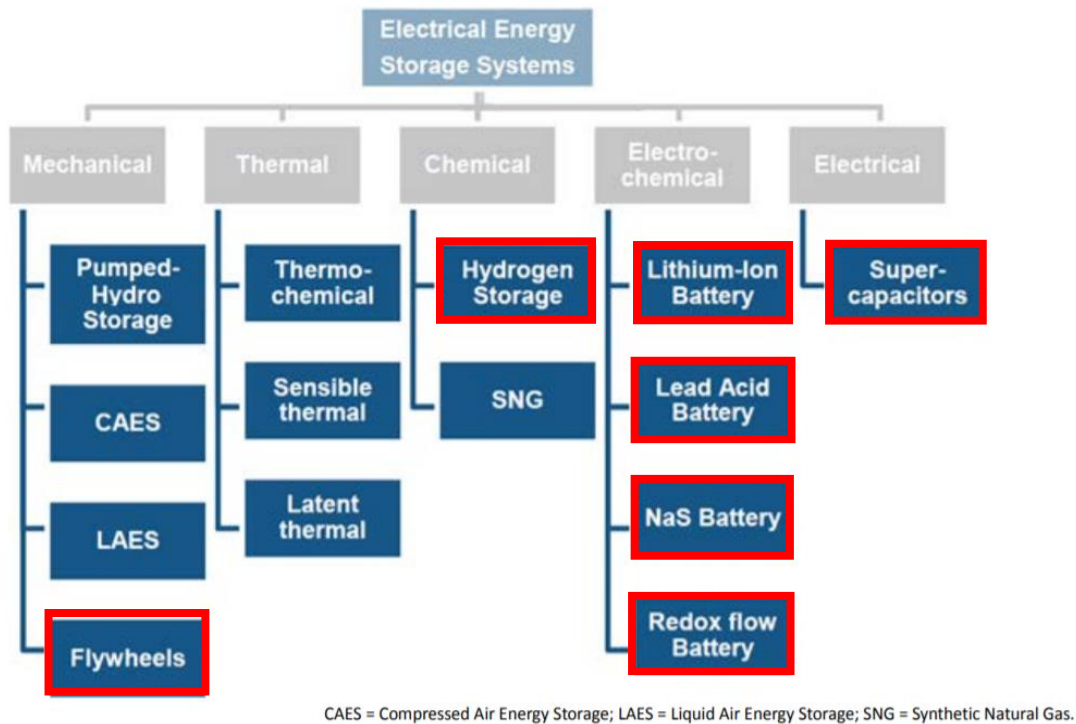


Fig. 3.6. Examples of energy storage systems [22]

In this section, the technologies highlighted in red will be addressed in the following subsections, while the rest will not be studied due to their little use or relevance for the proposed objective.

3.2.1. Flywheel

A flywheel is a mass that rotates around an axis, which can store energy in the form of kinetic energy. The amount of energy stored is proportional to its rotational speed and the moment of inertia [21]. The flywheel can be low-speed, with operating speeds up to 6000 rpm, or high-speed with operating speeds up to 50.000 rpm [23]. These wheels are accelerated in a matter of minutes, rather than the hours required to recharge a battery. The high-speed flywheel container is either vacuum or helium filled to reduce aerodynamic losses and rotor stresses [23].

The main advantages of flywheel storage systems are high charge and discharge rates for many cycles. In addition, the high cycling capacity of the flywheel is one of its key characteristics and it is not dependent on the rate of loading or unloading. The limiting factor

in some applications is more likely to be the life of the steering wheel, which is typically cited as 20 years. Its energy efficiency is typically around 90% at rated power [24].

The main disadvantages of the flywheel are the high cost and the relatively high losses. The friction losses of a 200-ton flywheel are estimated to be around 200 kW. Using this hypothesis and the instantaneous efficiency of 85%, the overall efficiency would drop to 78% after 5 h, and to 45% after one day. Long-term storage with this type of device is not foreseeable [25].

The flywheel can be integrated with renewable energy sources. The amount of energy produced by renewable sources varies significantly from hour to hour. Even when conventional technologies generate electricity at a constant rate, there are fluctuations in demand throughout the day. This load mismatch with the electrical supply means that power is not always available when required and at other times, there is excess power. Flywheel technologies can be used to provide power when not enough power is generated, and to store excess production and act in the event of a power grid failure [21].

3.2.2. Electrochemical batteries

Electrochemical batteries are based on chemical reactions and have the double function of storing and releasing electricity, alternating the charging and discharging phases, without noise or emissions [25].

There is a wide range of technologies used in the manufacture of these accumulators, such as lead-acid, nickel-cadmium, nickel-metal hydride, nickel-iron, zinc-air, iron-air, sodium-sulfur, lithium-ion, lithium-polymer, etc. and their main strengths are their high energy density and the maturity of some of these technologies. However, their main drawback is their relatively low durability for high amplitude cycles [25].

According to DTI Report [26], large-scale storage was rare until recently and some batteries contain toxic material, and therefore, the environmental impact of discarding these batteries must be considered. For Karpinski, et al. [27] batteries that are in use or potentially suitable for large-scale storage are lead-acid, nickel-cadmium, sodium-sulfur, sodium nickel chloride, and lithium-ion.

Currently, the electrochemical batteries widely applied today are lead-acid batteries, nickel-based batteries, and lithium-based batteries. In addition to these the three, there are some additional types, albeit with low market penetration. These are the sodium-sulfur (NaS), the redox flow storage system, and the metal-air battery [26][27].

3.2.2.1. *Lead-acid*

Lead-acid batteries are the oldest of the rechargeable type and are based on chemical reactions involving lead dioxide (cathode), lead (anode), and sulfuric acid that acts as an electrolyte [28]. Lead-acid batteries are highly energy-efficient (between 85 and 90%), are easy to install, and require a relatively low level of maintenance and a low investment cost [21]. Moreover, they provide competitive costs, but they have a relatively limited lifetime, low energy density, and can cause a large environmental impact [27].

3.2.2.2. *Nickel Cadmium*

In these batteries, nickel hydroxide is used in the positive electrode, while cadmium hydroxide is used in the negative. The electrolyte is an aqueous solution of potassium hydroxide with some lithium hydroxide. NiCd batteries have a high energy density (50-75 Wh/kg), robust reliability, and very low maintenance requirements, but a relatively short cycle life (2000-2500) [29]. The main disadvantages of these batteries are a relatively high cost due to the expensive manufacturing process, and the fact that cadmium is a toxic heavy metal, and therefore poses problems associated with the disposal of NiCd batteries [32].

3.2.2.3. *Lithium-ion (Li-ion)*

In these batteries, the cathode is a lithiated metal oxide and the anode is made of graphitic carbon with a layered structure. The electrolyte is composed of lithium salts dissolved in organic carbonates [26]. The self-discharge rate is very low, with a maximum of 5% per month, and the battery life reaches about 1500 cycles [30]. However, the life of a lithium-ion battery is temperature-dependent and can be severely shortened by deep discharges. Also, lithium-ion batteries are fragile and require a protection circuit to maintain

safe operation. Built into each battery pack, the protection circuit limits the maximum voltage of each cell charge and prevents the cell voltage from dropping too low on discharges [21].

3.2.2.4. *Sodium sulfur (NaS)*

Sodium sulfur batteries consist of a positive molten sulfur electrode and a negative molten sodium electrode separated by a sodium beta-alumina ceramic electrolyte [31]. NaS batteries have an expected operational duration of 15 years considering 2.500 cycles (charge and discharge) for a depth of discharge of 100% (DOD). They have a high energy density, three to five times more than a lead-acid battery. Besides, 98% of the material used in NaS batteries can be recycled, only sodium cannot be reused [32].

3.2.2.5. *Vanadium redox flow*

Redox technology offers significant advantages, such as the absence of self-discharge and degradation for deep discharge [21]. The cell efficiency can be as high as 85%. This type of battery is suitable for a wide range of energy storage applications for electric utilities and industrial end-users. Most development work has focused on stationary applications due to the relatively low energy density [26].

3.2.2.6. *Metal-air*

Metal-air batteries are the most compact and potentially the least expensive technology [26]. It offers a high energy density (compared to lead-acid batteries) and long life. However, tests have shown that metal-air batteries have a limited operating temperature range [21]. Among the various metal-air batteries, the lithium-air battery is an attractive option. Nevertheless, the high reactivity of lithium with air and humidity can cause a fire, which is a high safety risk. Currently, only a zinc-air battery is technically feasible [33].

3.2.3. Ultracapacitors

The ultracapacitors (UC), also known as supercapacitors, fill the gap between the classic capacitors used in electronics and batteries in general, due to their almost unlimited cycle stability, as well as the extremely high power capacity and capacity of energy storage many orders of magnitude higher than traditional capacitors [33].

The two main characteristics of UC are extremely high capacitance values, on the order of many thousands of farads, and the possibility of very fast charging and discharging due to extremely low internal resistance, characteristics that are not available with conventional batteries. Other advantages are durability, high reliability, lack of maintenance, long service life, and operation over a wide temperature range and in various environments. The useful life reaches one million cycles (or ten years of operation) without any degradation, except for the solvent used in the condensers, which deteriorates in 5 or 6 years regardless of the number of cycles. They are environmentally friendly and are easily recycled or neutralized. Efficiency is typically around 90% and discharge times are in the range of seconds to hours [33]. Recent progress in electrochemical capacitors/UC could lead to much higher capacity and energy density than conventional capacitors, allowing for compact designs [26].

The cost of UC is a major concern for their commercial use in industrial applications. The cost is significantly higher compared to well-established storage technologies such as lead-acid batteries. Therefore, a drastic reduction in costs must be achieved, especially in the fields of carbon, electrolyte, and separator. Currently, the high power storage capacity of UC coupled with rapid discharge cycles makes them ideal for temporary energy storage to capture and store regenerative braking energy and to provide boost charging in response to sudden demands of energy [34]. At the same time, UC can provide short-duration peak power and short-term peak power backup for uninterruptible power supply applications. By combining a UC with a battery-based system, the life of the batteries can be extended [21].

There are a lot of UC developers. Leading companies include PowerCache (Maxwell, US), SAFT (France), NESS (Korea), ESMA (Russia), ELIT (Russia), PowerSystem Co. (Japan), and Chubu Electric Power (Japan), etc. [35].

3.2.4. Hydrogen

The hydrogen-based storage system includes three steps: electrolysis that consumes electricity during off-peak hours to produce hydrogen, the fuel cell that uses the hydrogen and oxygen from the air to generate electricity at peak hours, and a hydrogen reserve tank to guarantee adequate resources when needed [25].

Although the overall efficiency of hydrogen is low compared to storage technologies such as li-ion batteries, hydrogen is the only concept that allows the storage of large amounts of energy, up to a TWh range, for long periods [36]. Another advantage of hydrogen is that they can be used in different sectors, such as transport, mobility, heating, and the chemical industry [33].

There are different approaches to store hydrogen, either as a high-pressure gas, or chemically bounded on complex hydrides. However, for stationary applications, high-pressure gaseous storage is the most popular option [21]. Smaller amounts of hydrogen can be stored in tanks or bottles above the ground at pressures up to 900 bar. For large amounts of hydrogen, underground piping systems or even salt caverns with various volumes of 100.000 m³ can be used at pressures up to 200 bar [33].

3.2.5. ESS comparison

To compare the performance of the different types of storage systems, some criteria were taken into consideration such as cost, energy density, recyclability, durability, efficiency, allowing to define a performance index for the following four application categories [25]:

- Low power in isolated places, to power emergency terminals and transducers (Category 1).
- Medium power in isolated areas, for individual electrical systems (Category 2).
- Grid connection (Category 3).
- Power quality control (Category 4).

Storage system performance parameters are often expressed for a wide variety of types and applications. Fig. 3.7 shows a comparison of the different storage techniques. The comparison is based on the "performance index" defined as the applicability of the storage technique to the specified application, taking into account the categories mentioned above. The data represent typical systems in each category but may not cover all available products [25].

From the Fig. 3.7, it is possible to make the following statements: (i) For low and medium power in isolated places, the lithium-ion battery has the best performance index; (ii) if the objective is to connect the storage system to the grid, the UC shows a good performance index; and (iii) when the objective is the power quality control, the UC is interesting, followed by the flywheel.

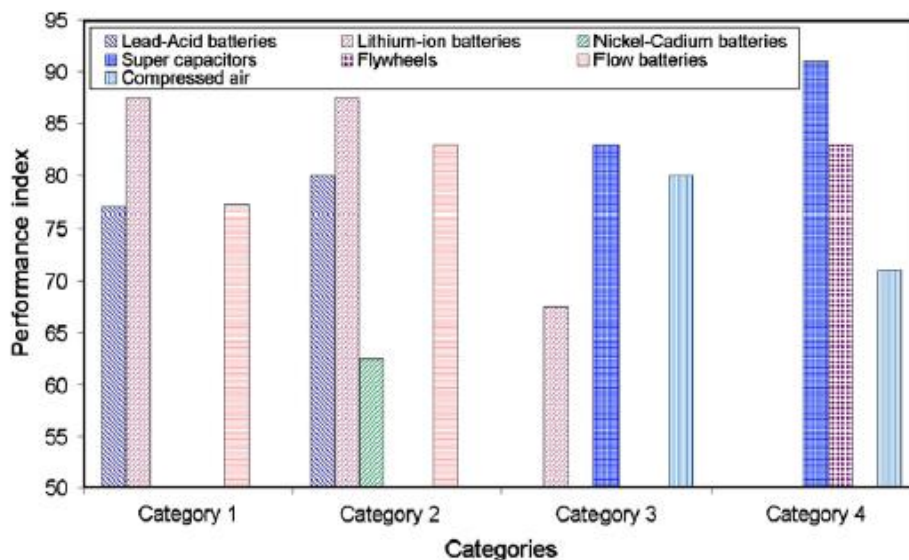


Fig. 3.7. Performance index for nine storage technologies for the four application categories [25].

Another perspective to analyze the most suitable storage system for a specific application is to compare the rated power of the system and the discharge time, as shown in Fig. 3.8. Large-scale permanent energy storage applications can be classified into three main operational categories:

- Power quality: the energy stored in these applications is only used for a few seconds or less to guarantee the quality of the energy delivered.

- Buffer and emergency storage: the energy stored in these applications is used from seconds to minutes to guarantee continuity of service when changing from one source of electricity to another.
- Grid management: storage systems are used in these applications to decouple the timing between power generation and consumption. A typical application is load leveling, which involves storing energy during off-peak hours (low energy cost) and using stored energy during peak hours (high energy cost).

Fig. 3.8 compares which of the storage options are more suitable according to the application and the intended power.

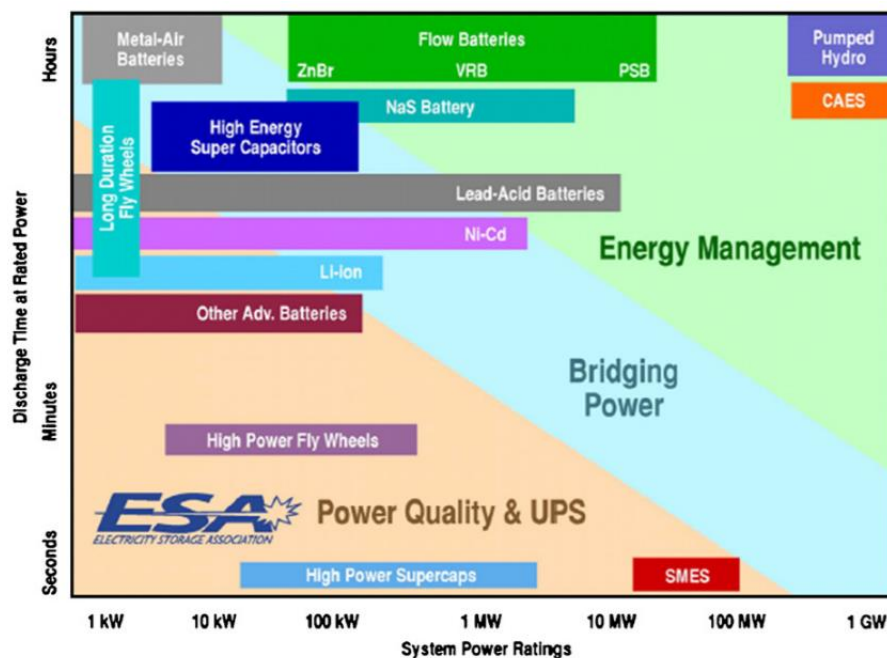


Fig. 3.8. Distribution of storage techniques according to the application [25].

The characteristics of the different storage techniques concerning efficiency and life cycle are illustrated in Figure 3.9. The two technologies with the longest lifespan and efficiency are the UC and the flywheel, and among the batteries, the li-ion technology presents a higher efficiency.

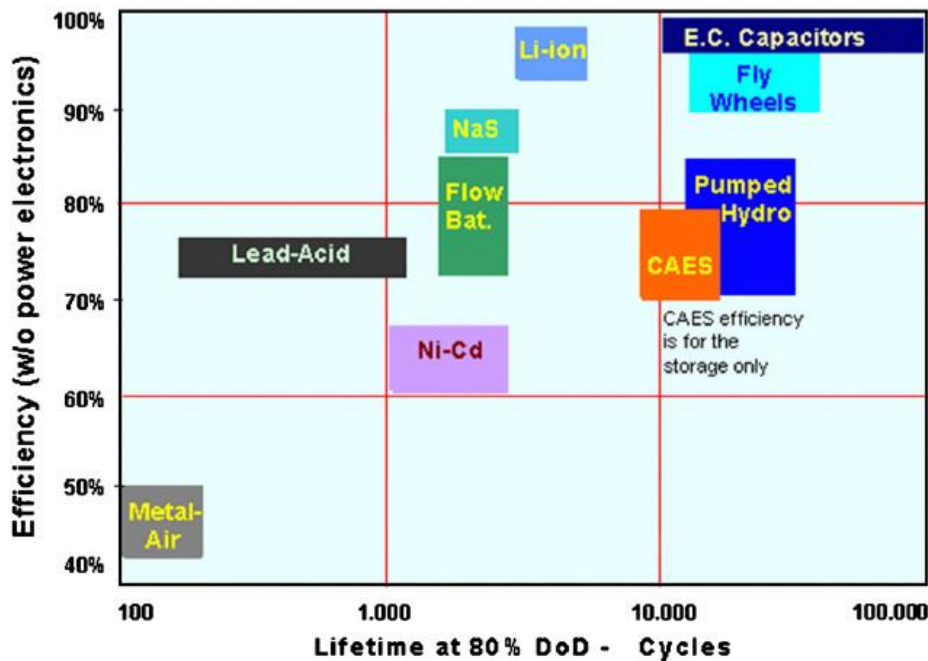


Fig. 3.9. Distribution of storage technologies based on efficiency and lifetime [25].

Energy efficiency and lifespan (maximum number of cycles) are two important parameters to consider, among others, before choosing a storage technology, as they affect overall storage costs. Low efficiency increases effective energy costs as only a fraction of the stored energy can be used. A short service life also increases long-term costs, as the storage unit must be replaced more frequently.

With regards to costs, the investment associated with a type of storage is an important economic parameter and affects the total price of energy production. Therefore, some types of storage systems can only be profitable if a certain minimum of energy is supplied. Then, the overall cost of the system (including durability of the equipment and cost of investigation) must be considered to achieve a complete analysis. For example, even though lead-acid batteries are relatively inexpensive, they are not necessarily the least expensive option for power management, due to their relatively low durability.

The cost of batteries per unit of power and energy is as shown in Fig. 3.10.

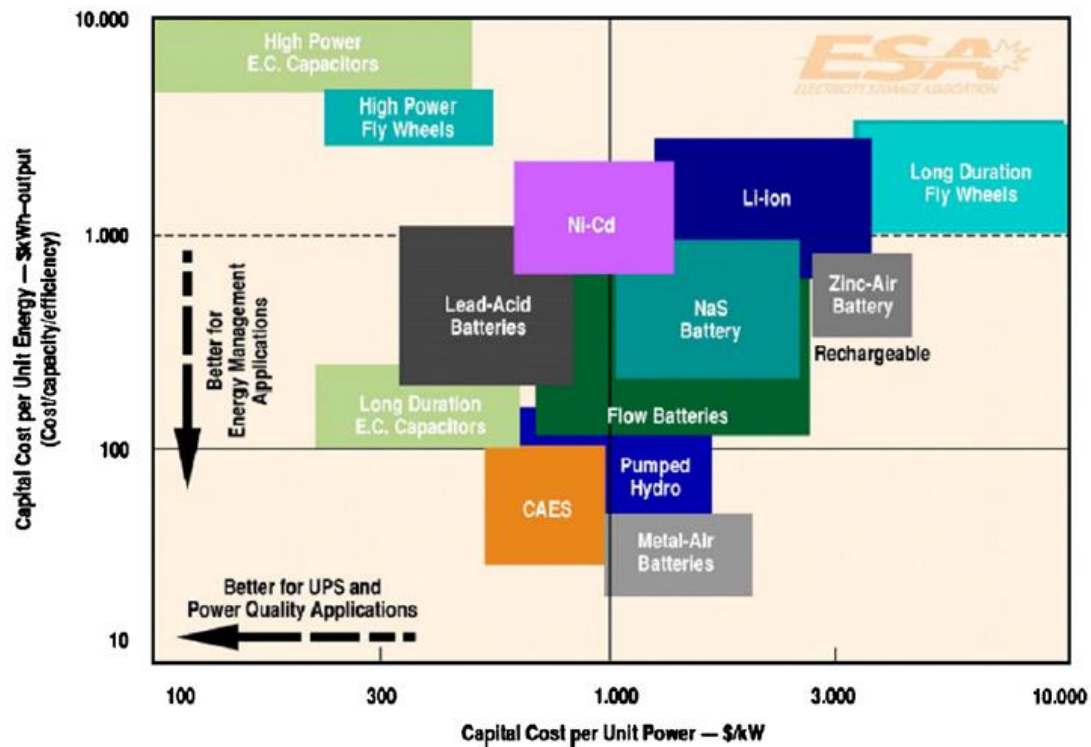


Fig. 3.10. Distribution of storage technologies as a function of investment costs per unit of power [25]

To conclude, from the data presented, it is possible to note that there is a great variety of storage technologies, each one intended for different applications. The choice of the best option is conditioned by the amount of energy to be stored, the time during which it is required to retain or release this stored energy, the available space and environmental restrictions, the cost, and the exact location of the network where storage is required.

It is clear from the review above that batteries are the dominant technology to be used when continuous power supply is primordial, while technologies such as flywheel and UC are most suitable for energy storage applications where a shorter power supply is demanded. Li-ion batteries are becoming increasingly important and have several advantages over traditional lead-acid batteries. Finally, fuel cell performance is constantly improving in terms of reliability and investment cost, yet the future penetration of fuel cells remains linked to costly hydrogen production and storage processes.

3.3. Converter technologies

Converters are elements capable of altering the characteristics of the voltage and current inputs, transforming them in a desired specific output [37]. The converters are responsible for adapting the energy generated by the PV solar panels, batteries, or any other source, to the necessary characteristics so that it can be injected into the electric grid or used in an isolated installation.

The desirable characteristics for a converter can be summarized in high efficiency, low no-load consumption, high reliability, protection against short circuits, safety, good regulation of the output voltage and frequency [38]. A common classification is through the relationship between the input and the output of the converter [39], being those the: DC-DC, AC-DC (also called rectifiers), AC-AC, DC-AC (also called inverters). When connected to the grid, the inverter should provide an alternating current that presents the same characteristics of the electrical network to which it is being connected, concerning the frequency, form, and effective value. Variations are practically not allowed, to avoid disturbances on the electrical distribution network.

The energy generated by DC sources needs to be converted before being delivered to the load or the grid. This conversion occurs typically in two stages. The first one is performed through a DC-DC converter, and in the second one, usually, a voltage source inverter (VSI) allows the connection to the grid [40]. When dealing with PV plants, typically, the DC-DC conversion stage boosts the voltage of the PV panels and implements the maximum power point tracking (MPPT) strategy for the PV generator, while the VSI is controlled to keep the voltage at the DC link constant and regulate the reactive power exchange with the grid [41]–[43].

Converters based on voltage or current source have the drawbacks of being a buck or boost converter and they cannot be a buck-boost converter. This means that the output voltage range is limited to higher or lower than the input voltage and their main circuits cannot be interchangeable [44].

To overcome these problems, the impedance source converter (ZSC) is a power converter that has buck and boost capabilities in a single conversion state. A single-stage conversion is an attractive option due to its reduced losses, low device count, and lower costs [45]. This type of device incorporates an impedance network between the power source and

the converter to overcome the technological barriers of traditional converters [46]. The structure of a ZSC is presented in Figure 3.11

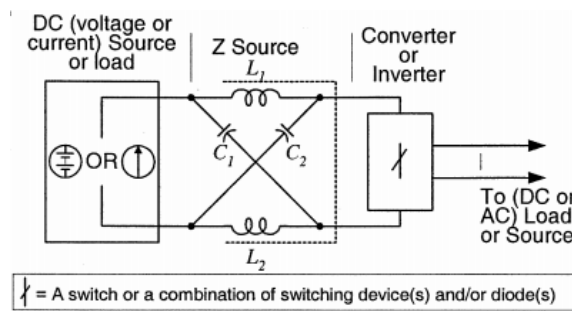


Fig. 3.11. General structure of a ZSC [46].

Another important advantage of the ZSC is that they have the possibility to work in a shoot-through state without damaging the power switches. The operating principle of this shoot-through state is based on taking advantage of the overlapping states, not allowed in VSI, to increase or decrease the voltage on the DC bus, thanks to the impedance network.

Several advantages of this type of converter were highlighted in [47], where the configuration based on DC/DC boost converter and VSI was compared to a configuration based on ZSC. ZSC achieved a better performance due to its shoot-through capability. However, their main drawbacks are a discontinuous input current in the boost mode and high voltage stress in the capacitors of the impedance network [48].

Several ZSC topologies were analysed in [49], [50]. Among them, the quasi-Z-source inverter (qZSI) is particularly attractive due to certain improvements compared to the ZSC [48]. For instance, the qZSI presents continuous input current and reduced current and voltage in the inductor L_2 and the capacitor C_2 , respectively. Furthermore, it can also work as a bidirectional converter replacing the diode with a bidirectional controlled switch. The DC/DC converter proposed in [51], is a variation of the traditional qZSI that can be coupled to the VSI. This converter improves the voltage gain in the DC/DC stage, on the other hand, it reduces the duty cycle range. A converter based on an impedance source is proposed in [52] which, in addition to a good duty cycle range, has a high voltage gain, while maintaining an acceptable degree of stress in the components. The converter proposed in [53], which is used in this work, in addition to a high degree of boost/buck capacity, reasonable efficiency, and stress on the components, has a linear duty cycle gain, making control much easier.

A qZSI can be modeled by a detailed or switched dynamic model (DM), which includes the modeling of all switches and their firing pulses. However, this model is not recommended for steady-state stability studies, long-term simulations, or large electric power systems due to its huge computation requirements. Therefore, a simplified model, which can represent accurately the system response while significantly reducing the computational time, is an interesting option for such studies. The small-signal model described in [44] has been presented as an alternative to the DM of the qZSI with lower computational efforts. However, it is based on the circuit analysis of the qZSI, rather than on the use of averaged voltage and current sources that can be easily implemented in an electric circuit representation of the qZSI. Fig. 3.12 presents the structure of a qZSI converter.

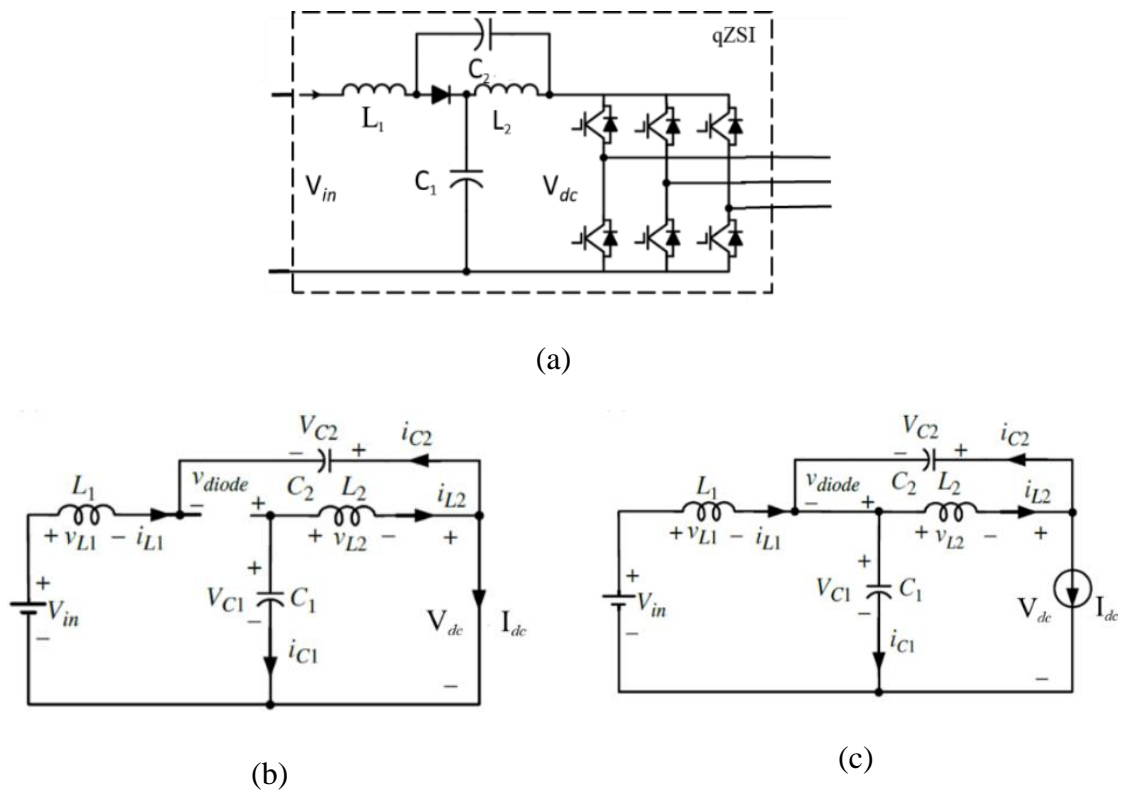


Fig. 3.12. (a) General structure of a qZSI converter, (b) shoot-through state; and (c) non-shoot-through state of the qZSI

Regarding the use of qZSI with renewable energies, several works on small-scale PV solar energy (with rated power below 10 kW) can be found in the literature. The qZSI was used in [54] and [55] for PV distributed generation with rated powers of 1 kW and 1.3 kW, respectively. In both papers, the closed-loop control of the output voltage/current was

applied through the voltage on the capacitor C_l of the impedance network. A model predictive control (MPC) technique was applied to a 550 W qZSI and PV array system in [56].

In Sections 5.2 and 5.3 the modeling of the qZSI and DC/DC-ZSC used in this thesis, is described in detail.

3.4. PV power plants with energy storage system

This section presents some of the applications for PV power plants with energy storage systems, in terms of topologies used, storage system, and control. It is a solution little used to date, with a great future, which requires more research for its development and implementation.

3.4.1. Small-scale PV power plants

The current situation of small-power PV plants, less than 100 kW, with energy storage, which corresponds to the vast majority of published works, is briefly discussed here. In this sense, some significant references have been chosen to show the current state of the use of energy storage in small PV power plants.

Even though lead and lithium-ion batteries are the most widely used options in [57] for isolated or grid-connected small plants, for the authors in [31], NaS batteries represent an efficient option as storage system in small PV power systems, as it is a well-developed technology already, that has a long useful life and high efficiency, requiring little space. This last factor is convenient, especially in areas of high population density. It is also noted that the use of NaS batteries is interesting to control energy peaks to increase the reliability of the system and increasingly include renewables in the grid.

In [58], an optimization of PV plants with grid-connected battery storage in commercial buildings in the UK is presented. The linear programming model developed finds the most cost-effective configuration of PV and battery systems, while providing information on how such systems should operate at half-hour intervals at different times of

the year. The technology selection and operation model has been tested using a case study in a food distribution center in London, UK. The results indicate that the most attractive technology configuration is a combination of lithium-ion batteries and monocrystalline silicon PV panels, and that financial payback is completed in eight years. However, this does not mean that this is always the best option, as each building is different and no solution fits all the applications. The result found in general terms indicates that, without incentives or reductions in the cost of the technology, PV and battery systems constitute a questionable investment for most of the organizations that establish short periods of investment recovery (less than 3 years). This finding implies that, if there were not the incentives set by the UK government, much of the installed capacity so far would not have taken place.

Other examples, considering PV systems with qZSI/ZSI for small-scale applications can be found in the literature [54], [59]–[63]. An optimization based on a novel perturbation and observation algorithm was proposed in [59] to achieve the MPPT of a 4.5 kW PV system connected to the grid through a qZSI. In [60]–[62], different modulation techniques were applied to ZSI/qZSI in small-scale PV system applications. A control strategy based on model predictive control was implemented for a three-phase qZSI in [63], while control loops with conventional PI controllers were used in [54].

Some of the first applications of qZSI connected to small-scale PV systems and integrating energy storage systems can be seen in [64], [65]. After these first applications, other research works with the same elements were also published, connecting the inverters in the cascaded multilevel topology [66], managing the battery state-of-charge (SOC) [67], or the power flow [68].

3.4.2. Large-scale PV power plants

Concerning LS-PVPP, until 2016 seven of the ten largest PV systems in terms of installed capacity were located in the USA. Among these top ten, the installed capacity has been increasing since the last decade, as the capacity went from 250 MW in 2011 to 580 MW by the end of 2015. There is a tendency to increase the global installed capacity until 2050, especially in China and USA, reaching 1800 GW and 500 GW respectively [69] [70], as shown in Fig. 3.13. In this graph, two situations are considered for China, one with an

optimistic forecast (indicated by "x" in yellow) considering a high PV penetration through government incentives, and another in case of continuing to follow the current patterns (red triangles). The mentioned data justify the importance of developing studies on LS-PVPP to improve their quality and spread their use.

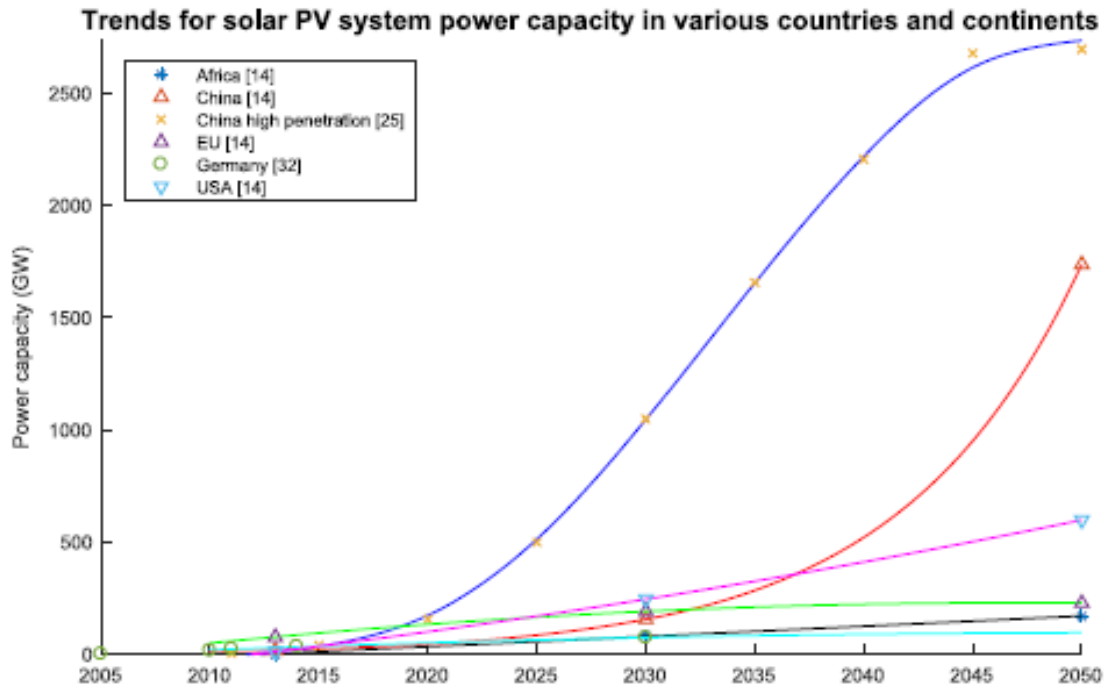


Fig. 3.13. Trends for installed PV power systems by countries/continents [70].

One important parameter to take into account to improve LS-PVPP is the study and evaluation of the most suitable configuration according to technical criteria. To guarantee the best design, control, and operation of the PV power plants, the PV generation components are being investigated, as well as the internal design of the plants. Hence, the topologies used in PV plants are investigated next.

Four topologies for large-scale power plants are analyzed in [18]. In the central topology, all PV panels are interconnected with an inverter. In the string topology, a PV string is connected to an inverter. The multi-string topology presents a PV string connected to a DC/DC converter, with 4 or 5 DC/DC converters connected to a DC/AC inverter. The fourth topology, module integrated, has one inverter for each PV module, but until the present date, it has not been used in large-scale plants.

It can be affirmed that the central topology has the following advantages: robustness, low AC energy losses, low variation of AC voltage, and reasonable installation and maintenance costs in contrast with the other topologies. The general characteristics of the string and multi-string topologies are very attractive, but their main drawback is the installation and maintenance costs as the number of inverters increases. The string topology has characteristics similar to the multi-string topology, but its use is recommended when each PV string has different orientation angles. The multi-string topology has better efficiency because it has a dedicated MPPT control per string. However, the complexity of the installation and the large number of inverters needed make this topology less attractive to investors.

Four different configurations for PV plants were evaluated in [71]. The contribution of energy storage systems was also considered in this paper. Furthermore, the connection to the grid of the configurations was analyzed. The configurations evaluated are: independent, AC-Coupled, DC-Coupled, and DC tightly coupled.

The independent configuration represents the way that the vast majority of large-scale storage and PV systems are currently implemented. In this configuration, the PV generators and the ESS can be located in completely different locations and do not share common components or control strategies. The ESS can be charged with any source in the network that provides low-cost power, and it can discharge during periods of high demand.

In the AC-Coupled configuration, the PV and ESS are located together and share a point of common coupling to the AC network. Because the plant does not share any component, the ESS can still act independently of the PV system, that is, it can store energy from the PV plant or from the network.

The systems in which the PV plant and the ESS are coupled on the DC side of a shared inverter are the DC-Coupled and the DC tightly coupled configuration. The DC-Coupled system includes a bidirectional inverter that allows the storage system to be charged from the network, in addition to being charged from the PV. The DC tightly coupled system assumes that the ESS can only store energy from the PV panels, not from the grid.

For LS-PVPP, different converter models have been implemented. For example, the topology used in [72] is connected to the grid through two conversion stages, consisting of two parallel-connected triple-port dual active bridge (DAB) combined into a two-level

inverter. Each triple-port DAB integrates a PV and a battery-based ESS through a multi-winding transformer. The high power density, galvanic isolation, seamless switching between the different operating modes, and the modular nature, are notable features of the triple-port DAB-based DC/DC converter modules. All these features make this PV-ESS integrated triple-port DAB converter interfaced to an inverter an attractive solution for LS-PVPP integration to the grid.

Other works found in the literature suggest the use of ZSI and qZSI with ESS. A large voltage boost in a single-stage can be achieved by Z-source inverters (ZSI), which include an impedance network before the VSI. Different topologies for ZSI can be found in [73], [74]. A modified topology with a bi-directional power flow was proposed in [73]. An improved boost capability and low voltage stress in the impedance source of a ZSI were analyzed in [74]. A variation of ZSI is the quasi-Z-source inverter (qZSI), which presents differences in configuration while maintaining the same operating principle. The benefits of the qZSI, when compared to the ZSI, are a lower component rating, no need for extra filtering capacitors, reduced switching ripples, and constant DC input current from the PV panel [65].

When analyzing the qZSI topologies integrated with ESS, two feasible configurations include a battery energy storage system (qZSI-BES) connected in parallel with the capacitors C_1 or C_2 , as shown in Fig. 3.14 (a) and (b).

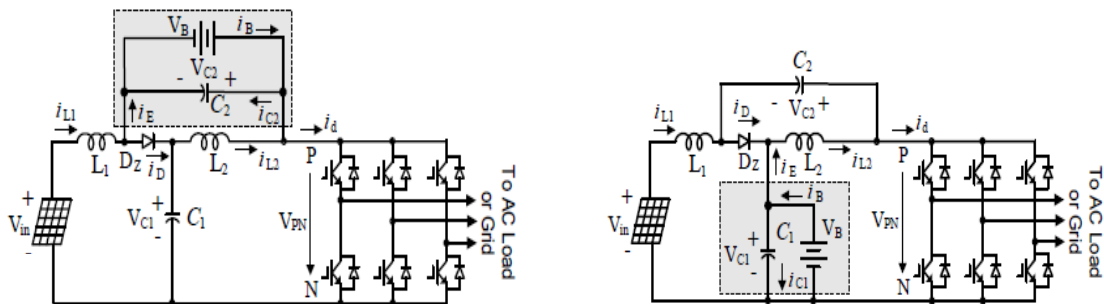


Fig. 3.14. qZSI with battery (a) in parallel with C_2 , (b) in parallel with C_1 . [9]

The authors in [75] proposed the use of the configuration presented in Fig. 3.14 (a) for three hybrid modules with their outputs connected in series. Each module includes a PV panel, a battery, and a qZSH-bridge inverter. The battery is included to reduce the intermittency of the PV generation. The control scheme develops the MPPT strategy of the

PV panels, provides the desired power to the grid, and balances the power of each battery between the different modules. For the MPPT, the perturb and observed (P&O) algorithm was implemented delivering the voltage reference at the output. A PI regulator was applied to track the voltage reference by regulating the duty cycle (D). Here, D was not only used to implement the MPPT but also to boost the PV voltage to a higher voltage level. In the case of grid power control, the phase angle of the grid voltage was measured by using a phase-locked loop and then used to produce the phase reference for the grid current. For battery energy management, the SOC was controlled to operate in a safe range between the minimum and maximum limits. Therefore, when the battery reached the minimum SOC, this module could not be discharged any deeper, and when it reached the maximum SOC, the battery could not be charged any further. To achieve this objective, the proposed controls were implemented and the simulation results confirmed the effectiveness of the system.

The configuration presented in Fig. 3.14 (b) was chosen by the authors in [65]. This paper proposed this new topology to overcome the power limitation due to the wide range of discontinuous conduction mode during the battery discharge. This occurs when the battery is paralleled with C_2 . The intention here was to test the new topology, to control the PV panel output power, and, as a result, to control the battery power. Regarding the control strategy, the PV panel power or the battery power can be controlled through D , and the inverter output power can be controlled by the modulation index (M). For the PV panel power control, the battery voltage changes with the SOC of the battery. Also, the voltage of the PV panel is highly current-dependent. Therefore, for a given battery voltage higher than both the open-circuit voltage of the PV panel and the inverter line-to-line output voltage, the input voltage of the PV panel can be controlled to track its maximum power point (MPP) through D . The PI regulator is employed in the PV voltage closed-loop control to find the desired variation of the shoot-through duty cycle for a PV voltage reference variation. As a result, in this control method, D was used to control the input voltage to track the maximum power of the PV panel, thus controlling the input power. For the battery power control, the shoot-through duty ratio D was used to control the battery current directly through changing the voltage of capacitor C_1 connected in parallel to the battery, thus controlling the battery power. Moreover, M was used to control the inverter output power, while the input PV power was indirectly controlled. With the proposed qZSI plus battery and the two suggested control methods, it was possible to develop the MPPT strategy in the PV module effectively and to

inject the active/reactive power into the grid through the inverter independently. It also controlled the energy flow from/to the battery. These are key features in most PV energy systems, which demonstrates the suitability of the proposed solution for this type of application.

Knowing the existing configurations is important, since one of the aims of the thesis is to study and evaluate the most suitable configuration for a PV plant with hybrid ESS according to technical criteria.

3.4.3. Energy storage systems

Although RES present the advantages of a vast fuel source and lower emissions of pollutants, their intermittent nature requires special attention for their integration into the grid. If this integration is not dealt properly, excessive PV generation may lead to voltage instability, power fluctuation, or malfunctioning of the voltage regulation equipment, among other issues [2]. The use of energy storage systems with RES is an effective way to address the fluctuation and intermittency of the RES generation. A robust sizing of hybrid PV systems with battery is recommended when considering future variations of meteorological data and consumption profiles [76].

Among the existing large-scale energy storage technologies, batteries are widely employed [32], [77]. Batteries can operate in charge or discharge mode according to the desired system operation. Most of the configurations with batteries and PV panels also include an additional DC-DC converter for the battery connection and a VSI for grid connection [78]–[80]. For the authors in [42], the electrochemical ESS that are suitable for PV systems is the Redox flow battery (RFB), the sodium-sulfur battery (NaS), the nickel-cadmium battery (Ni-Cd), the lead battery, and the lithium-ion (Li-ion) battery.

However, energy-stored qZSI represents a very interesting alternative for hybrid PV-battery systems without needing an additional DC/DC converter dedicated to the battery, since the battery is integrated into the impedance network of the qZSI in the energy-stored qZSI. This configuration allows an appropriate MPPT control of the PV panels, stable regulation of the DC voltage, and adjustable reactive power exchange through the control of the single inverter in the qZSI.

In the literature, qZSI has been used with energy storage systems in applications such as microgrids [81], [82], induction motors for water pumps [83], stand-alone wind turbines [84], and electric vehicles [85]. All these applications share the common objective of providing a stable power supply and enabling an efficient use of RES. A microgrid is “a group of Distributed Energy Resources (DER), including RES and ESS, plus loads that operate locally as a single controllable entity” [86].

To reduce the intermittent characteristic of the RES, the authors in [32], [87]–[89] proposed the use of ESS. Although the ESS market is expanding, there is a lack of standards and methods for comparing the efficiency and performance of ESS in a PV system [32]. According to the same authors, the high uncertainty and fluctuation of the PV power cause poor power quality and control issues. The energy storage and dispatch strategies could play an important role in the stability of future power systems with high PV penetration.

Reference [87] discussed the use of batteries with large renewable generation as one of the effective technologies to deal with power fluctuation and intermittency. The proposed battery energy management strategy was applied to meet the real-time power requirement and ensure energy balance and availability. However, the current high cost of batteries is indeed a problem that cannot be ignored. According to this work, in order to use the battery more efficiently, further research, development, and verification associated with the operation and application technologies of the large-scale batteries need to be continued.

Table 3.2 presents the ten largest EES, by nominal power capacity under commission or in operation for the electrical grid as of 2016. From this table, it can be seen that six of the ten technologies used in the ESS are lithium-ion. In addition, it is also noted that three of the ten plants are located in Japan and two are located in the USA.

TABLE 3.2. THE TEN LARGEST ESS (BY POWER CAPACITY) UNDER COMMISSION OR IN OPERATION FOR THE ELECTRICITY GRID AS OF 2016 [70].

Name	Location	Technology	Power capacity (MW)	Energy capacity (MWh)	Status	Description
AES Alamos Energy Storage Array	Long Beach, California, United States	Li-ion	100	400	Contracted	The EES will be placed in a large building named Alamos Power Center and will be used as replacement of peaking power plant. It will also be used for balancing intermittent renewables.
Solar Energy Corporation of India (SECI) -100 MW	Ananthapuramu, Andhra Pradesh, India	Electro-chemical	100	400	Announced	The EES will be built as an addition to the recent commissioned 750 MW solar farm.
Kingfisher Project (Stage 2)	Roxby Downs, South Australia, Australia	Li-ion	100	400	Under construction	The EES will be paired with a 100 MW solar farm and will be in operation by the end of 2017.
Kyushu Electric - Buzen Substation - Mitsubishi Electric / NGK Insulators	Buzen, Fukuoka Prefecture, Japan	Sodium-sulphur	50	300	In operation	Mainly used for stabilizing power flow and frequency introduced by renewables. It can also optimize the operation of the system by efficient coordination of EES and dispatchable sources.
Gyeongsan Substation ESS - 48 MW ESS - KEPCO / Wookin / LG Chem	Gyeongsan-si, Gyeongsangbuk-do, South Korea	Li-ion	48	12	In operation	The EES is mainly used for transmission congestion relief, voltage support and frequency regulation.
Nishi-Sendai Substation - Tohoku Electric / Toshiba	Sendai, Miyagi Prefecture, Japan	Li-ion	40	20	In operation	The EES was built to minimize the frequency fluctuation from PV plant.
40 MW - AES / National Grid Corp. of the Philippines (Kabankalan)	Kabankalan, Negros Occidental, Philippines	Li-ion	40	Unknown	In operation	The EES is one of the largest electrochemical storage systems in Asia. It provides voltage support and frequency regulation and aims to improve the ancillary services.
Minami-Soma Substation - Tohoku Electric / Toshiba	Minamisoma, Fukushima Prefecture, Japan	Li-ion	40	40	In operation	The EES aims to provide better energy management and improve renewable energy supply and demand balance.
Notrees battery storage project - Duke Energy	Goldsmith, Texas, United States	Advanced lead-acid	36	24	In operation	The EES was built to relieve the intermittency issues created by a 153 MW wind power farm in western Texas. A grant from U.S. Department of Energy Office of Electricity American Recovery and Reinvestment Act was issued to support the project development.
Non-gong substation EES - 36 MW EES - KEPCO/Kokam	Non-gong substation, South Korea	Lithium nickel manganese cobalt	36	13	Contracted	The EES was built to provide frequency regulation at the Non-gong substation. The project began in June 2016 has an expected completion date by Dec. 2016.

In [88], the ESS consisted of a combination of battery and UC that complemented each other in terms of power and energy. The coordinated use of the battery and the UC can provide an excellent combination that can cover a wide range of power and energy requirements, especially in PV systems.

The use of hydrogen as an ESS for a PV power plant, with simulations based on real data from a 1.62 MWp plant located in central Italy, was analyzed in [89]. The system was used to supply power to the load directly from the PV field, or by converting in the fuel cell the chemical energy of the hydrogen into electricity. The conclusions of this work suggest that, due to the losses of efficiency in the system, the direct delivery of energy from PV plants to the grid is generally the best option. However, in areas where the local network experiences a low quality of service due to sudden variations in the injected energy, a flat injection curve can reduce the need to invest in transmission lines and become a viable commercial proposal. In cases when the grids are stable and adequately sized, a hydrogen system that helps a PV plant would be more suitable, from an economic point of view, for off-grid or backup power supply applications. Furthermore, if performance improvements occur and system costs decrease, the business proposal can be attractive even for grid stabilization and balance services.

In [90], the PV system supplies power to a DC load. When the power of the PV source is insufficient, the electricity grid compensates for the energy deficit. On the other hand, if the load is satisfied and the PV source can still supply energy, the excess energy is diverted to its own storage unit that produces hydrogen gas through water electrolysis. The difference between the authors of [89] and [90] is that in [90] a pump is not used to control the flow of water for the electrolysis process, and they propose the idea of replacing the function of the pump by the action of gravity.

Solomon *et al.* described ESS for large-scale power plants in [88]. According to the authors, only one type of ESS is not enough to meet all the needs for this type of plant. However, it should be possible to devise a hybrid storage system, composed of subunits of various ESS technologies, that would have appropriate qualities for large PV grid penetration.

To the best of our knowledge, no published paper dealing with LS-PVPP with qZSI and two types of ESS exists up to date. Based on this fact, it will be considered in this thesis

the use of two storage units in a hybrid system into the PVPP, such as batteries, UC, or hydrogen systems, combining the advantages of different ESS, also called hybrid energy storage system (HESS). This will be one of the main novelties and contributions of this thesis.

3.4.4. Control techniques

To guarantee the proper functioning of RES using battery energy storage, it is necessary to monitor and control the energy flow between sources and loads or the grid [91]. This control is performed by an energy management system (EMS).

There exist numerous control techniques that can be used depending on the desired application. Among these techniques, some of the most used are the PI/PID controllers, due to their degree of development and simple implementation.

The representation of the global system used in [1] is shown in Fig. 3.15. In this system, batteries are designed to store electric energy for later use, providing slow system dynamics and an efficient means of smoothing power fluctuations. A bi-directional buck-boost converter is used to connect the batteries to the DC bus. UCs are used to provide or absorb significant powers with fast dynamics, with low internal resistance and low voltage, and also to carry out very fast charges and discharges, as they have a large number of cycles without degradation and with high efficiency. The UCs are also connected to the DC bus through the use of a buck-boost converter.

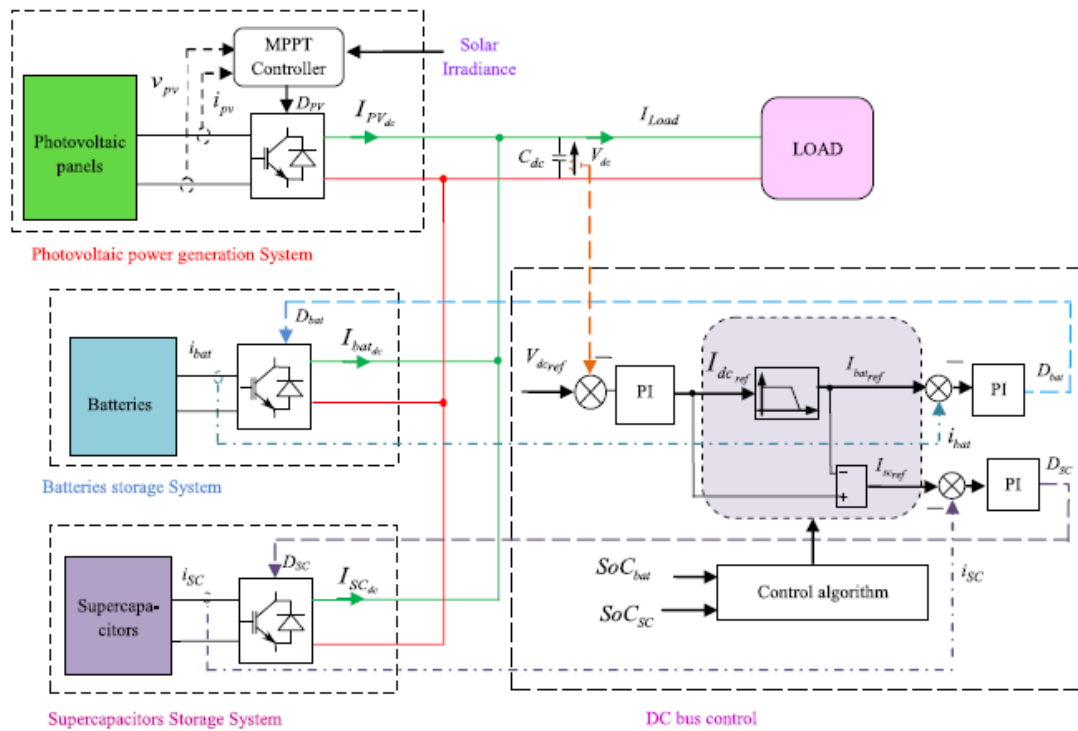


Fig. 3.15. Configuration considered in [1] with PV plant and HESS

The DC bus control is based on a PI controller, which calculates the reference current $I_{dc\,ref}$ to keep the DC bus voltage at the reference voltage V_{ref} . An energy management strategy provides the reference currents for the battery and UC converters. These currents guarantee the maintenance of the DC bus voltage regardless of the behavior of the load and the value of the energy extracted from the PV panels. If a problem occurs in a PV generator, the batteries and/or the UC ensure the regulation of the DC bus voltage. At any time, the sum of the reference currents, $I_{sc\,ref}$ and $I_{bat\,ref}$, must equal $I_{cc\,ref}$.

The control algorithm in charge of establishing the reference currents to the batteries and the UC for different cases of state of charge (SOC) is the following:

- If the DC bus reference current is negative (when the PV panels provide more power than desired) and the UC SOC is higher than 95% (the UC are saturated), the reference current of the UC must be null. If the SOC is below 95%, the UC starts charging.
- If the DC bus reference current is positive (when the PV panels do not provide the desired power) and the UC SOC is below 25%, the UC reference current must be

zero, that is, they must not supply any power. If the SOC is greater than 25%, the UC starts discharging.

- The reference current of the DC bus is zero when the PV panels produce the necessary power for the load.

To demonstrate the effectiveness of this hybrid storage system, some operating simulations are performed in [47]. The simulation results demonstrate that the integration of UC in the energy storage system of a PV plant leads to a low charge/discharge current rate of the battery and reduces stress levels, improving the battery life cycle. Nevertheless, the lack of robustness and the need to adjust different parameters are considered some disadvantages of this traditional PI control technique. In this context, artificial intelligence (AI) algorithms are becoming popular nowadays, playing an important role in enhancing the performance of PV systems [92].

AI techniques can be programmed to learn from examples, they can perform predictions at high speed, they are able to deal with nonlinear problems, and are fault-tolerant in a manner that they can handle noisy and incomplete data. Some of the AI techniques used in the PV field are Neural Networks (NN), Fuzzy Logic (FL), Genetic Algorithm (GA), and also hybrid techniques, combining the advantages of more than one AI algorithm [93]. A hybrid technique was applied in [94], in which the EMS between a renewable energy system, a battery, and the grid was performed using an adaptive neuro-fuzzy (ANFIS). The control strategy based on ANFIS improved the overall control capacity and provided better performance when compared to a PI-based control.

AI algorithms have been used in many aspects of sizing, modeling, and control of PV systems. For instance, a two-level coordinated control strategy with FL was proposed in [95] to adequately adjust the total active power supplied to a grid by LS-PVPP with the aim of regulating the grid frequency. The results of the simulation for the frequency control strategy showed an improved performance compared to the conventional strategy based on the complete MPPT mode. An EMS based on fuzzy logic was used in [96] to maximize the duration of the power supply according to the availability of renewable sources and storage systems. An intelligent EMS of a hybrid system with storage in isolated applications (stand-alone) based on fuzzy logic was developed in [97]. Moreover, a control strategy using fuzzy gain scheduling of PID controller for a hybrid system, composed of PV and battery,

subjected to different climatic conditions was used in [98]. A two-level control system structure was implemented combining PID and fuzzy logic control for MPPT.

In [99], a fuzzy logic two-level coordinated control strategy is proposed to properly adjust the total active power supplied to a grid by large-scale PV plants to regulate the grid frequency. Each solar plant is connected to a DC/DC converter, treated as agents, and a central coordinating controller. The central controller uses a frequency regulation module based on a new self-adjusting FLC scheme to calculate the appropriate reference value according to the total power required. Then, the individual reference value is defined for each local controller. Each local controller governs all the power electronic converters installed in the PV agent to inject energy into the grid according to the individual reference value received. In addition, each local controller uses an algorithm to manage the state of charge of the battery bank installed, so that it remains in the safe range of 20 to 80% while operating near the desired value of 50% in the stationary state. In addition, a special control mode is integrated into the overall strategy to help the fast recovery of the grid frequency in emergency conditions.

The techniques based on model predictive control (MPC) are also gaining popularity due to their capability to control various variables at the same time, including constraints, dealing with different kinds and magnitude of controlled variables [93]. These techniques are versatile and can be used for the control of converters, as well as for supervisory control. An example of the application of MPC for PV systems was presented in [95], which proposed control and optimization methods for a grid-connected PV plant with ESS. The control system had two main objectives. The first one was to benefit from unequal prices, and the second one was to smooth the intermittent power output of the PV plant. A MPC was used to allow storage units to adapt automatically and dynamically to changes in PV production while responding to requests from external system operators or price signals. From the results obtained, it is clear that, although MPC does not guarantee optimality, it generally shows almost optimal results.

Another objective of this thesis is the design of new control systems based on advanced control techniques for the PV power plant with hybrid ESS, as well as the supervisory control system for the coordinated control of the inverter and ESS, in order to

improve the results obtained by the existing solutions in terms of energy efficiency, management, and operation.

The aforementioned arguments lead to the conclusion that the topic covered in this thesis is timely, of interest, and worth of greater research efforts, as it has been shown in the review of the state of the art carried out in this section. In particular, there are very few works published that address the study of large-scale PV hybrid plants that combine qZSI with two types of ESS, and pursuing an efficient management and integration of the plant in the grid. Those aspects will be addressed in this thesis to provide new knowledge and relevant results, and they represent the main developments and contributions of this thesis.

Chapter 4

Methodology

The research methodology followed during this thesis consists of the logic steps presented in this section. The main tool used for modeling, control design, and simulation was the software MATLAB/Simulink®. The experimental validation was performed in the Hardware-in-the-Loop (HIL) platform TYPHOON HIL-402-AP and the control board dSPACE MicroLabBox. Therefore, the research methodology for this study consists of the following tasks:

- *Task 0. Literature review and conceptual modeling*

The objective in this task was to learn the state of the art of the topic under study, performing a detailed review of the existing literature. LS-PVPP with ESS were analyzed to identify common aspects present worldwide in terms of configuration, technologies, control, and management of the plant. During the comprehensive review of the available literature, a critical observation was carried out in order to identify possible constraints, limitations, and research questions to be solved. After that, points of action were structured to address the weaknesses and find solutions.

- *Task 1. Determination of the plant under study*

The characteristics of the plant in terms of configuration, solar modules, converters, and ESS, were selected in this task. The solar modules were chosen according to their efficiency, material, and reliability. Regarding the ESS, the possibility to combine different technologies was analyzed, in order to procure a short-term energy storage with fast response time, and/or a long-term energy storage with slow response time.

- *Task 2. Evaluation of different types of internal configuration.*

In this task, the connections and topologies within the plant were defined, evaluating the best connection point for the ESS and PV system. The viability to connect one or both storage systems in parallel to the capacitors in the qZSI was analyzed, as well as the need to use a DC/DC converter between one of the ESS and the qZSI to control both ESS. This study helped defining the internal configuration considering aspects such as voltage levels, control, and operation strategies.

- *Task 3. Dynamic modeling of the main components.*

Dynamic models of the plant components were developed using the software MATLAB/Simulink®. The models available in the libraries were adapted according to the needs. For ESS, accepted models of recognized validity in the field of electric power systems were also used. The design and sizing processes followed the technical characteristics provided by manufacturers or suppliers. Simulations were performed under different operating conditions, evaluating and verifying the correct response of the models. The designs were implemented, assessed, and validated experimentally on laboratory scale through a TYPHOON HIL system (a compact, extremely powerful HIL device that allows modeling and simulating in real-time ESS, power converters and grids, and testing power electronics controllers for a wide range of applications).

- *Task 4. Design and evaluation of the control systems for the energy sources*

This task focused on the design of a control strategy for the power converters. Simulations and experimental tests were performed for their validation under different operating conditions and under changes in the references of the control variables. The control system was implemented on a dSPACE MicroLabBox control board, and the real-time measurement of the input/output signals of the controller and the response of the controlled system were evaluated and analyzed. The results obtained with the different control systems implemented were compared to observe the improvements achieved. Finally, a supervisory control system was developed to verify the correct operation of the plant through simulations and experimental tests.

- *Task 5. Design of the supervisory control system for energy management of the hybrid power plant.*

In this task, the study and design of different supervisory control systems, based on fuzzy logic control, were carried out. The aim was to perform an adequate coordinated operation of the inverter and the HESS that improved the generation capacity and energy management capabilities of the hybrid PV plant. Within the control strategy, variables such as the active power of the PV generator, the reactive power exchanged with the grid, the internal voltage of the plant or the electric grid, the power demanded by the system operator and the power of the ESS and its SOC, were taken into account. Finally, simulations and experimental tests were carried out under different operating conditions of the hybrid PV plant. The results obtained through the different supervisory control systems implemented, were analyzed in depth.

- *Task 6. Analysis of the results and thesis writing*

Here, the objective was to gather the results obtained, establish conclusions and write the thesis. Comparisons were made to prove that the proposed configurations and control strategies outperform other existing solutions.

III

Modeling and Control Systems

In this section, the modeling of the elements in the plant under study is presented. The overall configuration is presented and described, explaining the proposed control strategy afterwards. The control loops implemented are described in detail, paying special attention to the energy management control strategy, for which three different schemes are considered.

Chapter 5

Configuration and Modeling

In this chapter, the configuration of the system under study and the modeling of the components are presented. The system is based on a grid-connected PV power plant composed of the PV panels, the BES-qZSI, the DC/DC-ZSC, the UC, an LCL filter, and a transformer.

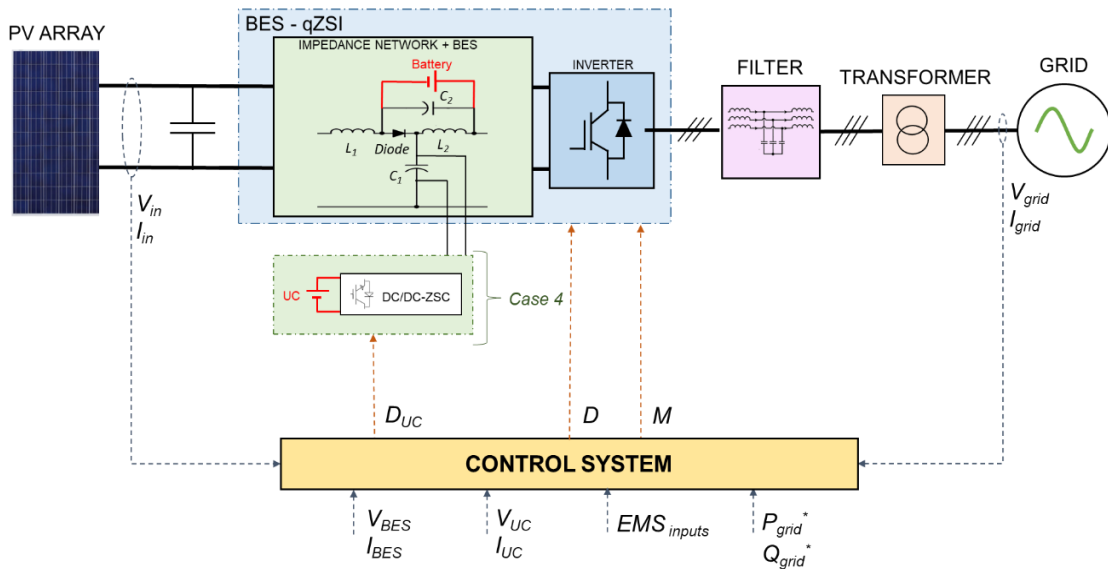


Fig. 5.1. General configuration of the plant under study

Note that the mentioned configuration was applied for the simulation results presented in Case 4 (Section 8.4). For Cases 1, 2, and 3 the DC/DC-ZSC converter and the UC were not considered.

5.1. PV Panels

A PV system is composed of many cells connected in series and in parallel, in order to supply a power output depending mainly on the incident irradiance and also on the

temperature. A single-diode model was chosen to represent the behavior of the PV panels, being a model widely accepted and used by many research papers in the literature [100][101]. The elements in this model are a diode, a controlled current source, a series resistor, and a shunt resistor. The PV model receives the irradiance and temperature as inputs, while the I-V characteristics are outputted.

The mathematical modeling for the output current is given by Eqs. 5.1 – 5.3.

$$I_{pv} = I_L - I_{sat} \left(e^{\frac{q(V_{pv} + I_{pv}R_s)}{NkT_{pv}}} \right) - \frac{(V_{pv} + I_{pv}R_s)}{R_{sh}} \quad (5.1)$$

$$I_L = I_{L0} (1 + K_0 (T - 300)) \cdot \frac{G}{G_n} \quad (5.2)$$

$$I_{sat} = I_{sat,n} \left(\frac{T_n}{T} \right)^3 e \left[\frac{qE_g}{ak} \left(\frac{1}{T_n} - \frac{1}{T} \right) \right] \quad (5.3)$$

where I_{L0} , I_L are the solar-induced current at 300 K and the solar-induced current (A), respectively. $I_{sat,n}$, I_{sat} are the nominal saturation current of the diode and the saturation current (A). The Boltzmann constant ($J \cdot K^{-1}$) is represented by k . The elementary charge of an electron (C) is represented by q . K_0 is a constant depending on the characteristics of the PV panel. T and T_n are the operating and the nominal temperature (K) of the PV panel. E_g is the bandgap energy of the semiconductor (eV). a is the diode ideal constant. R_{sh} and R_s are the shunt resistance and series resistance (Ω), respectively. G and G_n are the irradiation and the nominal irradiation ($W \cdot m^{-2}$) on the device surface, respectively.

The solar monocrystalline module SunPower SPR-335NX-BLK-D [102] was the model considered in this study. It can reach a maximum power of 335 W, with a voltage of 57.3 V at the maximum power point. As described in the literature review, the monocrystalline technology presents good efficiency, and its cost is decreasing over the years with its popularization.

The other characteristics of this module are an open-circuit voltage equal to 67.9 V, a short circuit current of 6.23 A, and a current at the maximum power point of 5.85 A.

5.2. Detailed model of the Quasi Z-source inverter

The typical qZSI configuration consists of a three-phase voltage source inverter (VSI) and an impedance network with two capacitors (C_1, C_2) and two inductors (L_1, L_2). These components are sized to limit the switching frequency current and voltage ripple [103].

The qZSI allows two possible operation states, called the shoot-through and the non-shoot-through states. In the shoot-through state, both switches of a leg are active simultaneously, thus short-circuiting the DC side of the converter. On the other hand, in the non-shoot-through state, the qZSI allows the two zero states and the six active states of a conventional VSI (i.e., at least one of the switches open in each leg) [104].

The capacitance C and inductance L are the main components to be designed in the qZSI. According to [104], the inductance of the Z network can be calculated as:

$$L = \frac{1}{2} \cdot T_{0\max} \cdot \frac{M_{\min} v_{in}}{r_i I_{in}} \quad (5.4)$$

where I_{in} and v_{in} are the input current and voltage of the qZSI, respectively, r_i is the current ripple of the inductors, which is limited to 20%, and T_0 is the shoot-through period, given by:

$$T_{0\max} = \frac{2 - \sqrt{3} M_{\min}}{2 f_s} \quad (5.5)$$

Where f_s is the switching frequency.

The minimum modulation index M_{\min} for the space vector modulation technique applied herein, namely ZSVM6 [61], is calculated as follows:

$$M_{\min} = \frac{\pi G_{\max}}{3 G_{\max} \cdot \sqrt{3} - \pi} \quad (5.6)$$

where the maximum gain of the inverter G_{\max} is expressed as:

$$G_{\max} = \frac{v_{ac}}{v_{in\min} / 2} \quad (5.7)$$

being v_{ac} the peak phase-to-phase voltage.

The capacitance C is obtained from (5.8), setting the voltage ripple r_v to 1%:

$$C = 2T_{0\max} \cdot \frac{I_{in}}{r_v \hat{v}_{dc}} = \frac{2T_{0\max} I_{in} (1 - 2D_{\max})}{r_v v_{in}} \quad (5.8)$$

where \hat{v}_{dc} is the DC voltage at the output of the Z network.

Finally, the maximum duty ratio D_{\max} is obtained from:

$$D_{\max} = 1 - \frac{3\sqrt{3}M_{\min}}{2\pi} \quad (5.9)$$

5.3. Simplified model of the Quasi Z-source inverter

The model presented in Section 5.2 is called the detailed model (*DM*) or fully switched model, since all the components are modeled, including the impedance network and the switches of the qZSC. An alternative option to represent the converter dynamics with sufficient accuracy while using a less complex model than the DM is the simplified model (*SM*), as proposed in [105]. This model is based on averaged values of the variables, voltage/current sources, and the same control circuit as the DM, except for the switching pulses of the power switches. The SM allows a faster time-domain simulation and is useful for control design and dynamic analysis purposes.

Because the firing pulses of the switches are not considered in the SM, the data processing is reduced notably (the sample time can be increased), while obtaining a performance similar to the DM. Thus, the proposed model does not present the current and voltage harmonics, but it reproduces the dynamic performance of the DM, which is relevant when it comes to managing the power flow.

The proposed SM is composed of a controlled current source in the PV system side, three controlled voltage sources on the grid side, a controlled voltage source for the terminals of the capacitor C_2 and a controlled voltage source for the terminals of the capacitor C_1 . As in the DM, the battery is connected to C_2 . The voltage source for the capacitor C_1 , was only considered in the configuration with UC. Fig. 5.2 illustrates a scheme of the SM proposed for the qZSI.

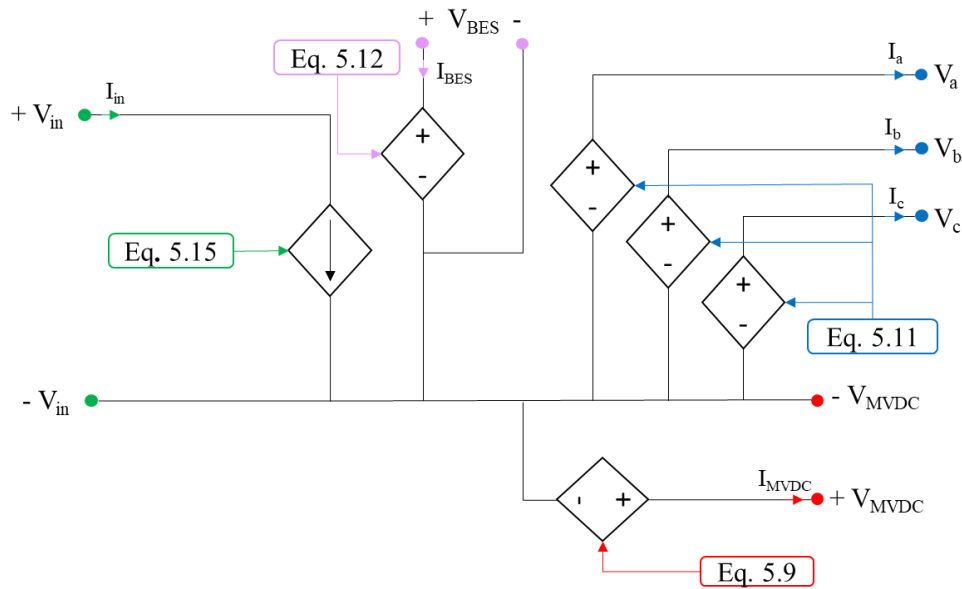


Fig. 5.2. Proposed qZSI simplified model

In a lossless qZSI, the input voltage (V_{in}) and the voltage across the capacitor C_1 (V_{C1}) or the MVDC bus voltage (V_{MVDC}) are related through Eq. (5.9), where D is the shoot-through period. Eq. (5.10) shows the relation between V_{in} and the output voltage of the impedance network (V_{dc}). V_{dc} and the AC voltages are related through m_a , m_b , and m_c , as described by Eq. (5.10), where B is the boost gain. The values of D and $m_a(t)$, $m_b(t)$ and $m_c(t)$ are obtained from the control loops shown in Fig. 6.1, described in section 6.4. These are needed for a proper control of the power flow among the components of the MVDC.

$$V_{C1} = V_{MVDC} = \frac{1-D}{1-2D} \cdot V_{in} \quad (5.9)$$

$$V_{DC} = \frac{1}{1-2D} \cdot V_{in} = B \cdot V_{in} \quad (5.10)$$

$$v_{abc} = \frac{1}{\sqrt{3}} (V_{DC} \cdot m_{abc})$$

Now, substituting V_{dc} from Eq. (5.9) into Eq. (5.10), a direct relation can be obtained between the input voltage of the energy source (V_{in}) and the AC output voltage as in Eq. (5.11).

$$v_{abc} = \frac{B}{\sqrt{3}} (V_{in} \cdot m_{abc}) \quad (5.11)$$

The voltage in the capacitor C_2 (V_{C2}) can be obtained from V_{in} , as shown in Eq. (5.12). In this configuration, this V_{C2} voltage also corresponds to the voltage of the BES (V_{BES}).

$$V_{BES} = V_{in} \cdot B \cdot D \quad (5.12)$$

The value of the controlled current source is obtained from the power balance principle ($P_{grid} - P_{dc} = P_{PV} + P_{BES}$) calculated in the PV side terminals.

$$P_{grid} = i_a \cdot v_a + i_b \cdot v_b + i_c \cdot v_c$$

$$P_{in} = V_{in} \cdot I_{in}$$

$$P_{BES} = V_{C2} \cdot I_{BES} = V_{BES} \cdot I_{BES}$$

$$P_{DC} = V_{C1} \cdot I_{C1} = P_{UC} \quad (5.13)$$

where P_{DC} is the power in V_{dc} , which comes from the UC and P_{in} is the PV power.

Substituting Eq. (5.11) in Eq. 5.13, derived from the PV terminals, Eq. 5.14 is then obtained. . Notethat the voltage in the BES is equivalent to $V_{in} B D$, .

$$P_{grid} = \frac{V_{in}}{\sqrt{3}} B \cdot (i_a \cdot m_a + i_b \cdot m_b + i_c \cdot m_c)$$

$$P_{in} = V_{in} \cdot I_{in}$$

$$P_{BES} = V_{in} \cdot B \cdot D \cdot I_{BES}$$

$$P_{DC} = V_{in} \cdot B \cdot (1-D) \cdot I_{C1} \quad (5.14)$$

Finally, if the power balance is carried out, the input current can be calculated.

$$I_{in} = \frac{B}{\sqrt{3}}(i_a \cdot m_a + i_b \cdot m_b + i_c \cdot m_c) - D \cdot B \cdot I_{BES} - B \cdot (1 - D) \cdot I_{C1} \quad (5.15)$$

where I_{in} is the current generated by the PV system (input current to the impedance network).

5.4. DC / DC Converter based on Z-Source

Fig. 5.3 illustrates the averaged model of the DC/DC ZSC used to connect the UC. This model consists of a controlled current source at the input and a controlled voltage source at the output, and it is based on the converter designed in [53].

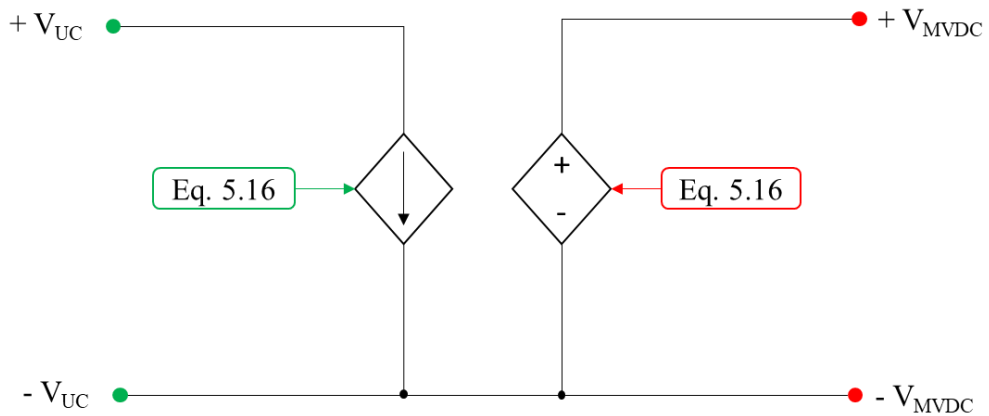


Fig. 5.3. Averaged model of the DC/DC ZSC

This converter reaches a high boost gain regulated with a duty cycle, making it more suitable and providing good control for power regulation. The voltage gain G of this converter is given by Eq. (5.16).

$$G = \frac{V_{out,zsc}}{V_{in,zsc}} = \frac{24.8 \cdot D_{UC} - 0.8569 \cdot D_{UC}^2}{0.0146 \cdot D_{UC} + 0.3919} \quad (5.16)$$

where D_{UC} is the shoot-through duty cycle in the DC/DC-ZSC. In the configuration of the charging station, $V_{out,ZSC}$ corresponds to V_{MVDC} while $V_{in,ZSC}$ is related to the voltage of the UC.

Finally, considering the power balance in the converter, the relation between the input and output current is obtained as follows.

$$G = \frac{I_{in}^{ZSC}}{I_{out}^{ZSC}} = \frac{V_{out}^{ZSC}}{V_{in}^{ZSC}} \quad (5.17)$$

5.5. Battery

The BES is connected in parallel with the capacitor C_2 of the qZSI and it acts as a secondary energy source supporting the intermittent PV generation. The MATLAB/SimPowerSystems® library [106] contains an electrochemical battery model based on a controlled voltage source in series with an equivalent internal resistance that was used in this study. This model calculates the battery instantaneous voltage (V_{BES}) as a function of several design parameters and the actual operating conditions of the device according to Eq. (5.18).

$$V_{BES} = E_{BES} - R_i \cdot i_{BES} \quad (5.18)$$

where E_{BES} is the open-circuit voltage, which depends on the charge or discharge of the device, R_i is the internal resistance of the battery, and i_{BES} is the instantaneous battery current.

Another important parameter of the BES is the state of charge (SOC), which needs to be controlled to avoid a deep discharge or an overcharge. The BES SOC can be obtained through Eq. 5.19:

$$SOC(\%) = SOC_0(\%) - 100 \left(\frac{\int I_{BES} \cdot dt}{Cap} \right) \quad (5.19)$$

where SOC_0 is the initial BES SOC state and Cap is the battery capacity (Ah).

The main advantage of the model is that the parameters can be obtained and adjusted from discharge curves of the manufacturer, or from experimental results of tests carried out on the battery. However, some assumptions need to be taken into account. In this sense, the internal resistance of the battery is considered constant during the charging and discharging

processes, the model does not include aging or temperature effects, and the self-discharge of the battery is not considered. Additionally, the parameters of the model are determined from discharge curves and assumed the same for the charge process.

A lead-acid battery is used in Cases 1, 2, and 3, associating in series and parallel to reach the appropriate voltage and capacity, obtaining a rated power of 18.75 kW, as shown in Table 5.2. This battery type presents a low cost, high reliability, and high efficiency [32]. Moreover, these batteries are suitable for energy management, which means that they can provide power for long periods, as presented in the literature review. This characteristic is an important advantage since only the battery is considered as ESS in Cases 1, 2, and 3.

In Case 4, in which the battery has the support of the UC, the technology chosen is the li-ion, due to reduced environmental impact in the disposal process when compared to the lead-acid. In addition, li-ion batteries have a good life-cycle, high efficiency, deep discharge depth, and fast charging capabilities [107]. The total power of the battery pack is 111 kW in this case, as shown in Table 5.2. The batteries are associated in series to reach the adequate output voltage of 370 V for the connection to the capacitor C_2 . Then, the batteries are connected in parallel to provide a nominal capacity of 300 Ah.

5.6. Ultra-capacitor

Like the BES, the UC model is also obtained from the MATLAB/SimPowerSystems library. This element consists of a generic UC model composed of a voltage source and an equivalent series resistance.

Ultracapacitors present a very fast response time (< 5 ms), high energy efficiency (85 – 98%), long life cycle (> 100.000 cycles), and high power density (500 – 5000 W/kg). Moreover, they can be charged and discharged quickly [108], being these characteristics very suitable for the proposed application, where the fast response of the UC will be required as discussed in the results section (Chapter 8).

The energy consumed/released by the UC bank is directly proportional to the capacitance and the change in the terminal voltage, as given by Eq. 5.20 [109]. A positive value of E_{UC} corresponds to an energy release in the UC, while it absorbs when E_{UC} is negative.

$$E_{UC} = \frac{1}{2} C (V_i^2 - V_f^2) \quad (5.20)$$

where C is the capacitance of the UC (F), V_i is the initial voltage before discharging starts (V), and V_f the final voltage after discharging ends.

The necessary voltage level can be obtained connecting multiple UC in series. The required capacitance can be obtained by the number of UCs connected in parallel. The total capacitance can be obtained through Eq. 5.21, and the internal resistance through Eq. 5.22.

$$C_{UC}^{total} = n_p \cdot \frac{C}{n_s} \quad (5.21)$$

$$r_{UC}^{total} = n_s \cdot \frac{ESR}{n_p} \quad (5.22)$$

where n_p is the number of UCs connected in parallel, n_s is the number of UCs connected in series and ESR is the equivalent series internal resistance (Ω).

Moreover, the UC SOC can be expressed as a function of the rated UC voltage (namely SOC_{UC} and V_{UC}^{rated} , respectively), as in Eq. (5.23) [110].

$$SOC_{UC} (\%) = 100 \cdot \frac{V_{UC}}{V_{UC}^{rated}} \quad (5.23)$$

Some assumptions need to be taken into account regarding this UC model. The most relevant are the following: the internal resistance of the UC is constant during the charging and discharging processes, the model does not include aging or temperature effects, and the current through the UC is assumed continuous.

In this work, the UC chosen was an association of the model BMOD0008 E160 B02, from the manufacturer Maxwell Technologies [102]. The UC bank is connected to the DC/DC – ZSC, as shown in the system configuration in Fig. 5.1.

5.7. LCL Filter

Filters are used to reduce the harmonic components generated during the conversion process. The three most commonly used passive filters are the L, LC, and LCL filters [111]. L and LC filters are used in low power applications, while LCL filters are usually preferred in large-scale applications, especially due to their higher harmonic attenuation and their suitability for renewable energy applications [111].

To size the filter, the base impedance Z_b and capacitance C_b are determined first.

$$Z_b = \frac{V_0^2}{P_0} \quad (5.24)$$

$$C_b = \frac{1}{Z_b \omega_n} \quad (5.25)$$

where ω_n is the grid angular frequency, V_0 is the nominal line voltage and P_0 the nominal inverter power.

To reach acceptable values for the filter, the following criteria have to be followed: 1) The inductor impedance X_{LI} must be lower than 10% of the base impedance to limit the voltage drop; 2) The capacitance C_f is limited to absorb less than 5% of the rated reactive power of the converter; 3) To avoid resonance problems, the resonant frequency f_{res} must remain between ten times the grid frequency and half of the switching frequency [112]. The resonant frequency can be obtained through (5.26):

$$f_{res} = \frac{1}{2\pi} \sqrt{\frac{L_{1f} + L_{2f}}{L_{1f} L_{2f} C_f}} \quad (5.26)$$

To calculate the inductor on the converter side L_{1f} , a maximum percentage of the allowable current ripple ΔI_{LI} (%) must be defined. With the inverter power P_0 and the nominal line voltage V_0 , the maximum tolerable current ripple ΔI_{LI} is given by:

$$\Delta I_{L1f} = \Delta I_{L1f} (\%) \cdot \sqrt{2} \cdot \left(\frac{P_0}{3 \cdot \frac{V_0}{\sqrt{3}}} \right) \quad (5.27)$$

where $\Delta I_{Ll} = I_{max} - I_{min}$.

The value of L_{1f} is then obtained through [113]:

$$L_{1f} = \frac{V_0}{2 \cdot \sqrt{6} \cdot f_s \cdot \Delta I_{L1f}} \quad (5.28)$$

The percentage of the impedance X_{L1f} in relation to Z_b is given as follows:

$$\% X_{L1f} = \frac{2 \cdot \pi \cdot f_r \cdot L_{1f}}{Z_b} \quad (5.29)$$

If this percentage is higher than 10%, a lower value should be chosen for ΔI_{L1f} (%) and ΔI_{L1f} should be recalculated. A value of 12% was considered for ΔI_{L1f} in this work.

For the calculation of the filter capacitor C_f , the reactive power absorbed by the filter under nominal operating conditions is taken into account. Thus, C_f is given by [112]:

$$C_f = X_f \cdot C_b \quad (5.30)$$

where X_f represents the percentage of reactive power absorbed, set to 5% in this work. The grid side inductance L_{2f} is calculated according to [112]:

$$L_{2f} = r \cdot L_{1f} \quad (5.31)$$

where r represents the ratio between inductances L_{2f} and L_{1f} , and it can be obtained through:

$$\frac{I_{2(h)}}{I_{1(h)}} = \frac{1}{|1 + r(1 - C_b L_{1f} \omega_s^2 X_f)|} \quad (5.32)$$

where $I_{1(h)}$ and $I_{2(h)}$ are the harmonic currents of the converter at the switching frequency f_s . It was suggested in [112] that this relation should be less than 20%.

If the resonant frequency is not satisfied, a damping resistance R_d can be added in series with C_f [114]. The value of this resistance can be calculated through (5.33):

$$R_d = \frac{1}{6\pi f_{res} C_f} \quad (5.33)$$

5.8. System parameters considered in the simulation cases

After showing the mathematical modeling of the system components, the values of the main parameters are listed herein. The same general configuration (PV, qZSI-BES, filter, and grid) was considered for all the simulated cases. There is a single variation corresponding to Case 4, where a DC/DC-ZSC and an UC are added to the system. Hence, different parameters were considered throughout the study, with an initial situation of low voltage in the DC side (LVDC) in Cases 1 and 2, evolving to MVDC in Cases 3 and 4.

The same system parameters were considered for Cases 1 and 2, presented in Section 8.1 and 8.2, respectively. These are given in Table 5.1:

TABLE 5.1. SYSTEM PARAMETERS FOR CASES 1 AND 2

Parameter	Value
PV panels	$P_{pv \text{ rated}}$ 172 kW
	$V_{pv \text{ rated}}$ 515 V
Battery	Capacity 50 Ah
	$V_{BES \text{ rated}}$ 375 V
qZSI	$P_{qZSI \text{ rated}}$ 190 kW
	$V_{DC \text{ rated}}$ 900 V
	L_1, L_2 79.5 μ H
	C_1, C_2 2200 μ F
AC filter	L_{1f} 230 μ H
	L_{2f} 8.6 μ H
	C_f 175 μ F
Transformer	$V_{nom \text{ prim}}$ 465 V
	$V_{nom \text{ sec}}$ 25 kV
	L_{prim}, L_{sec} 230 μ H
	R_{prim}, R_{sec} 23 m Ω
	L_{mag} 1 H
	R_{mag} 377 Ω
	Connection Y/ Δ
Grid	f_{rated} 60 Hz
	$V_{grid \text{ rated}}$ 25 kV

The parameters considered for Cases 3 and 4 are given in Table 5.2:

TABLE 5.2. SYSTEM PARAMETERS FOR CASES 3 AND 4

Parameter	Value
PV panels	$P_{pv \text{ rated}}$ 374 kW
	$V_{pv \text{ rated}}$ 1031 V
Battery	Capacity 300 Ah
	$V_{BES \text{ rated}}$ 370 V
Ultra-capacitor	$V_{UC \text{ rated}}$ 550 V
	$V_{UC \text{ initial}}$ 350 V
	Capacitance 13 F
AC filter	L_{1f} 472 nH
	L_{2f} 17,6 nH
	C_f 86 nF
Grid	f_{rated} 60 Hz
	$V_{\text{grid rated}}$ 930 V

Chapter 6

Control Strategy

The overall control strategy is presented in Fig. 6.1. The maximum power extraction from the PV system, the active/reactive power, and the battery/UC power control loops are shown in this figure. For the detailed model, an impedance-space-vector modulation technique (ZSVM) is applied. Therefore, the modulation index and the shoot-through duty cycle (namely M and D) are the terms that control the power flows in the system. In the configuration with an added UC, an additional duty cycle (D_{UC}) is provided by the UC control loop, which regulates the gain of the DC/DC-ZSC converter.

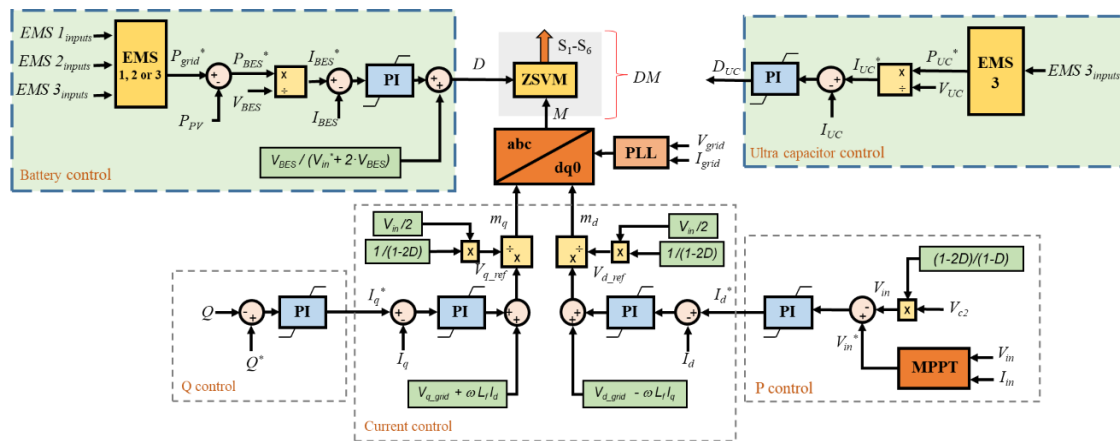


Fig. 6.1. Overall system control

It is worth mentioning that in EMS 3, the battery reference power (P_{BES}^*) is obtained at the output of the EMS. Hence, the step of subtracting the grid reference power (P_{grid}^*) to P_{PV} does not exist.

The EMS inputs are described in detail in Chapter 8, but they are also briefly introduced here for a basic comprehension of the BES and UC control loops. The EMS 1 inputs are the P_{PV} , the battery SOC, the power demanded by the system operator (P_{SO}), the reactive power demanded by the system operator (Q_{SO}) and the energy price. The EMS 2 inputs are the battery SOC, the energy price, and the P_{PV} . The EMS 3 inputs are the battery

SOC, the UC SOC, the primary power of BES (P_{BES}^{Prim}), and the primary power of the UC (P_{UC}^{Prim}).

6.1. MPPT

An MPPT strategy is necessary to benefit from the maximum solar radiance received by the PV modules. In the proposed configuration, a perturb and observe (P&O) algorithm was used, where the value of the maximum voltage is continuously tracked. The MPPT algorithm provides the reference voltage at the output of the PV panels (V_{in}^*), which is then compared with the voltage measured at the panels (V_{in}) in the active power control loop.

6.2. Z-Space Vector Modulation

The ZSVM technique is only applied for the DM, since there are no power switches in the SM of the ZSC, as they are represented by controlled current and voltage sources that do not require a gate signal.

The main objective of the modulation techniques is to provide a minimum harmonic distortion and maximum fundamental component in the output. Many control strategies based on pulse width modulation (PWM) have been used for the control of the duty ratio. Typical modulation techniques applied to the qZSI are the simple boost control (SBC) [115], the maximum boost control (MBC) [116], the maximum constant boost control (MCBC) [117], and the ZSVM. According to the switching pattern, several options appear for the latter, such as ZSVM6, ZSVM4, ZSVM2, and ZSVM1. These ZSVM techniques are described in detail in [61].

Fig. 6.2 illustrates the relationship between the ZSVM technique and the conventional sinusoidal PWM (SPWM), which includes the SBC, MBC, and MCBC algorithms. The smallest ON circle (SPWM) allows a maximum magnitude of the output voltage of $V_{dc}/2$, achieved with a maximum modulation index of 78.55%. The OM circle (ZSVM) has a ratio equal to $V_{dc}/\sqrt{3}$, achieving a higher modulation index of 90.7% [118].

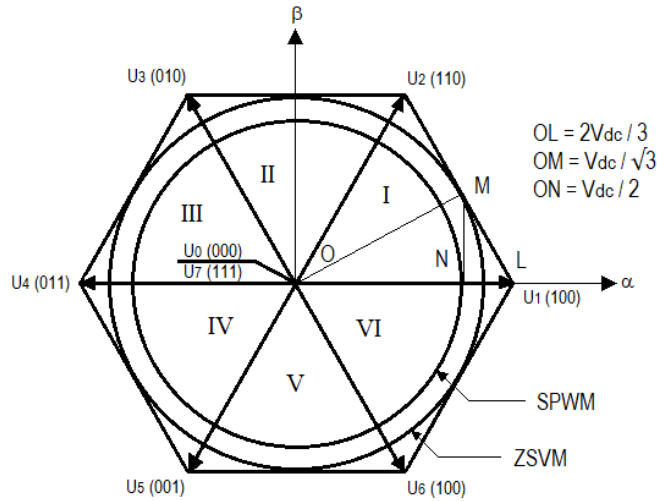


Fig. 6.2. Comparison between SPWM and ZSVM

In this work, ZSVM6 is applied due to two main advantages over other techniques, such as a higher voltage gain, and lower voltage stress for the same voltage gain [61].

To implement the ZSVM algorithm, an abc to $\alpha\beta$ reference frame transformation is necessary. Thus, eight space vectors are obtained, named U_0 to U_7 . U_0 and U_7 are the zero vectors, while U_1 to U_6 are the active vectors.

The traditional SVM applied to three-phase VSI has six active states and two zero states, generating eight space vectors that create six possible sectors as shown in Fig. 6.2. When the SVM is applied to qZSI, one additional state, named the shoot-through state, is added. According to [61], the ZSVM algorithm can be implemented through Eq. 6.1, where U_{ref} is the reference for the voltage at the AC output of the qZSI, T_1 is the time of application of the active vector U_1 , T_2 is the time of application of U_2 , T_s is the sample time of the ZSVM, T_{sh} is the shoot-through time ($T_{sh} = D \cdot T_s$), M is the modulation index given by $M = \sqrt{3}U_{ref}/V_{dc}$, θ is the angle between U_{ref} and U_1 , i represents the sector (from 1 to 6) and V_{sh} is the shoot-through voltage vector.

$$\begin{aligned}
 T_1 &= T_s M \sin \left[\frac{\pi}{3} - \theta + \frac{\pi}{3}(i-1) \right] \\
 T_2 &= T_s M \sin \left[\theta - \frac{\pi}{3}(i-1) \right] \\
 T_s &= T_0 + T_1 + T_2 + T_{sh}
 \end{aligned} \tag{6.1}$$

$$U_{ref} = U_1 \frac{T_1}{T_s} + U_2 \frac{T_2}{T_s} + U_0 \frac{T_0}{T_s} + V_{sh} \frac{T_{sh}}{T_s}$$

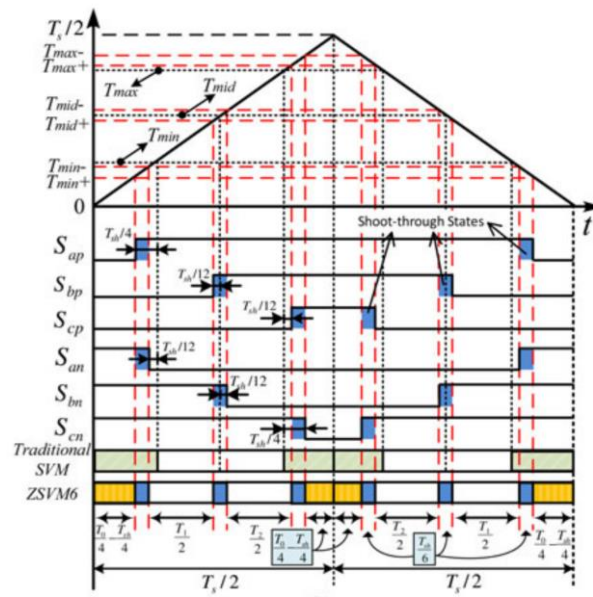
Fig. 6.3 shows all the switching time sequences, referring to sector 1 modified from the traditional SVM for ZSVM6. The switching times for the three legs of the bridge, T_{max} , T_{mid} , and T_{min} are the maximum, medium, and minimum times, and are described in Eq.6.2.

$$\begin{cases} T_{min} = \frac{T_0}{4} \\ T_{mid} = \frac{T_0}{4} + \frac{T_1}{2} \\ T_{min} = \frac{T_s}{2} - \frac{T_0}{4} \end{cases} \quad (6.2)$$

In the ZSVM, in addition to T_1 and T_2 , it is necessary to calculate the intermediate times. These times occur during the shoot-through periods, and, for the ZSVM6 technique implemented herein, the switching times are calculated by [119]:

$$\begin{cases} T_{max+} = T_{max} + \frac{T_{sh}}{12} \\ T_{max-} = T_{max} + \frac{T_{sh}}{4} \\ T_{min+} = T_{min} - \frac{T_{sh}}{4} \\ T_{min-} = T_{min} - \frac{T_{sh}}{12} \end{cases} \begin{cases} T_{mid+} = T_{mid} - \frac{T_{sh}}{12} \\ T_{mid-} = T_{mid} + \frac{T_{sh}}{12} \end{cases} \quad (6.3)$$

To summarize, the algorithm implemented initially identifies the sectors through the angle theta. Then, all the times are calculated, and finally, the trigger signals for all sectors with the switching states described in Fig. 6.3 are generated. A complete list of the switching states applied to the converter with ZSVM6 can be seen in Fig. 6.3b.



(a)

■ = STS

Sector 1

S_1, S_3, S_5	000	100	100	110	110	111	111
S_2, S_4, S_6	111	111	011	011	001	001	000
	0	T_{min+}	T_{min-}	T_{mid+}	T_{mid-}	T_{max+}	T_{max-}

Sector 2

S_1, S_3, S_5	000	010	010	110	110	111	111
S_2, S_4, S_6	111	111	101	101	001	001	000
	0	T_{min+}	T_{min-}	T_{mid+}	T_{mid-}	T_{max+}	T_{max-}

Sector 3

S_1, S_3, S_5	000	010	010	011	011	111	111
S_2, S_4, S_6	111	111	101	101	100	100	000
	0	T_{min+}	T_{min-}	T_{mid+}	T_{mid-}	T_{max+}	T_{max-}

Sector 4

S_1, S_3, S_5	000	001	001	011	011	111	111
S_2, S_4, S_6	111	111	110	110	100	100	000
	0	T_{min+}	T_{min-}	T_{mid+}	T_{mid-}	T_{max+}	T_{max-}

Sector 5

S_1, S_3, S_5	000	001	001	101	101	111	111
S_2, S_4, S_6	111	111	110	110	010	010	000
	0	T_{min+}	T_{min-}	T_{mid+}	T_{mid-}	T_{max+}	T_{max-}

Sector 6

S_1, S_3, S_5	000	100	100	101	101	111	111
S_2, S_4, S_6	111	111	011	011	010	010	000
	0	T_{min+}	T_{min-}	T_{mid+}	T_{mid-}	T_{max+}	T_{max-}

(b)

Fig. 6.3. (a) Switching time sequences in ZSVM6, (b) Complete switching states in the six sectors for ZSVM6

6.3. Battery and Ultra-Capacitor

The active power reference for the battery P_{BES}^* is provided by the EMS. This value is then divided by the measured battery voltage V_{BES} to obtain the current reference I_{BES}^* , as illustrated in Fig. 6.1. Due to technical constraints of the device, the battery current must remain between maximum and minimum values. The deviation between the actual and the desired battery current is inputted to a PI controller that generates ΔD as an output. Finally, D is computed by adding D_0 to ΔD . D_0 is obtained through Eq. 6.4, where V_{BES}^{nom} is the nominal voltage of the BES, and V_{in}^* is the input voltage of the qZSI at standard conditions of the PV system. Note that D_0 is constant. In the detailed model, D is inputted to the ZSVM algorithm to implement the shoot-through states in the converter. On the other hand, the simplified model requires the calculation of the battery voltage V_{BES}^* for the controlled voltage source that represents the battery in the averaged model of the converter. This voltage is calculated through Eq. 5.12, as shown in Section 5.3, and this is the equation implemented at the upper part of Fig. 5.2.

$$D_0 = V_{BES}^{nom} / (2 \cdot V_{BES}^{nom} + V_{in}^{std}) \quad (6.4)$$

The UC control is very similar to the BES, as it can be observed in Fig. 6.1, in which a reference UC power (P_{UC}^*) is outputted from the EMS, then divided by the UC voltage (V_{UC}), and the reference current (I_{UC}^*) is obtained and controlled with a PI regulator. The PI output is the duty cycle used in the DC/DC – ZSC, called D_{UC} , used to calculate the gain of the converter in Eq. 5.13.

6.4. Active and Reactive Power

As in a VSI, in the proposed control scheme, the qZSI is responsible for controlling the active and reactive power through M . For this reason, a dq reference frame oriented along the grid voltage is used to decouple active and reactive power control. Two cascaded control loops are used to control these powers [120], as shown in Fig. 6.1.

The outer control loops are dedicated to active and reactive power regulation, which can be calculated using Eq. 6.5 in the dq reference frame. It can be seen that controlling the

d and q components of the grid current ($I_{d,grid}$ and $I_{q,grid}$) is equivalent to controlling P_{grid} and Q_{grid} , respectively, because $V_{d,grid}$ is constant in a robust grid [44].

$$P_{grid} = \frac{3}{2} V_{d,grid} I_{d,grid}$$

$$Q_{grid} = \frac{3}{2} V_{d,grid} I_{q,grid}$$
(6.5)

The reference values for these currents (I_d^* and I_q^*) are generated by the outer control loops through PI controllers, one controlling active power indirectly through V_{in} , and the other one controlling reactive power. The reactive power reference is imposed externally, whereas the active power depends on the power extracted from the PV panels. In this sense, the MPPT controller defines the optimum DC input voltage for the qZSI (V_{in}^*) that allows maximum power generation in the PV system.

The inner loops are the current control loops, where two PI controllers regulate $I_{d,grid}$ and $I_{q,grid}$ to follow the reference values provided by the outer control loops. These PI controllers generate the compensation terms (V_d and V_q). With the contribution of the decoupling terms shown in Eq. 6.6, independent control of $I_{d,grid}$ and $I_{q,grid}$, and thus, active and reactive power, can be achieved through the d and q components of the modulating signal (namely m_d and m_q) [120].

$$m_d = \frac{\sqrt{3}}{V_{DC}} (V_d - L_f \omega I_{q,grid} + V_{d,grid})$$

$$m_q = \frac{\sqrt{3}}{V_{DC}} (V_q + L_f \omega I_{d,grid} + V_{q,grid})$$
(6.6)

where u_d and u_q are the dq components of the qZSI output voltage, L_f is the inductance from the qZSI output to the grid connection, and ω_0 is the electric angular frequency.

Once m_d and m_q are defined, they are transformed into m_a , m_b , and m_c through an abc to dq transformation to generate the switching pulses of the qZSI according to the ZSVM6 technique. A phase-locked loop (PLL) ensures the tracking of the grid voltage frequency [103]. The value of M can be obtained by m_d and m_q , through Eq. 6.7.

$$M = \sqrt{m_d^2 + m_q^2} \quad (6.7)$$

The control strategy for the SM is the same as for the DM, except for the absence of the ZSVM in the former.

Chapter 7

Energy Management System

In this section, three different EMS control strategies are presented, being each of them applied to a specific case study presented in Chapter 8.

7.1. Strategy considering one storage system (EMS 1)

The present strategy was applied to Cases 1 and 2, described in sections 8.1 and 8.2, and will be referred to as EMS 1 for nomenclature simplification.

This section describes the EMS implemented to control the power flow between the energy sources, i.e. the PV system and the battery, and the grid (namely P_{PV} , P_{BES} and P_{grid} , respectively). A flowchart of the proposed EMS is shown in Fig. 7.1.

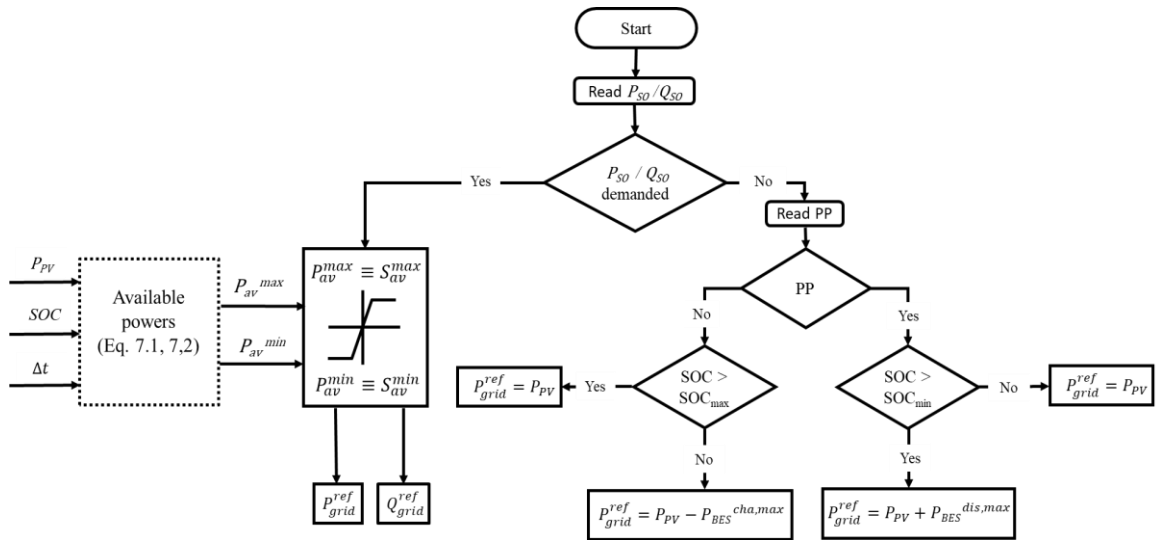


Fig. 7.1. The control scheme for the EMS 1

In the first stage, the EMS waits for instructions of the system operator (SO). The top priority of the EMS 1 is to comply with the active and reactive power requirements of the

SO (P_{SO} and Q_{SO}) as long as they remain between certain boundaries. If the SO does not set any operating instructions, then the system is operated to make an economic profit of the energy stored. These two possibilities are described in detail below.

To fulfill the SO requirements, P_{SO} must remain between the maximum and minimum available power (P_{av}^{max} and P_{av}^{min}) given by Eqs. (7.1) and (7.2) respectively. These boundaries are defined based on the maximum charge and discharge power of the battery ($P_{BES}^{ch,max}$ and $P_{BES}^{dis,max}$, respectively) according to Eqs. (7.3) and (7.4), which are computed considering the maximum and minimum SOC advised for the battery [121]. In this work, $SOC_{max} = 90\%$ and $SOC_{min} = 30\%$. This scheme protects the battery against overcharge and deep discharge. Additionally, the reactive power command Q_{SO} is limited by P_{SO} and the rated power of the converter. If both P_{SO} and Q_{SO} are set within the aforementioned limits, they become the active and reactive power references for the EMS ($P_{grid}^{ref} = P_{SO}$ and $Q_{grid}^{ref} = Q_{SO}$). Therefore, the SO must be informed of P_{av}^{max} and P_{av}^{min} to make a sensible selection of P_{SO} and Q_{SO} .

$$P_{av}^{max} = P_{PV} + P_{BES}^{dis,max} \quad (7.1)$$

$$P_{av}^{min} = P_{PV} - P_{BES}^{ch,max} \quad (7.2)$$

$$P_{BES}^{dis,max} = \min \left(P_{BES}^{max}, \frac{E_{BES}}{\Delta t} \left(\frac{SOC - SOC_{min}}{100} \right) \right) \quad (7.3)$$

$$P_{BES}^{ch,max} = \min \left(P_{BES}^{max}, \frac{E_{BES}}{\Delta t} \left(\frac{SOC_{max} - SOC}{100} \right) \right) \quad (7.4)$$

where E_{BES} is the nominal energy of the battery, Δt is the time interval of the demanded energy, and P_{BES}^{max} is the maximum power of the battery.

When no specific command is received from the SO, the battery is operated under economic profitability criteria. Because this paper does not focus on the detailed regulation of power generation in a complex electricity market, the EMS only discerns between valley periods (VP) and peak periods (PP). Nonetheless, the battery SOC limits still apply on this situation. In this sense, the EMS will charge the battery with $P_{BES}^{ch,max}$ during VP only if $SOC < SOC_{max}$. On the other hand, the EMS will discharge the battery with $P_{BES}^{dis,max}$ during PP if $SOC > SOC_{min}$. Storing energy in VP and releasing during PP increases the monetary profit of the hybrid system. However, if any of the SOC limits are reached either in VP or PP, the battery stops charging/discharging and only the PV generation is delivered to the grid ($P_{grid}^{ref} = P_{PV}$).

In the EMS proposed, P_{PV} , SOC , P_{SO} , Q_{SO} are used as inputs. Additionally, a binary variable PP is used to discriminate between PP (PP = 1) and VP (PP = 0) in the electricity market. Finally, P_{grid}^{ref} and Q_{grid}^{ref} are outputted from the EMS in any of the two scenarios considered: 1) SO command following; or 2) economic dispatch of the stored energy.

7.2. Strategy considering one storage system applying fuzzy logic control (EMS 2)

This strategy, named EMS 2, was applied to Case 3 presented in Chapter 8.3.

Fuzzy logic control (FLC) is a suitable control technique to perform the energy management of hybrid systems [122], presenting a wide range for operating conditions and a smooth response.

The EMS implemented in this section is responsible for defining the reference power to be stored in or provided by the battery (P_{BES}^*), taking into account the P_{PV} , the battery SOC, and the grid energy price, being these parameters the inputs to the FLC, as shown in Fig. 7.2. The EMS output and its posterior control are presented in Section 6.3.

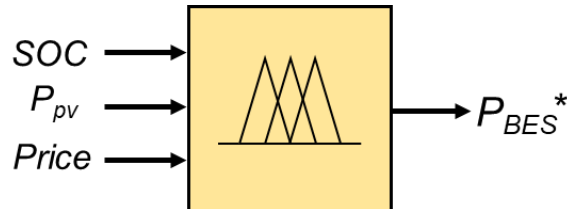


Fig. 7.2. EMS 2 inputs and outputs

The ranges of the inputs and the membership functions for the FLC with Mamdani rule-based structure are described below.

Four membership functions are used for P_{PV} , as shown in Fig. 7.3a. This power ranges from 0 to 374 kW depending on the solar irradiance, and the membership functions are structured as follows: 1) Low (L) membership function for P_{PV} between 0 and 100 kW; 2) Medium (M) for P_{PV} between 60-220 kW; 3) High (H) for P_{PV} between 180-320 kW; and 4) Very high (VH) for P_{PV} from 280 kW up to the maximum value.

For the battery SOC, three membership functions are used (Fig. 7.3b): 1) Low (L): SOC from 0 to 30%; 2) Medium (M) from 20 to 90%; and 3) High (H) from 80% to 100%. The SOC is an important parameter to guarantee an appropriate battery usage, avoid overcharging/overdischarging, and increase the battery lifetime. If the SOC is L, the battery is not allowed to discharge more, and if the SOC is H, the battery is not charged more. However, if the SOC is medium, the battery can be charged or discharged.

Fig. 7.4 shows the grid energy price obtained from the day-ahead hourly energy price in Spain (April 20th 2021) [123] and adapted for a 30s simulation. In this case, three membership functions were considered (Fig. 7.3c): Unfavorable (U), Normal (N), and Favorable (F). U means that the energy market has a low price to sell energy and it is better to store energy in the batteries, if allowed by the battery SOC. In this situation, the price varies from 66 EUR/MWh to 75 EUR/MWh. In N, the price varies from 71 EUR/MWh to 89 EUR/MWh, and in this case, the battery can store or release energy depending on the SOC.

The energy price is high in F (over 85 EUR/MWh), and thus, it is better to discharge the battery to make an economic profit, if the SOC is M or H.

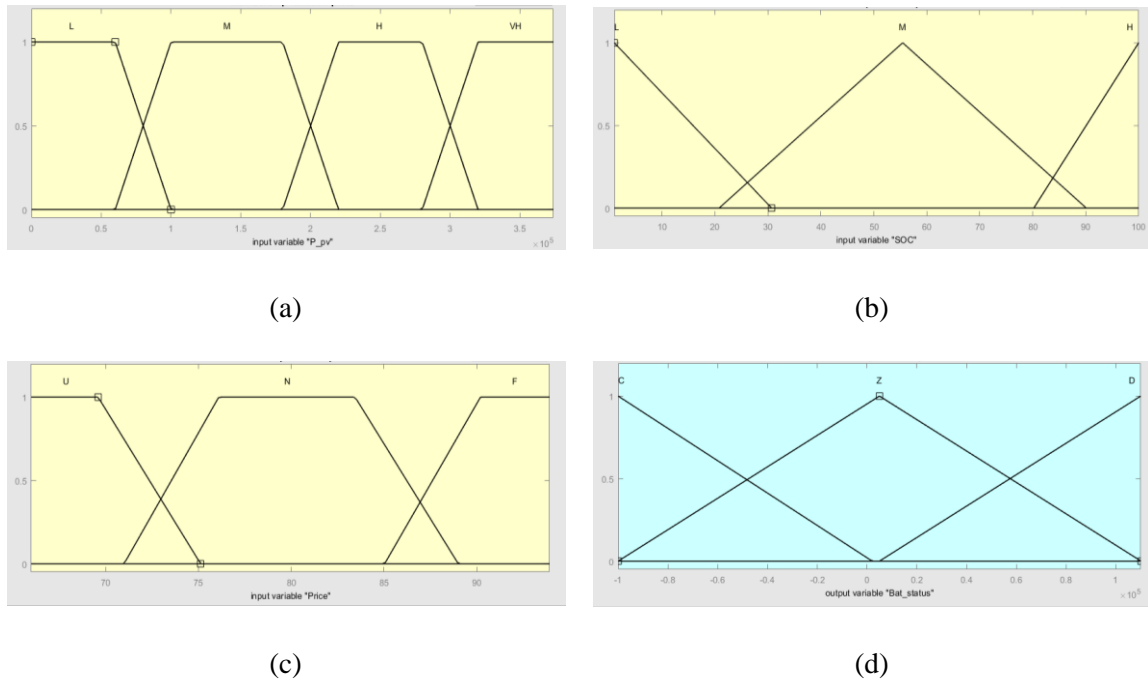


Fig. 7.3. Membership functions of the EMS 2 based on fuzzy logic for: (a) PV power (input), (b) SOC (input), (c) Price (input), and (d) Battery reference power (output).

The membership functions for the output P_{BES}^* are shown in Fig. 7.3d, which are defined as battery charge (C), discharge (D), and zero (Z), when the battery is not charging nor discharging. Table 7.1 shows the rule list for the proposed FLC. These rules illustrate the membership functions for C and D. In any other case not shown in Table 7.1, the output is Z.

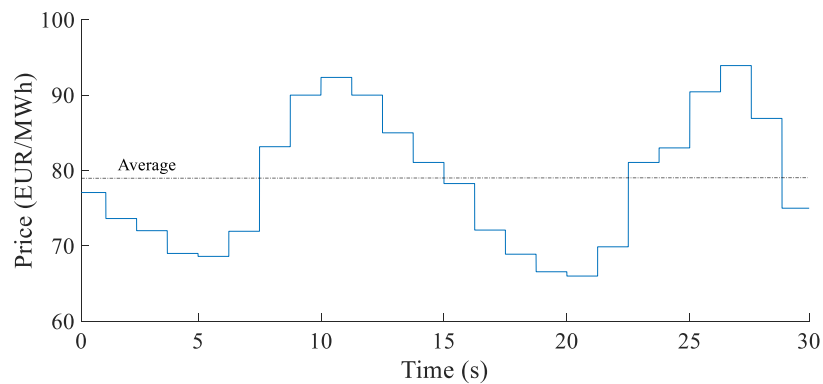


Fig 7.4. day-ahead hourly energy price in Spain (April 20th, 2021).

TABLE 7.1. RULE LIST OF THE FUZZY LOGIC CONTROLLER FOR EMS 2

P_{pv}	Inputs		Output
	SOC	Price	P_b^*
VH	L	U	C
VH	L	N	C
VH	M	U	C
VH	M	N	C
VH	M	F	D
VH	H	F	D
H	L	U	C
H	L	N	C
H	M	U	C
H	M	N	C
H	M	F	D
H	H	N	D
H	H	F	D
M	L	U	C
M	L	N	C
M	M	U	C
M	M	N	C
M	M	F	D
M	H	F	D
L	M	F	D
L	H	N	D
L	H	F	D

7.3. Strategy considering two storage systems and fuzzy logic control (EMS 3)

This strategy was applied to Case 4, presented in chapter 8.4, and it is referred to as EMS 3.

In the system configuration where EMS 3 is considered, an UC and a BES are combined. Hence, the EMS must be capable of managing the energy flow between various sources, i.e.: the HESS, the PV panels, and the grid. In this topology, the HESS is contributes reducing the power fluctuations of the PV generation. Specifically, the HESS compensates when the PV output power is lower than the power demanded by the system operator (P_{SO}). In contrast, the HESS stores the excess power when the PV plant generates more than the power requested by the SO. Therefore, the main objective of EMS 3 relies on obtaining the

power references for the BES and UC, benefiting from the inherited characteristic of each storage system, while maintaining safe SOC levels.

The UC presents fast response and low energy density, whereas the BES presents slow dynamics and high energy density. Considering the mentioned characteristics, the BES is responsible for handling the difference between the power demanded by the SO and the PV power generation.

The UC has three main functions: (i) Compensate the BES slow response; (ii) compensate small PV power variations; and (iii) complement a surplus power demand if the BES is operating at its limit. These three operating conditions are detailed below.

The UC will compensate the slow response of the BES, absorbing or delivering the necessary power during the transient states. This situation occurs due to the non-instantaneous response of the battery under quick power variations, similarly to the strategy proposed in [110]. Fig. 7.5 illustrates the idea behind this concept regarding the BES response and the UC compensation. In the second situation, the UC is responsible for covering low power requirements, such as small PV power variations due to partial shading from clouds, for instance. With this strategy, it is expected that the UC contributes to extend the life-cycle of the BES. With regards to the third strategy, the UC will support the BES power when necessary, for example, when the BES has low SOC.

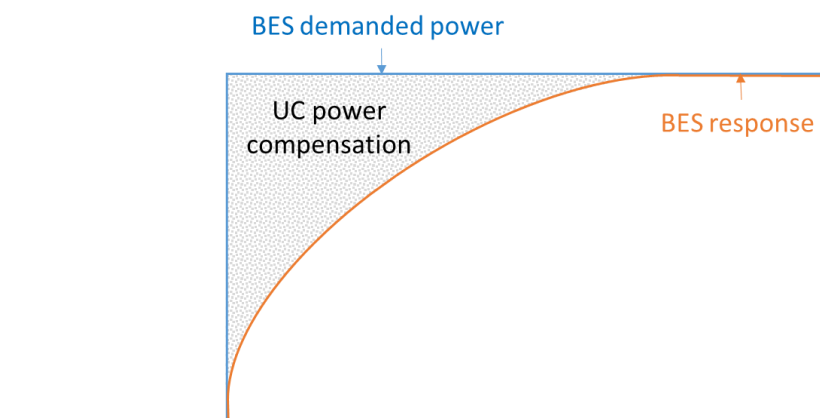


Fig. 7.5. UC power compensation to BES slow response

The EMS 3 has as inputs the SOC_{BES} , the state of charge of the UC (SOC_{UC}), an added term called the primary power of BES (P_{BES}^{Prim}), and another new term called primary power of UC (P_{UC}^{Prim}), being the last two calculated from Eq. 7.5 and 7.6. The P_{UC}^{Prim} is the power that the battery is not able to supply due to its slow response and the UC has to compensate, being P_{BES}^{res} the battery power response. The P_{BES}^{Prim} is the difference between the power demanded by the SO and the PV power generation. If P_{BES}^{Prim} is positive, then $P_{SO} > P_{PV}$ and the battery will be discharged. Contrarily, if $P_{PV} > P_{SO}$, the battery will be charged. It is noteworthy that the input constraint for the SO power demand is that P_{SO} must remain between the maximum and minimum available power (P_{av}^{max} and P_{av}^{min}) given by Eqs. 7.1 and 7.2, respectively, as in EMS 1, Section 7.1.

$$P_{BES}^{Prim} = P_{SO} - P_{PV} \quad (7.5)$$

$$P_{UC}^{Prim} = P_{BES}^{Prim} - P_{BES}^{res} \quad (7.6)$$

The EMS 3 output is given by a complementary power, called P_{compl} , which represents the power exchanged between the BES and the UC. Since the addition of a UC breaks the power balance, the BES absorbs/releases energy to recover the balance. In this sense, P_{compl} is subtracted from P_{BES}^{Prim} and added to P_{UC}^{Prim} . A positive P_{compl} , indicates that the UC is supporting the BES, while a negative value means that the BES is supporting the UC.

During the EMS execution process, the SOC of both storage systems are regulated between safe levels, that is $SOC_{min} < SOC_{BES/UC} < SOC_{max}$, being $SOC_{min} = 30\%$ and $SOC_{max} = 90\%$.

The EMS 3 structure is presented in Fig. 7.6.

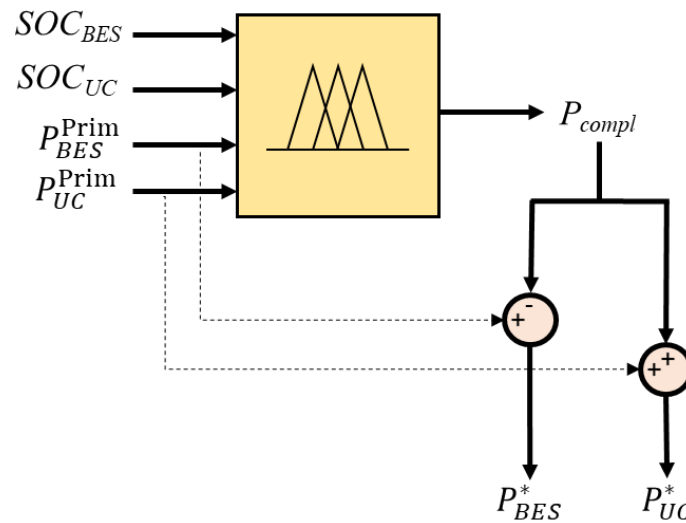


Fig. 7.6. EMS 3 inputs and outputs

A FLC was implemented as a strategy to obtain the EMS desired outputs. In [110], a FLC technique proved its superior performance in comparison to other EMS strategies that do not apply this technique. A prerequisite to implement the FLC is the definition of the member functions (MF) and the rules.

The MF for the BES and UC SOC have three possible levels: Low (L), medium (M), and high (H), varying from 0 to 1. The L level goes from 0 to 0.3, representing the SOC_{min} . The M goes from 0.2 to 0.9, and the H ranges from 0.8 to 1, representing the SOC_{max} .

The P_{BES}^{Prim} and P_{UC}^{Prim} MF have been classified in four possible states: Intense charge (IC), soft charge (SC), soft discharge (SD), and intense discharge (ID). In the intense charge state, the storage unit (BES or UC) receives a large amount of power and the SOC varies intensely. The intense discharge follows the same argument, but in this case, the storage unit releases power. In the soft charge/discharge MF, the BES and/or the UC absorb/release a low amount of power and SOC level will vary softly.

The power exchange between the storage sources, P_{compl} , outputted from the FLC has five possible symmetrical states: Zero (Z), positive small (PS), positive big (PB), negative small (NS), and negative big (NB). In the Z state, no power exchange is needed between the sources, whereas in the positive states the UC charges to support the BES with more (PB) or less (PS) intensity, and vice versa with the negative states. In Fig. 7.7 the MF of the inputs and output of the FLC are presented.

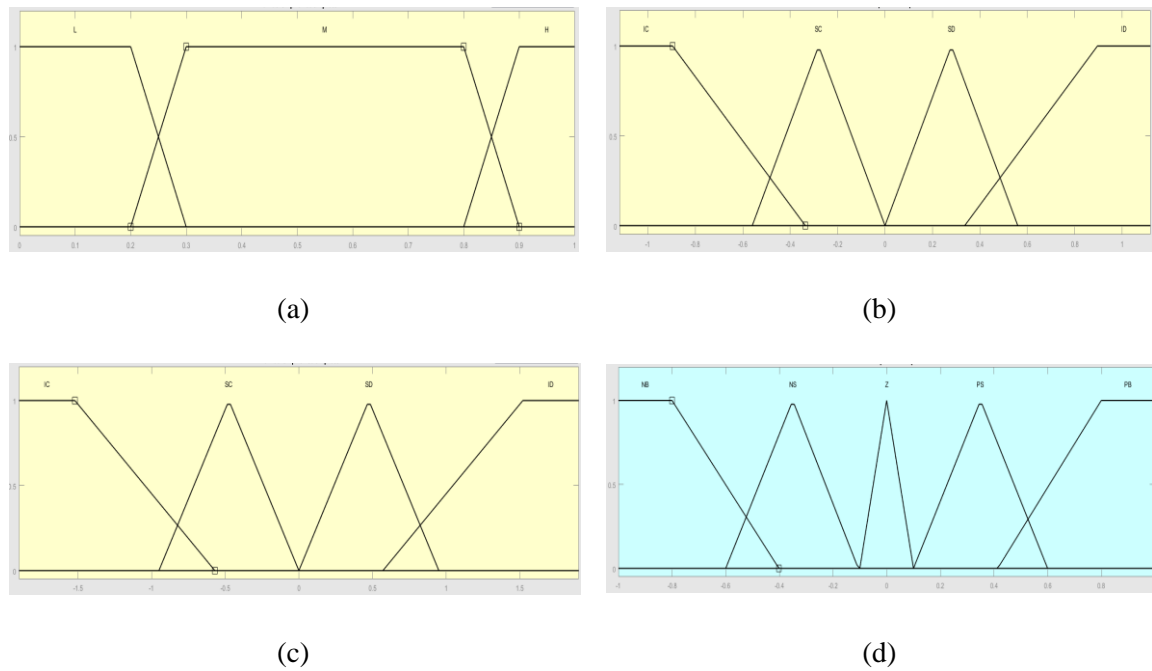


Fig. 7.7. Membership functions of the EMS 3 based on fuzzy logic control for: (a) Battery and UC state of charge (input). (b) Primary battery power (input). (c) Primary UC power (input). (d) Power complementary (output).

The FLC rules are presented in Table 7.2. A total of 144 rules were needed in order to cover all the MF possible states. In the literature, other studies have applied the same number of rules for hybrid renewable applications [124], [125], achieving enough precision and without strong fluctuations at the output.

TABLE 7.2. RULES OF THE FUZZY LOGIC CONTROLLER FOR EMS 3

<i>SOC_{BES} is L</i>				<i>SOC_{BES} is M</i>				<i>SOC_{BES} is H</i>			
Inputs			Output	Inputs			Output	Inputs			Output
<i>SOC_{SC}</i>	<i>P_{BES}^{Prim}</i>	<i>P_{UC}^{Prim}</i>	<i>P_{compl}</i>	<i>SOC_{SC}</i>	<i>P_{BES}^{Prim}</i>	<i>P_{UC}^{Prim}</i>	<i>P_{compl}</i>	<i>SOC_{SC}</i>	<i>P_{BES}^{Prim}</i>	<i>P_{UC}^{Prim}</i>	<i>P_{compl}</i>
L	IC	IC	Z	L	IC	IC	NB	L	IC	IC	NB
L	IC	SC	Z	L	IC	SC	NB	L	IC	SC	NB
L	IC	SD	NS	L	IC	SD	NB	L	IC	SD	NB
L	IC	ID	NS	L	IC	ID	NB	L	IC	ID	NB
L	SC	IC	Z	L	SC	IC	NS	L	SC	IC	NB
L	SC	SC	Z	L	SC	SC	NB	L	SC	SC	NB
L	SC	SD	NS	L	SC	SD	NB	L	SC	SD	NB
L	SC	ID	NS	L	SC	ID	NB	L	SC	ID	NB
L	SD	IC	PS	L	SD	IC	NS	L	SD	IC	NS
L	SD	SC	PS	L	SD	SC	NS	L	SD	SC	NS
L	SD	SD	Z	L	SD	SD	NB	L	SD	SD	NB
L	SD	ID	Z	L	SD	ID	NB	L	SD	ID	NB
L	ID	IC	PS	L	ID	IC	Z	L	ID	IC	Z
L	ID	SC	PS	L	ID	SC	Z	L	ID	SC	NS
L	ID	SD	Z	L	ID	SD	NS	L	ID	SD	NS
L	ID	ID	Z	L	ID	ID	NB	L	ID	ID	NB
M	IC	IC	Z	M	IC	IC	Z	M	IC	IC	NS
M	IC	SC	Z	M	IC	SC	Z	M	IC	SC	NS
M	IC	SD	Z	M	IC	SD	NS	M	IC	SD	NB
M	IC	ID	Z	M	IC	ID	NB	M	IC	ID	NB
M	SC	IC	PS	M	SC	IC	Z	M	SC	IC	NS
M	SC	SC	PS	M	SC	SC	Z	M	SC	SC	NS
M	SC	SD	Z	M	SC	SD	NS	M	SC	SD	NB
M	SC	ID	Z	M	SC	ID	NS	M	SC	ID	NB
M	SD	IC	PB	M	SD	IC	PS	M	SD	IC	Z
M	SD	SC	PB	M	SD	SC	Z	M	SD	SC	Z
M	SD	SD	PS	M	SD	SD	Z	M	SD	SD	NS
M	SD	ID	PS	M	SD	ID	NS	M	SD	ID	NB
M	ID	IC	PB	M	ID	IC	PS	M	ID	IC	Z
M	ID	SC	PB	M	ID	SC	PS	M	ID	SC	Z
M	ID	SD	PB	M	ID	SD	Z	M	ID	SD	NS
M	ID	ID	PB	M	ID	ID	Z	M	ID	ID	NS
H	IC	IC	PB	H	IC	IC	PS	H	IC	IC	Z
H	IC	SC	PS	H	IC	SC	PS	H	IC	SC	Z
H	IC	SD	Z	H	IC	SD	Z	H	IC	SD	NS
H	IC	ID	Z	H	IC	ID	NS	H	IC	ID	NB
H	SC	IC	PB	H	SC	IC	PS	H	SC	IC	PS
H	SC	SC	PS	H	SC	SC	PS	H	SC	SC	PS
H	SC	SD	PS	H	SC	SD	Z	H	SC	SD	NS
H	SC	ID	PS	H	SC	ID	NS	H	SC	ID	NB
H	SD	IC	PB	H	SD	IC	PB	H	SD	IC	PB
H	SD	SC	PB	H	SD	SC	PS	H	SD	SC	PS
H	SD	SD	PB	H	SD	SD	PS	H	SD	SD	Z
H	SD	ID	PS	H	SD	ID	Z	H	SD	ID	NS
H	ID	IC	PB	H	ID	IC	PB	H	ID	IC	PB
H	ID	SC	PB	H	ID	SC	PB	H	ID	SC	PS
H	ID	SD	PB	H	ID	SD	PS	H	ID	SD	Z
H	ID	ID	PB	H	ID	ID	Z	H	ID	ID	Z

III

Results and Discussion

In this third part, the correct functioning of the studied system is analyzed under different circumstances. The proposed simplified model is compared to the detailed model, in which a substantial simulation time reduction was verified. The three EMS strategies were verified, for different system configurations, considering a single storage system and a hybrid storage configuration.

Chapter 8

Simulation Results

In this section, two topologies are studied, one composed by the PV power plant, and the BES-qZSI (Cases 1, 2, and 3), and the other one composed by the previous configuration with the addition of the DC/DC-ZSC converter and the UC (Case 4). For each case, a different EMS strategy is evaluated, being EMS 1 for Cases 1 and 2, EMS 2 for Case 3, and EMS 3 for Case 4. For Case 1, the dynamic performance of the proposed SM and the DM of the BES-qZSI is evaluated, including experimental results. In Case 2, a long simulation is presented where it can be observed that the battery reaches its SOC limits and operates in the safe zone, confirming the suitability of the proposed system for dynamic analysis purposes in long-term simulations. For Case 3, an EMS based on FLC is implemented. In Case 4, a UC is added and a new EMS strategy to handle two storage units is developed.

8.1. Case 1.

8.1.1. Comparison of the detailed and simplified models

The dynamic performance of the proposed SM and the DM of the BES-qZSI is evaluated and compared under changes in the solar irradiation, electricity market, and reactive power reference. Moreover, a voltage sag as a grid disturbance is presented.

In this case, a 30 s-long simulation is carried out to evaluate the performance of the models with changes in the solar irradiation and the electricity market.

Fig. 8.1 shows the irradiation profile used in this case, which represents the irradiation of a typical cloudy summer day, but compressed in 30 s of simulation. This irradiation profile allows to evaluate the behavior of the system with changes in the PV power, and thus, in the management of the power stored in/provided by the battery (P_{BES}) and the power injected into the grid (P_{grid}). The simulation is performed assuming an initial

battery SOC of 50%. The MPPT algorithm allows the PV array to operate with the maximum power at every instant.

It can be seen in Figs. 8.2a-8.2c that the proposed SM achieves the expected objective, as the results obtained with the SM for the active power flow (P_{PV} , P_{BES} , and P_{grid}) are similar to those shown by the DM. Moreover, since the SM resembles the DM, it can be stated that the loss of information when using an averaged model of the VSI does not pose a significant drawback in this sort of simulation, since only the high switching frequency of the switches in the DM is neglected in the SM, while reducing the simulation time and computational efforts notably.

In this simulation, the SO does not define any reference power. Therefore, the battery operates searching for an economic benefit in the electricity market. Subsequently, during the VP (indicated with the red background in Fig. 8.2d) the energy is stored in the battery. The energy stored is released later during the PP (green background), making a monetary profit due to the difference in the energy price between both periods.

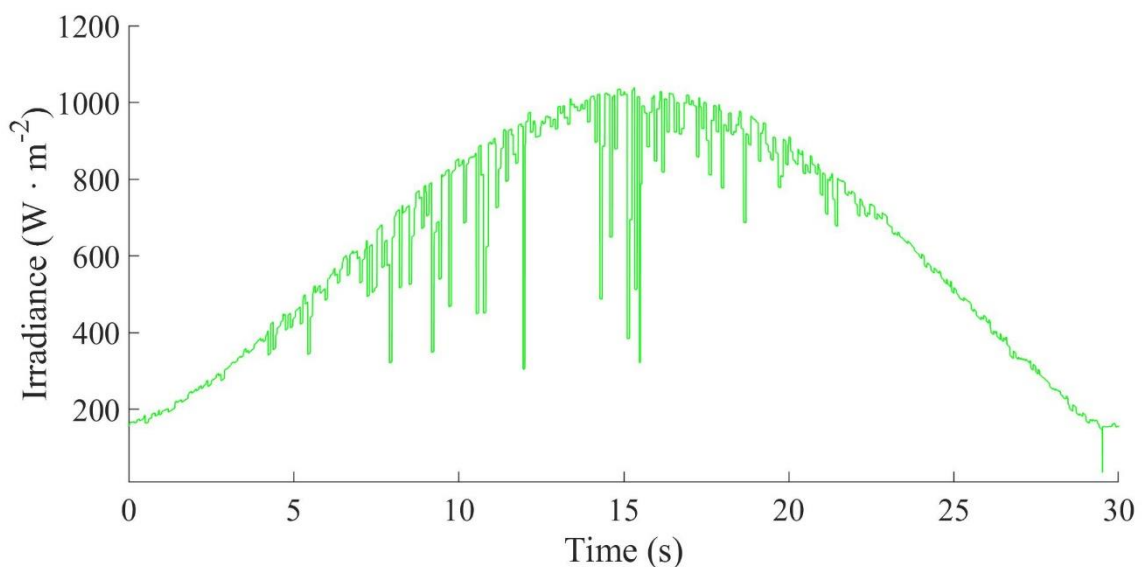
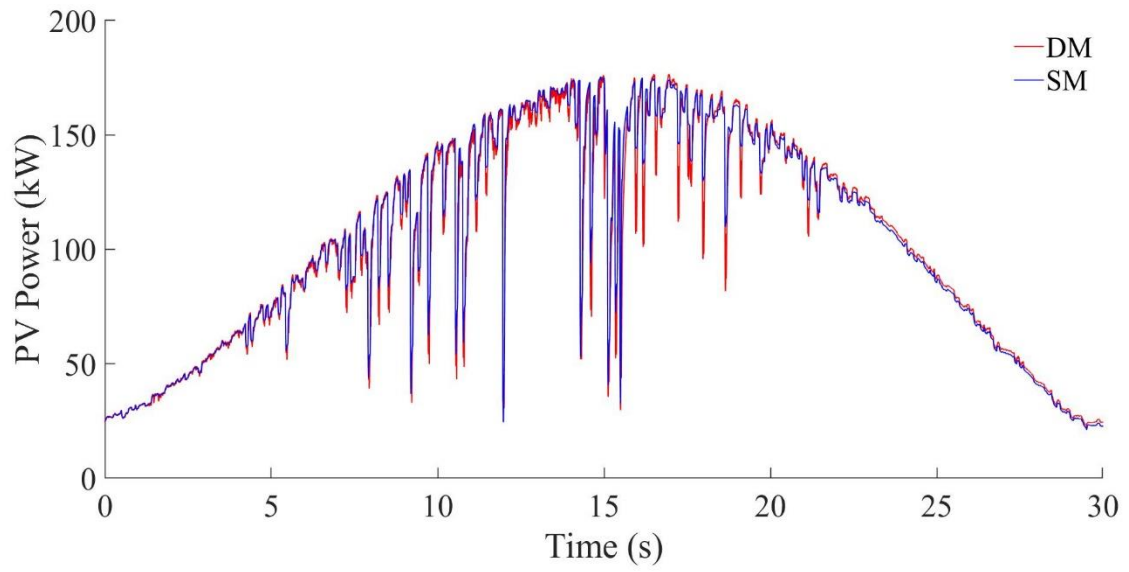
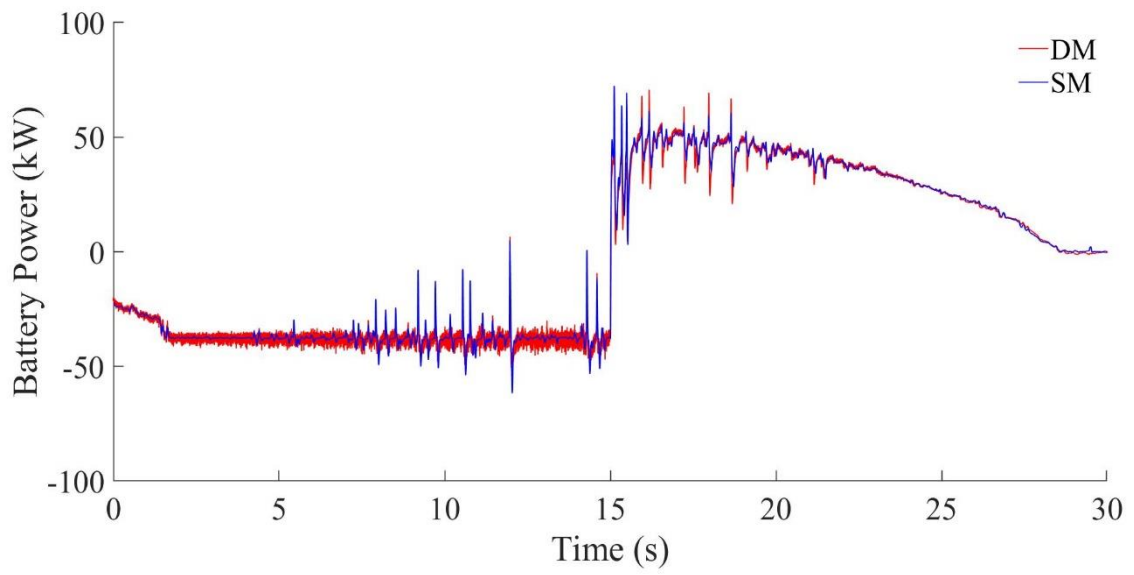


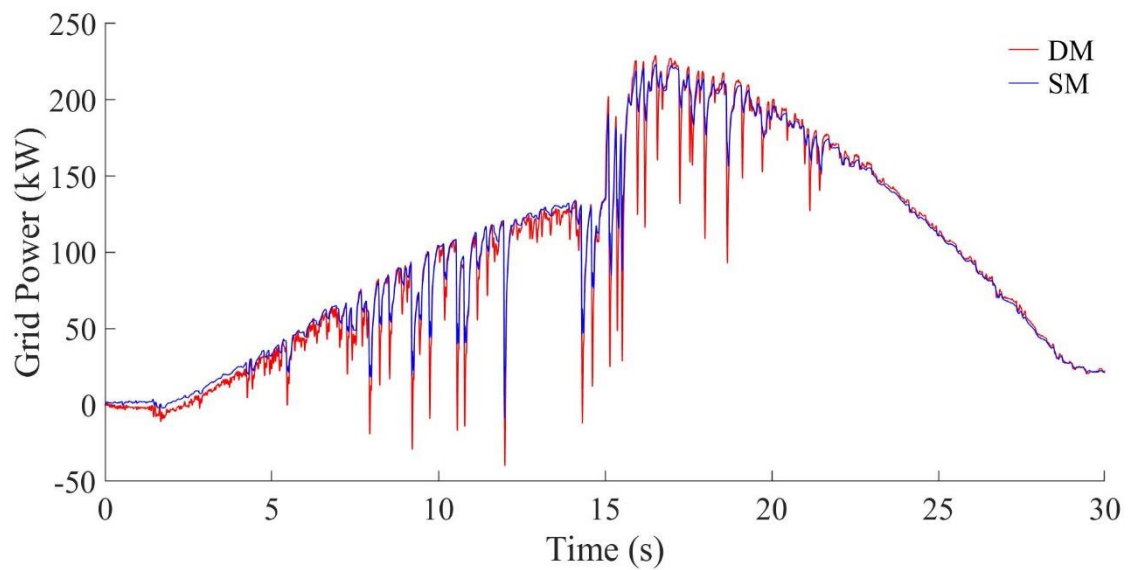
Fig. 8.1. Irradiation profile for case 1



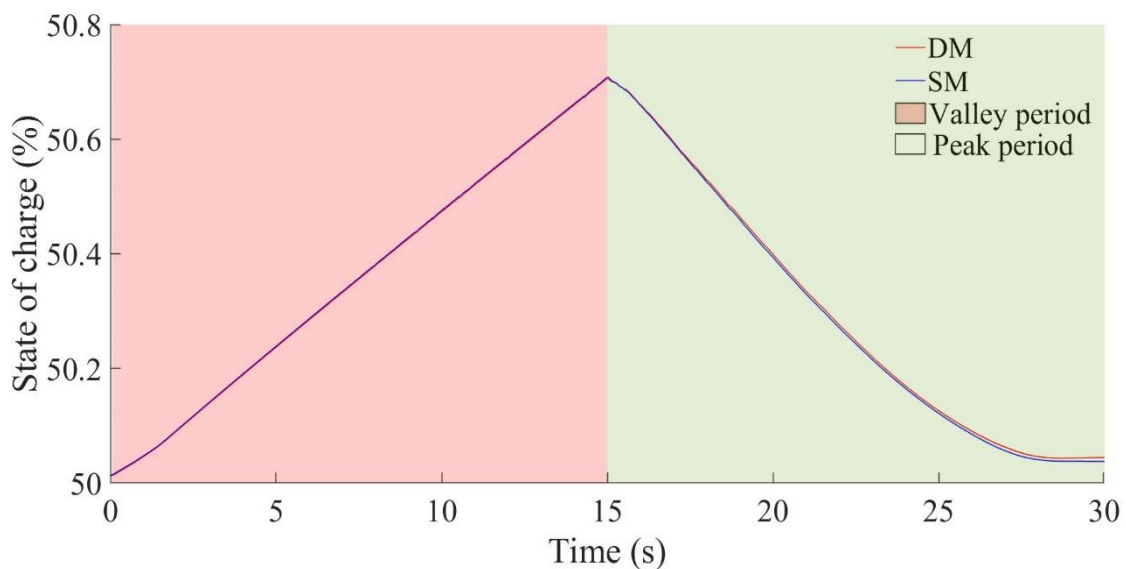
(a)



(b)



(c)



(d)

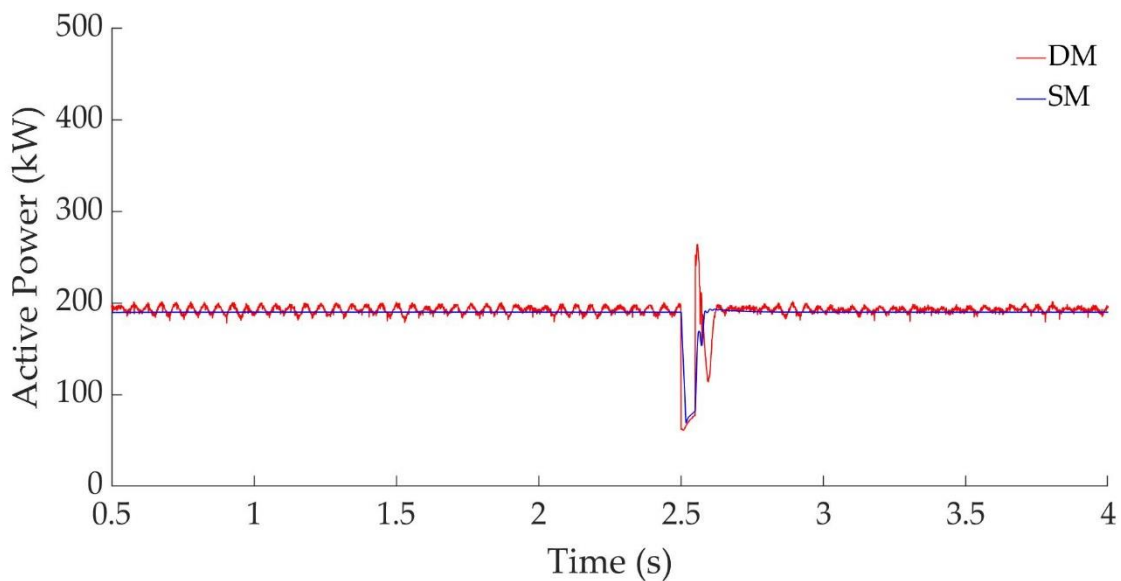
Fig. 8.2. Case 1: (a) PV power (b) Battery power (c) Grid power (d) SOC

This simulation focuses on evaluating the proposed SM and the control system under transient states that may occur in the system, such as changes in the reactive power reference imposed by the SO and a grid disturbance (grid voltage sag of 0.7 p.u. at 2.5 s with a duration of 50 ms).

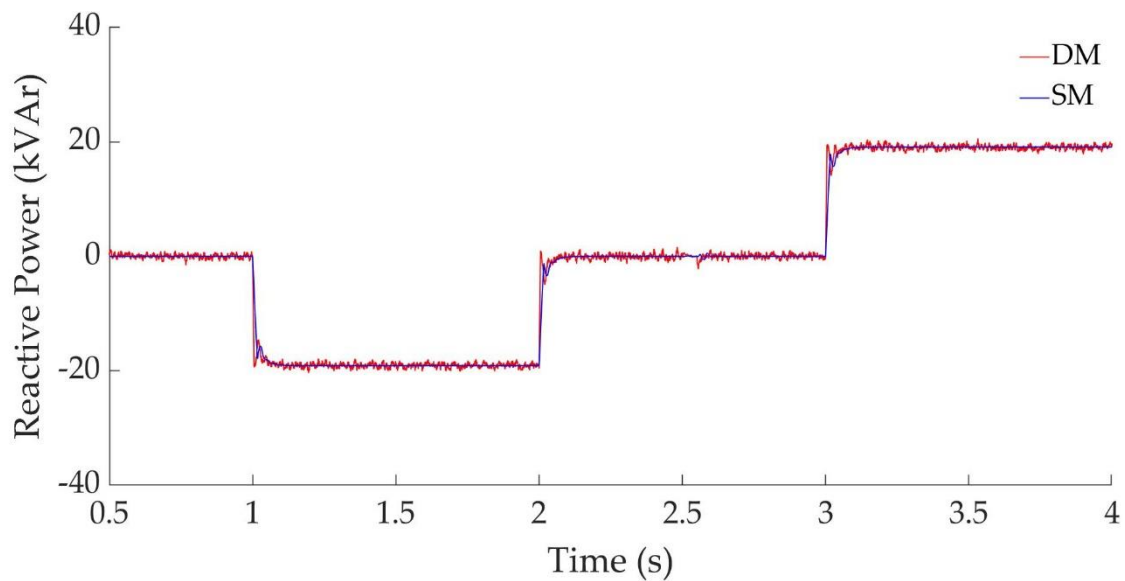
Fig. 8.3 illustrates the grid active and reactive power obtained in this case study, where the system is simulated under the following operating conditions: 1) the irradiation is

assumed constant at 1000 W/m^2 ; b) the SO demands a P_{SO} of 190 kW, where the PV system contributes with 171 kW and the battery with 19 kW; 3) the system operates with unity power factor (reactive power equals to zero), except from 1 to 2 s, where the SO demands a Q_{SO} of -0.1 p.u. (equivalent to -20 kVAr), and from 3 to 4 s, where +0.1 p.u. (+20 kVAr) are requested.

Regarding the voltage sag, the system operates with an active power of 190 kW and unity power factor right before the disturbance. During the voltage sag, the active power falls equally in both models (DM and SM) due to the voltage drop. When the disturbance is cleared and the grid voltage recovered, the active power increases and stabilizes at the pre-fault value. The SM presents less variability in the transient and reaches the pre-fault conditions earlier than the DM, provided that the operation of the power switches in the VSI is only considered in the latter. During the rest of the simulation, the results obtained by the proposed SM perfectly match those achieved by DM, even when the changes in the reactive power happen.



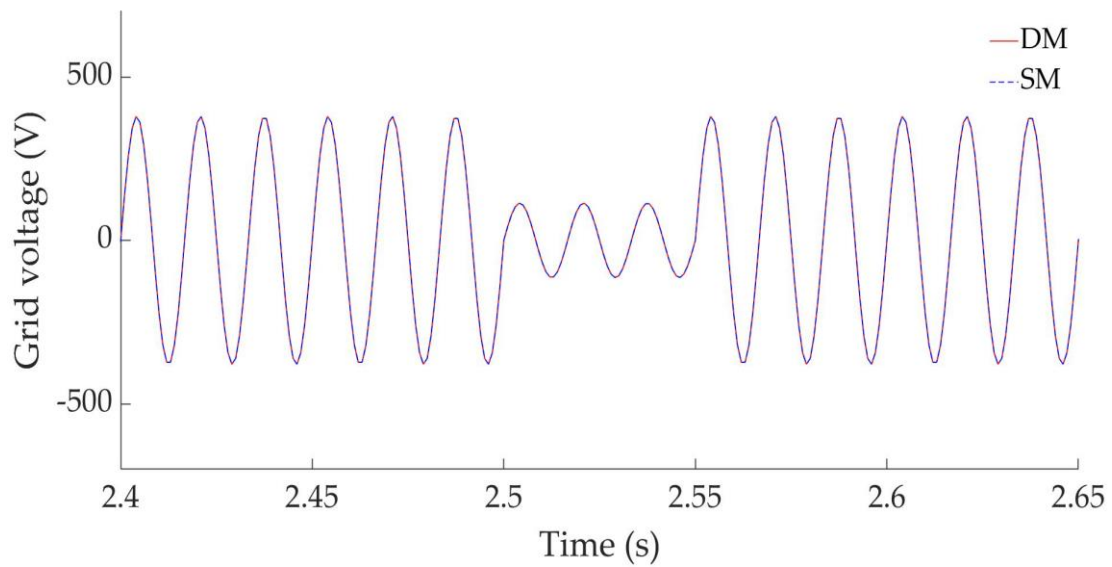
(a)



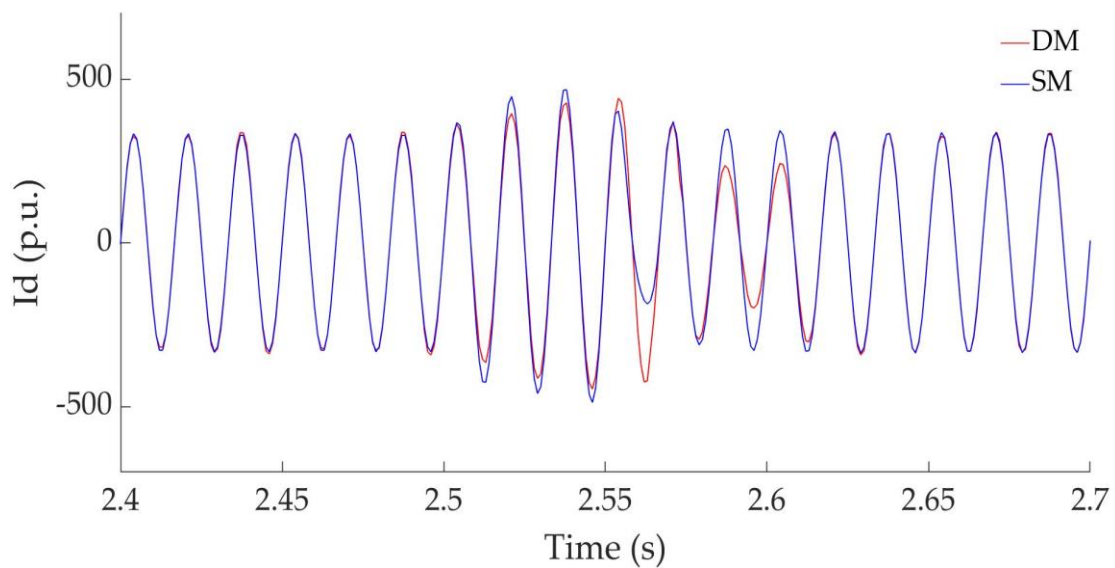
(b)

Fig. 8.3. Case 1: (a) Grid active power. (b) Grid reactive power

Fig. 8.4 illustrates the effect of the voltage sag on the phase-A grid voltage and current. Since the grid is modeled as an ideal source, only a single voltage waveform is represented in Fig. 8.4a, because it is exactly the same in the two models compared. Regarding the grid current in Fig. 8.4b, only small differences between the DM, and the SM appear during and after the fault. It can be seen that the transitory state in the grid current observed for the DM is slightly more intense than for the SM due to the simplifications made in this model. Nevertheless, the response of the SM is completely valid for its target simulations, and it should only be discarded if a very detailed study of the fault dynamics was required, which is not the case in this work. Finally, the stabilization of the grid current after the fault indicates that the PV power plant and the battery are controlled satisfactorily once the grid voltage is recovered.



(a)



(b)

Fig. 8.4. Case 1: (a) Phase-A grid voltage. (b) Phase-A grid current during the voltage sag

8.1.2. Comparison of the computational efforts of the models

Due to the simplifications applied to the DM to obtain the SM, the latter can be used for long-term simulations. In this sense, Table 8.1 presents a comparison of the computational efforts experienced for simulations using the DM and the SM. In Table 8.1,

the simulation horizon represents the simulation time set on Simulink, whereas the second column shows the simulation time reduction of the SM compared to the DM. The computer used for the simulations is equipped with an Intel® Core™ i7-10510U CPU @ 2.3 GHz processor, and 32 GB of RAM. In this case, the PV power plant is simulated as in the case presented in 8.1.1, but without any changes in the reactive power reference or voltage sags. Furthermore, the irradiation is assumed constant at 1000 W/m^2 , and P_{SO} equals 190 kW, where the PV system provides 171 kW and the battery 19 kW.

The results show an average time reduction of 85% with the SM compared to the DM.

TABLE 8.1. COMPARISON OF THE COMPUTATIONAL EFFORT OF THE DM AND SM MODELS

Simulation horizon (s)	SM vs DM
	Time reduction (%)
5	81%
10	85%
15	86%
20	86%
30	86%
8100	85%
Average time reduction	85%

8.1.3. Experimental HIL validation

This section presents the experimental results that allow testing and comparing the real-time performance of the DM and the proposed SM.

Fig. 8.5 presents the experimental HIL setup built for the validation of the simulation results. The power plant runs in real-time in a *Typhoon HIL402* device. This real-time machine is programmed through the software *Typhoon HIL Control Center*, which also

allows monitoring the most relevant parameters of the power system in real-time. The control system runs in a *dSPACE MicroLabBox*, programmed with Simulink, and using *dSPACE ControlDesk* to monitor the signals of interest. Finally, the figures presented in this section are obtained through a *Yokogawa DLM4038* oscilloscope that measures the inputs and outputs of both real-time simulators.

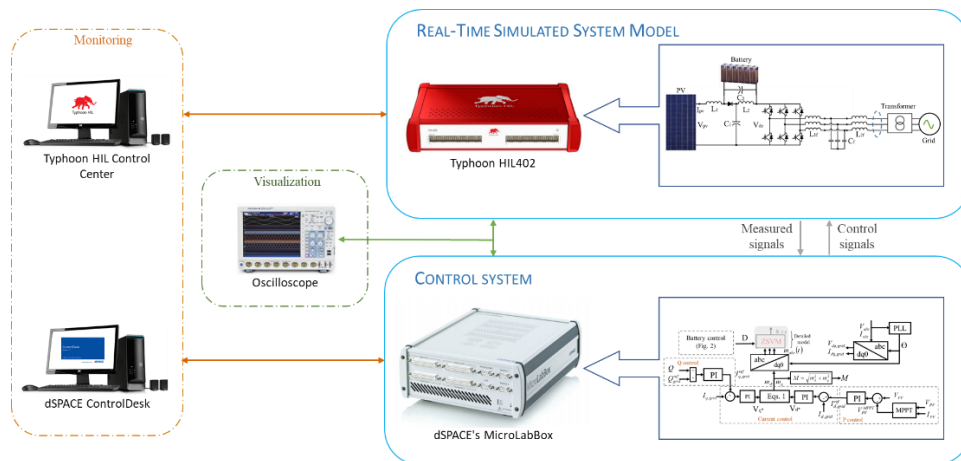
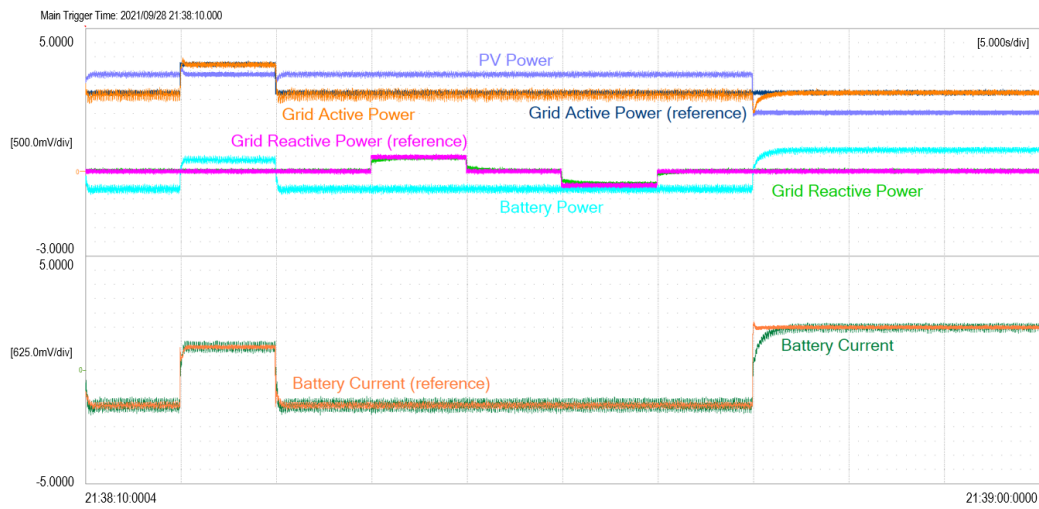
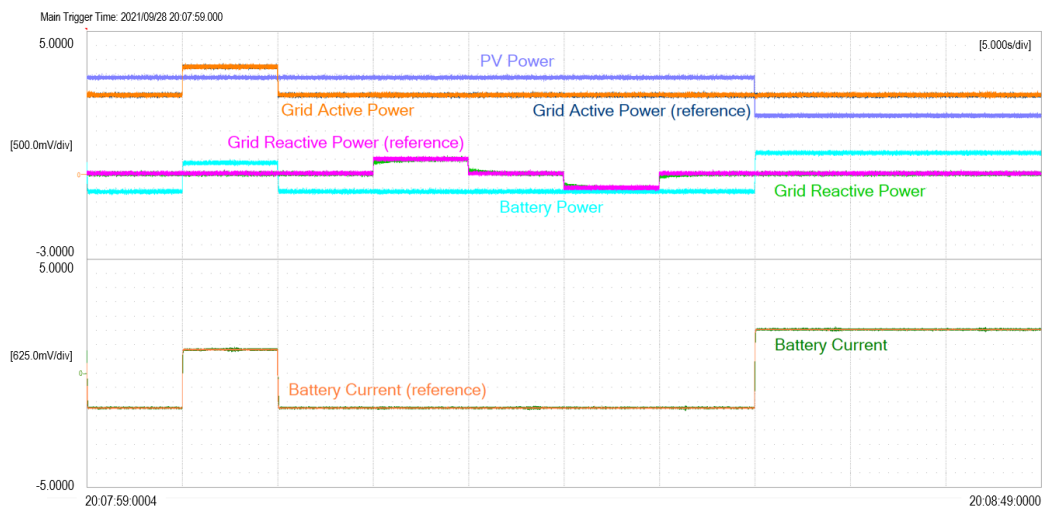


Fig. 8.5. HIL experimental setup

As it can be observed in Fig. 8.6 and 8.7, the results obtained with the experimental setup reveal that the proposed SM responds similarly to the DM under different operating conditions. In this sense, Fig. 8.6a shows that the DM tracks the references for the active and reactive powers satisfactorily, as well as the battery current. This indicates a proper operation of the control systems implemented. Additionally, the PV power generation and the battery power are also represented in this figure. The former varies with the irradiation input, and the latter is calculated from the battery voltage and current outputs. Fig. 8.6b illustrates an analogous scenario for the SM. As seen, the SM responds similarly to the DM under changes in the active and reactive powers, and the battery current and no relevant differences can be highlighted.



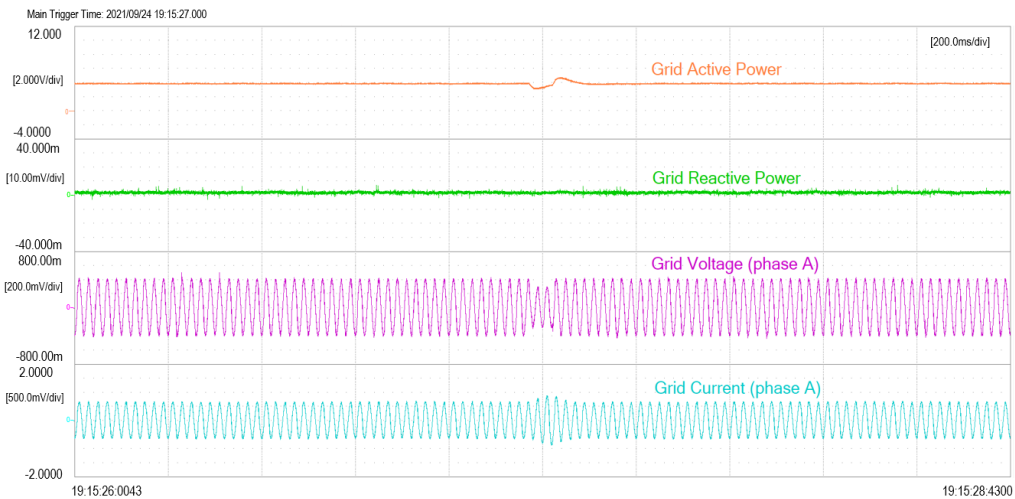
(a)



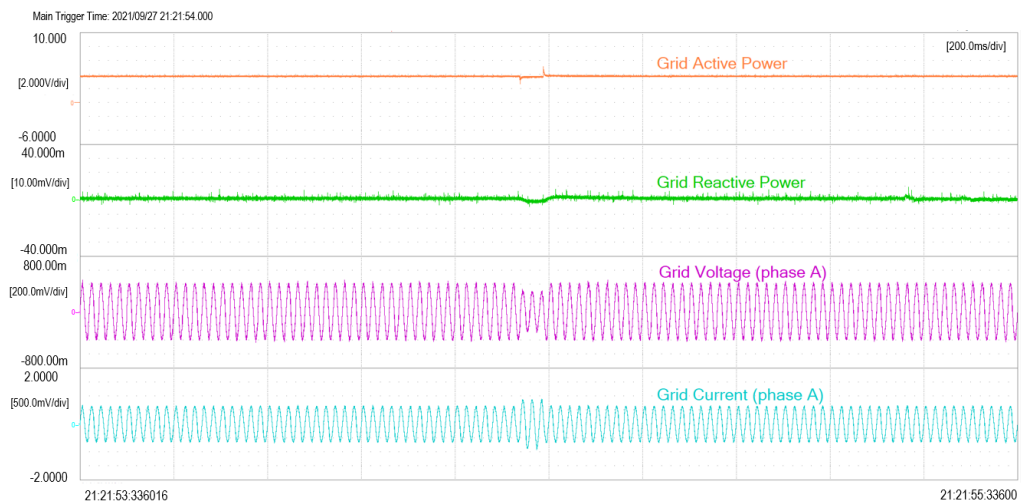
(b)

Fig. 8.6. Experimental results with power variation and battery current control for: (a) Detailed model. (b) Simplified model.

Fig. 8.7 depicts the results of the experimental setup during a sag in the grid voltage of 0.7 p.u., during 50 ms. The grid active and reactive powers, plus the phase-A instantaneous voltage and current are represented for the DM and the SM (Figs. 8.7a and 8.7b, respectively). Even under this grid fault, both the DM and the SM are able to recover the control of the power system shortly after the fault clearance. Furthermore, similar results for the DM and the SM can be noticed when comparing Figs. 8.7a and 8.7b.



(a)



(b)

Fig. 8.7. Experimental results including a voltage sag for: (a) Detailed model. (b) Simplified model.

The experimental results shown in this section prove the adequacy of the SM to replace the DM in long-term simulations, large-scale electric power systems, control design and dynamic analysis purposes.

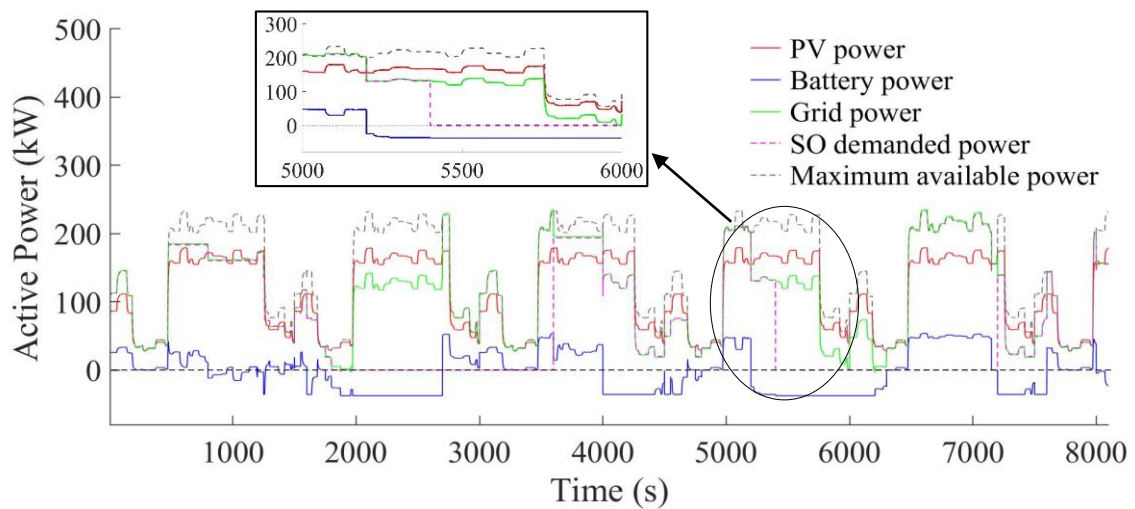
8.2. Case 2.

In Case 2, the behavior of the proposed SM is studied for long simulations with different operating conditions on PV generation, battery, and grid (changes in the electricity market and the power demanded by the SO).

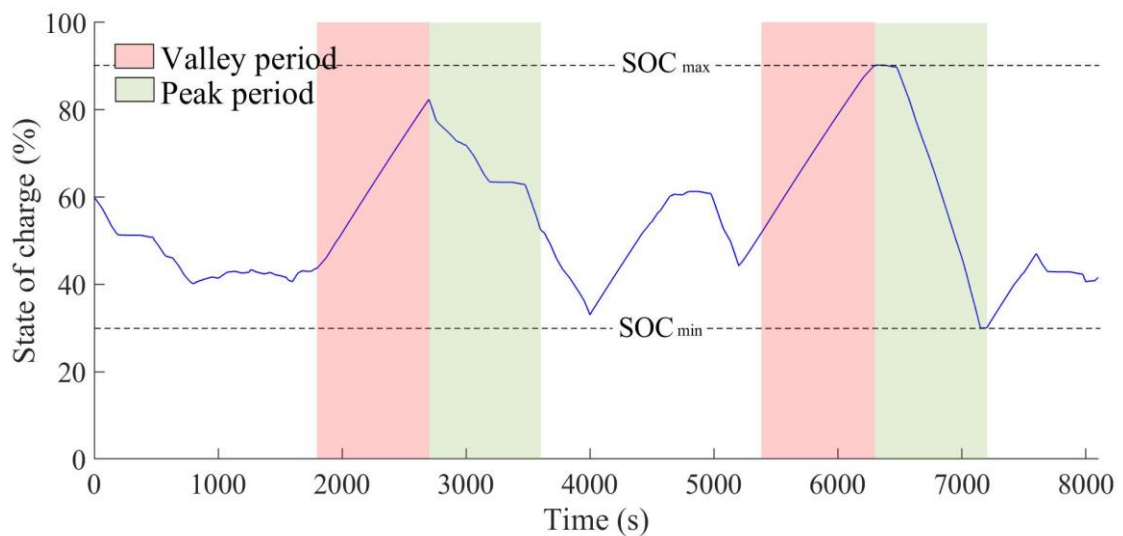
The results of an 8100 s-long simulation (equivalent to 2 hours and 15 minutes) are presented in this section. Since the performance of the proposed SM has proved similar to the DM in the previous case, only the SM is simulated in this scenario to confirm its suitability for dynamic analysis purposes in long-term simulations. For this simulation, a variable irradiance profile following the P_{PV} pattern shown in Fig. 8.8a and different operating conditions of the electricity market (Fig. 8.8b) are considered. This allows to evaluate the PV power plant and the proposed EMS under all the operating conditions described in Section 7.1 and Fig. 7.1.

Fig. 8.8a shows the power balance during the simulation for an initial SOC of 60% in the battery. It also presents the power demanded by the grid and the maximum available power. It can be noted from Fig. 8.8a that the demanded power is always lower than the maximum available power, and that when the SO demands a specific power, this request is addressed. From 0 to 1800 s, the SO defines a power demand. When the power requested by the SO is lower than the power generated by the PV panels, the exceeding energy is used to charge the battery. When the SO requests more power than the PV generation, the battery is discharged. From 1800 to 3600 s, the SO does not define any power demand, and the battery operates to achieve an economic benefit in the electricity market. In the first part of this period (from 1800 to 2700 s), the market is not favorable to sell energy (VP in Fig. 8.8b). Hence, the excess energy is stored in the batteries. On the other hand, in the second part (from 2700 to 3600 s) a PP is observed (Fig. 8.8b), and thus the battery is discharged. Approximately at the middle of the peak period, the battery is discharged with a lower intensity, limited by Eq. 7.3. From 3600 to 5400 s, P_{SO} is similar to the value set at the beginning of the simulation. However, this time the battery is charged and discharged more often because it coincides with periods where P_{SO} is either higher or lower than P_{PV} . From 5400 s onwards, it can be observed that the battery reaches and does not exceed the SOC limits.

Fig. 9b illustrates the battery SOC. It can be noted at 6300 s that, when the SOC reaches 90%, the battery is not allowed to charge beyond this point. On the other hand, when the battery SOC reaches 30% at 7100 s, a deeper discharge is not allowed. Moreover, it can be observed that, when the SO does not require a specific power, the battery is discharged during the PP, and charged during the VP. This behavior proves that the EMS avoids exceeding SOC limits, thus increasing the battery life cycle, while making an economic profit out of the smart energy dispatch implemented.



(a)



(b)

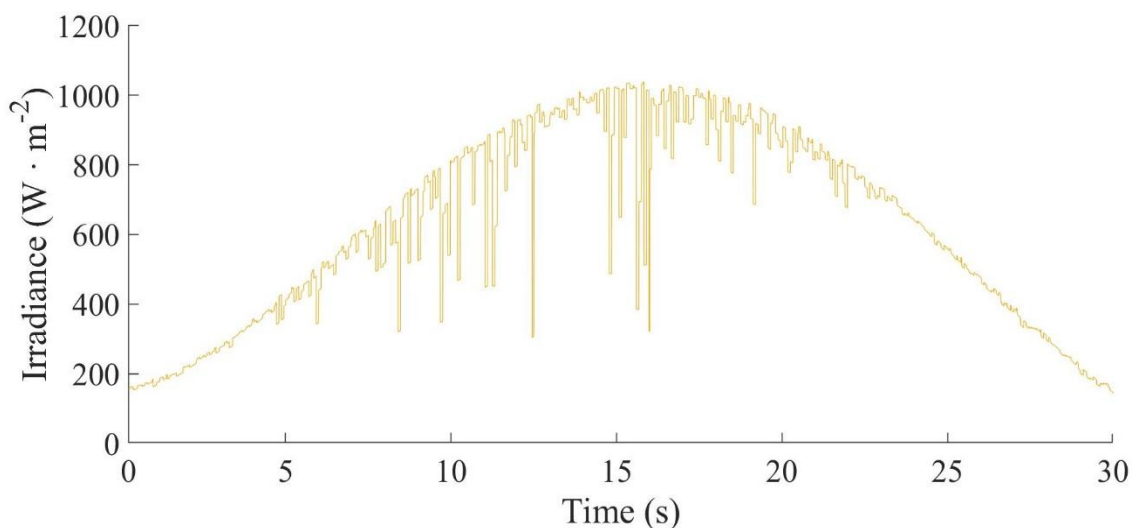
Fig. 8.8. Case 2: (a) PV power, battery power, grid power, SO demand, and maximum available power. (b) Battery SOC and trading in the electricity market

8.3. Case 3

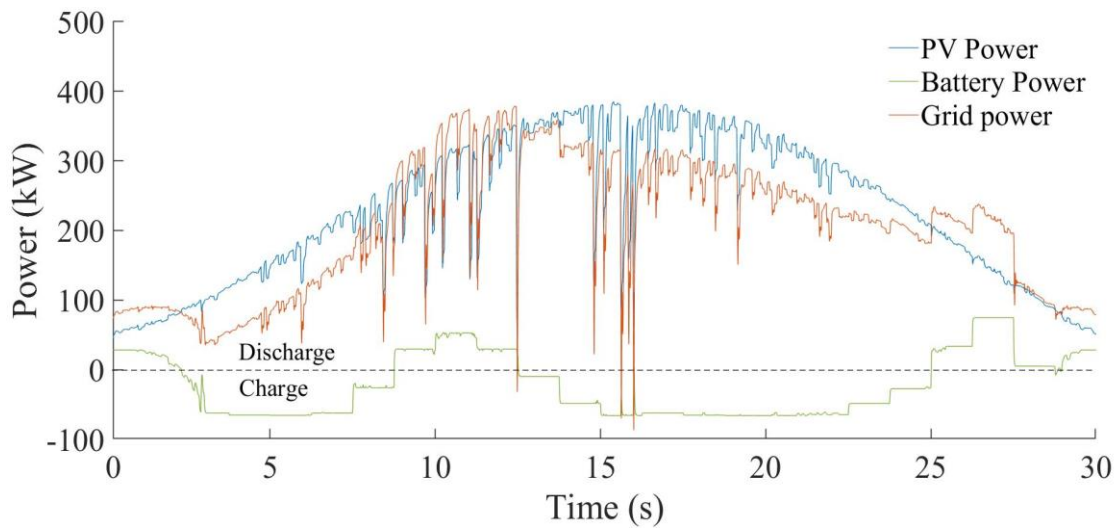
To evaluate the proposed fuzzy logic-based EMS applied to the system composed by PV panels, and a BES-qZSI, a simulation was performed considering an initial battery SOC of 50% and the PV power plant operation with unity power factor (reactive power reference equal to 0).

Fig. 8.9a shows the irradiation profile considered in the Case 2 simulation, which was obtained by adapting 14 h of a real cloudy summer day (from the sunrise to the sunset) to 30 s, to evaluate the system and the proposed control under different and variable operating conditions. The temperature profile was kept constant at 25°C during the whole simulation.

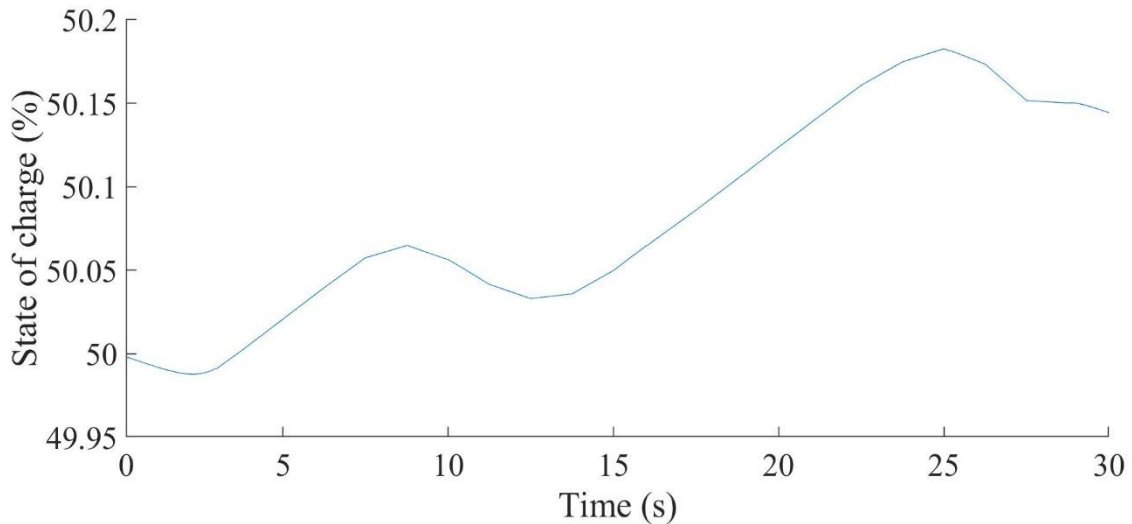
The power balance between the PV panels, battery, and grid is illustrated in Fig. 8.9b. It can be observed that the grid is the sum of PV and the battery power. When the battery is charging, the power is negative, and it is positive when the battery is discharging. Considering that the initial SOC is set at 50%, the battery can be charged or discharged according to the EMS implemented. Considering the price of the energy (Fig. 7.4), it can be seen that the battery is discharged when the price of the energy is high, and it is charged when the price is low. Fig. 8.9c depicts how the battery SOC increases when the battery is charged and decreases when the battery is discharged, following the power balance shown in Fig. 8.9b.



(a)



(b)



(c)

Fig. 8.9. Case 3: (a) Irradiation profile. (b) Power balance between PV panels, battery, and grid. (c) Battery SOC

The battery current control is illustrated in Fig. 8.10. As it can be seen, the measured current is able to follow the reference current, ensuring a suitable functioning of the battery charging and discharging, and as a consequence, ensuring the power balance between the sources (PV and battery) and grid.

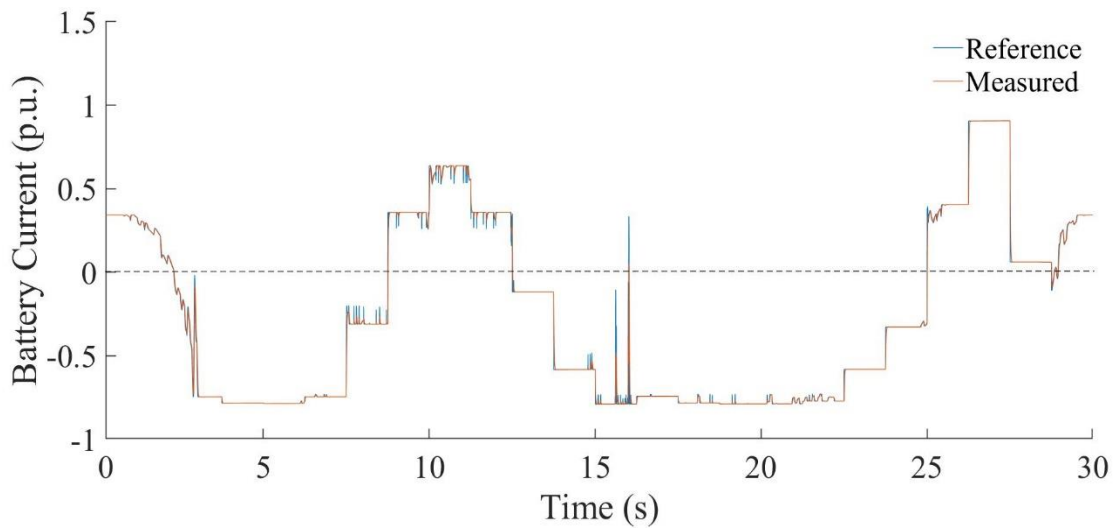


Fig. 8.10. Case 3: Battery current control

The DC input voltage to the inverter of the qZSI is about 1800 V (MVDC), as shown in Fig. 8.11. A voltage boost (B) of 1,79 is achieved by the qZSI from the PV panel output to the inverter DC side ($B = V_{dc}/V_{in}$), as expected.

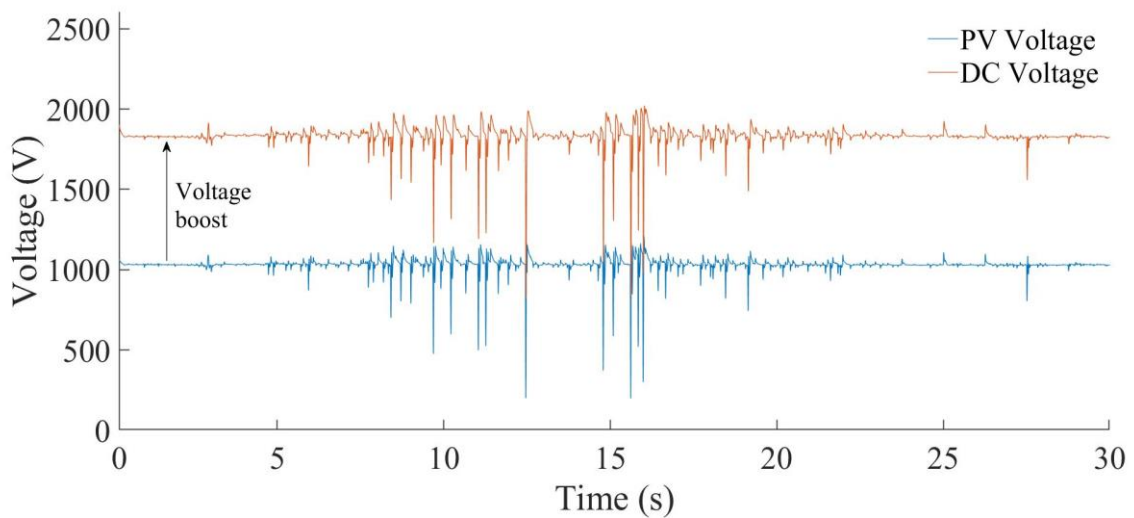


Fig. 8.11. Case 3: PV voltage, MVDC voltage, and voltage boost achieved from PV panels to DC side of the qZSI

D and M (Fig. 8.12) achieve values of 0,22 and 0,73, respectively, which confirms the voltage boost of 1,79, according to $B=1/(1-2D)$. It can also be observed that the control

system implemented complies with the premise that the sum of D plus M must be less than 1 to control the battery current and the AC grid current independently.

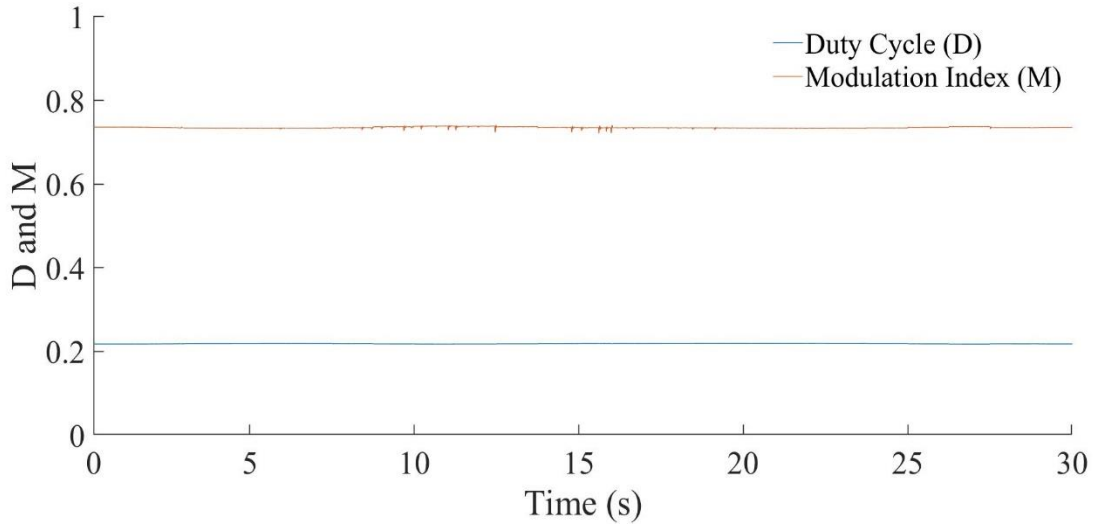
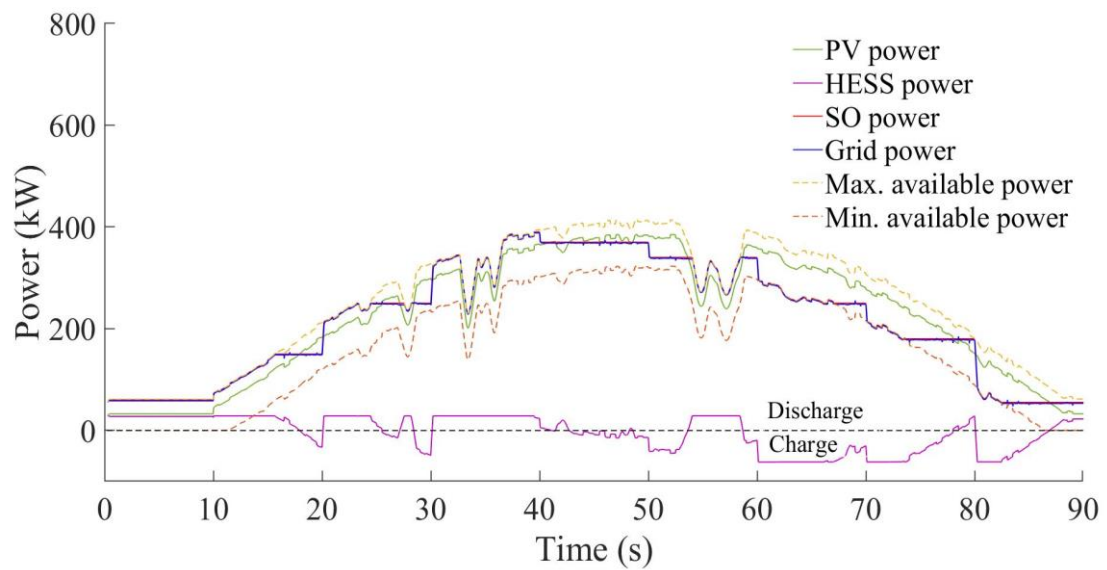


Fig. 8.12. Case 3: Duty cycle (D) and modulation index (M)

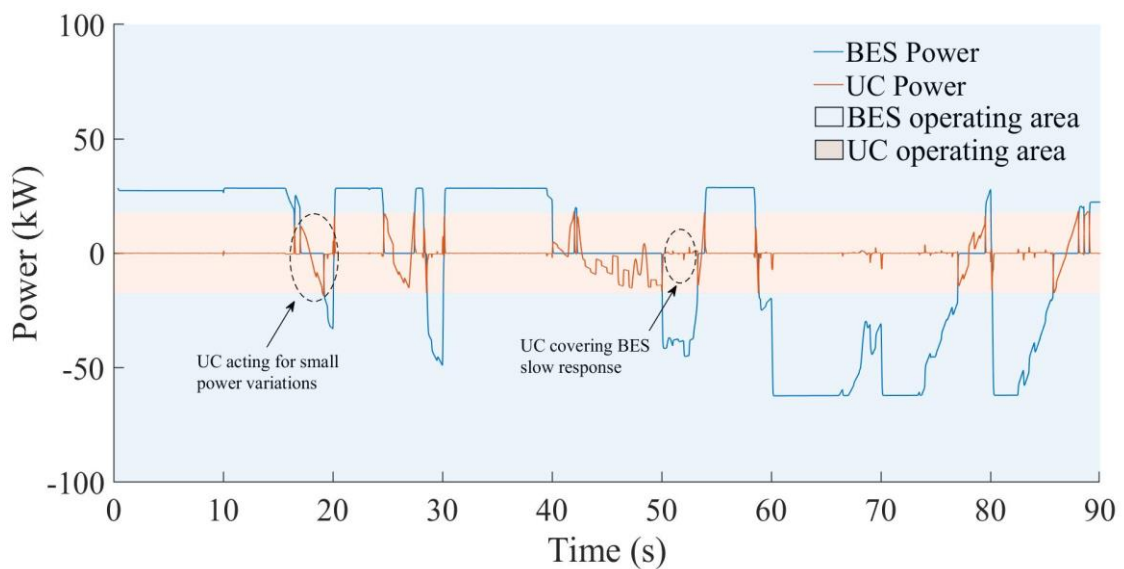
8.4. Case 4

In Case 4, the EMS 3 is designed to handle the power flow between the PV system, the grid, and the HESS system composed by the battery and the UC. This configuration is represented in Fig. 5.1. The strategy focuses on use the battery and the UC storage units to operate in a complementary manner.

From Fig. 8.13 to 8.16, the initial SOC of the BES is set to 50%. The power balance is represented in Fig. 8.13a. In this figure, it is possible to observe that P_{grid} is equal to P_{SO} , meaning that the power demanded by the SO is being attended throughout the whole simulation. This is possible due to the power gap compensation through the HESS. When the PV generation is different from P_{SO} , the HESS acts releasing or storing the power mismatch. Moreover, P_{SO} is between the allowed limits, according to Eq. 7.1 and 7.2. P_{BES} and the P_{UC} are illustrated in Fig. 8.13b. The UC covers low power fluctuations, as well as the BES slow response during changes on its power reference.



(a)



(b)

Fig. 8.13. Case 4: Hybrid system power balance (a) Power balance between PV, HESS, SO, and grid. (b) BES and UC power

In Fig. 8.14, it can be seen that the BES response presents a slight difference compared to the BES demanded power. This small difference is covered by the UC, as seen in Fig. 8.13b.

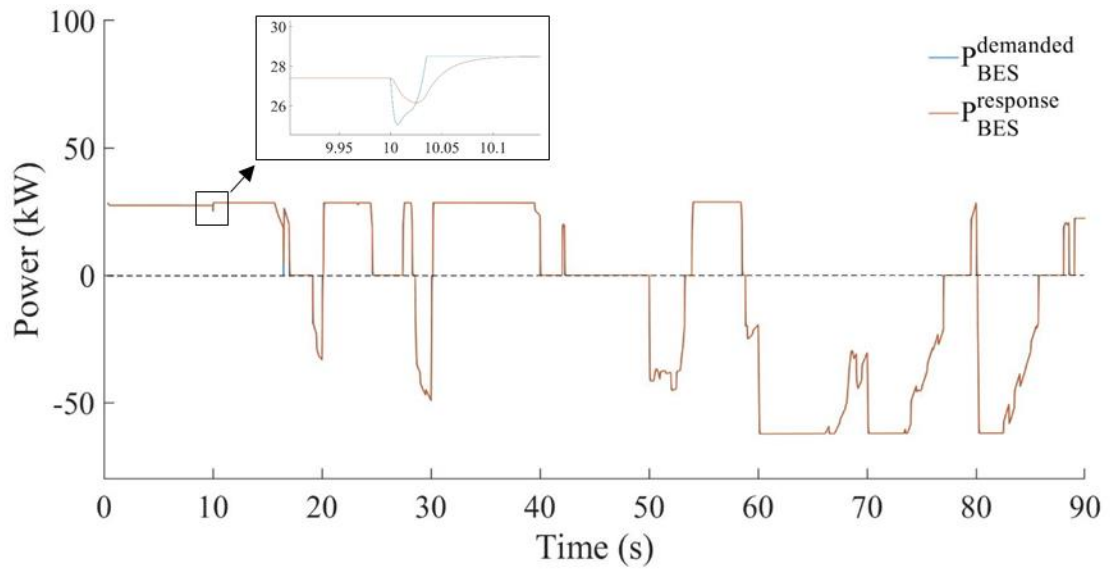
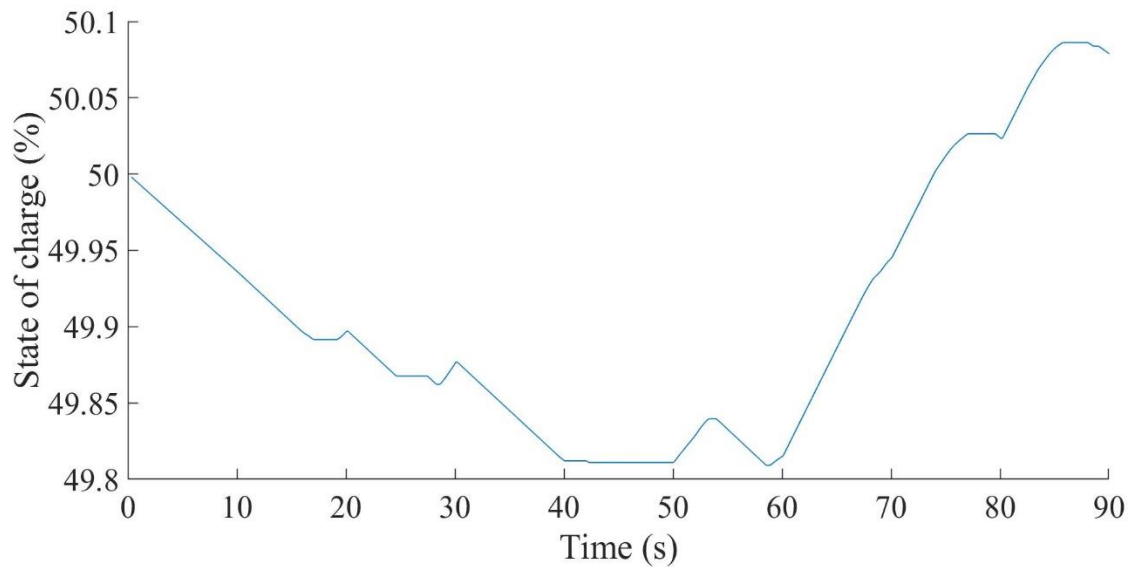
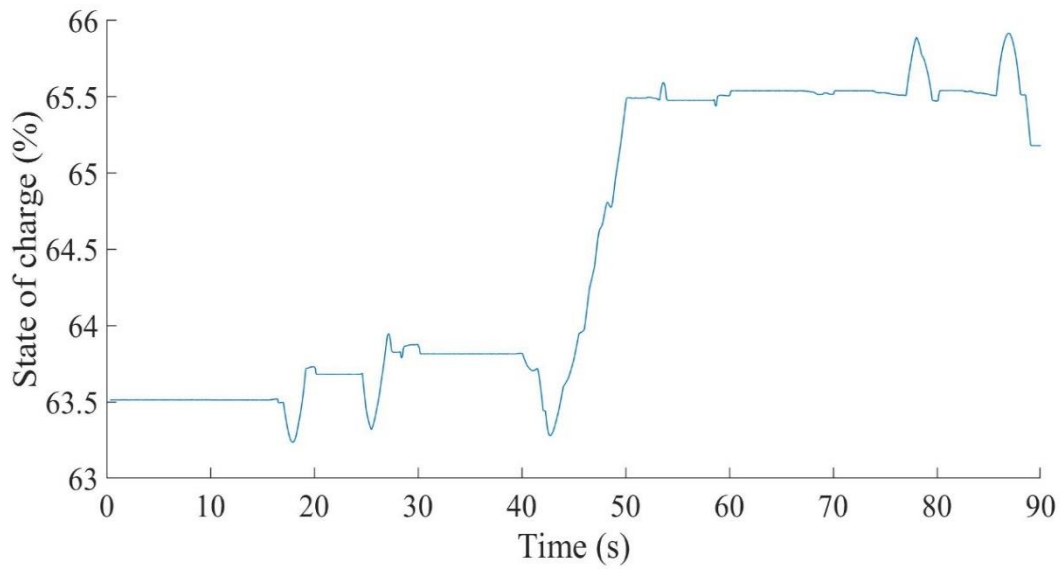


Fig. 8.14. Battery demanded power and battery response

BES and UC SOC are represented in Fig. 8.15 considering that the initial state is medium. In this case, three situations are possible for the BES: charge, discharge or maintain at the same level, depending on the power demanded by the SO.



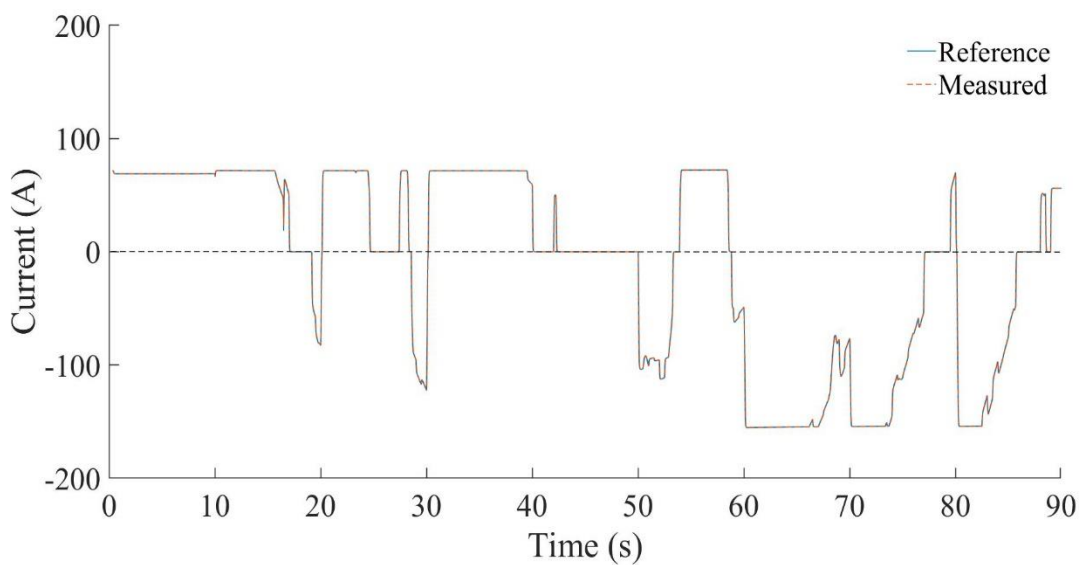
(a)



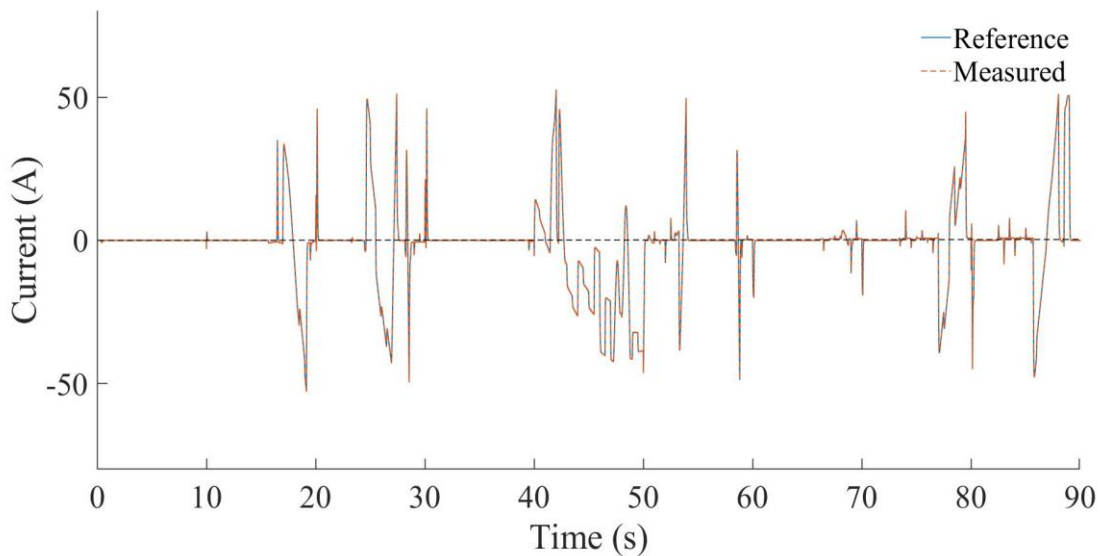
(b)

Fig. 8.15. Case 4: State of charge (a) BES. (b) UC

From Fig. 8.16, it is possible to conclude that the HESS control strategy is working satisfactorily, and that the BES (Fig. 8.16a) and the UC currents (Fig. 8.16b) are controlled, tracking their respective reference values.



(a)

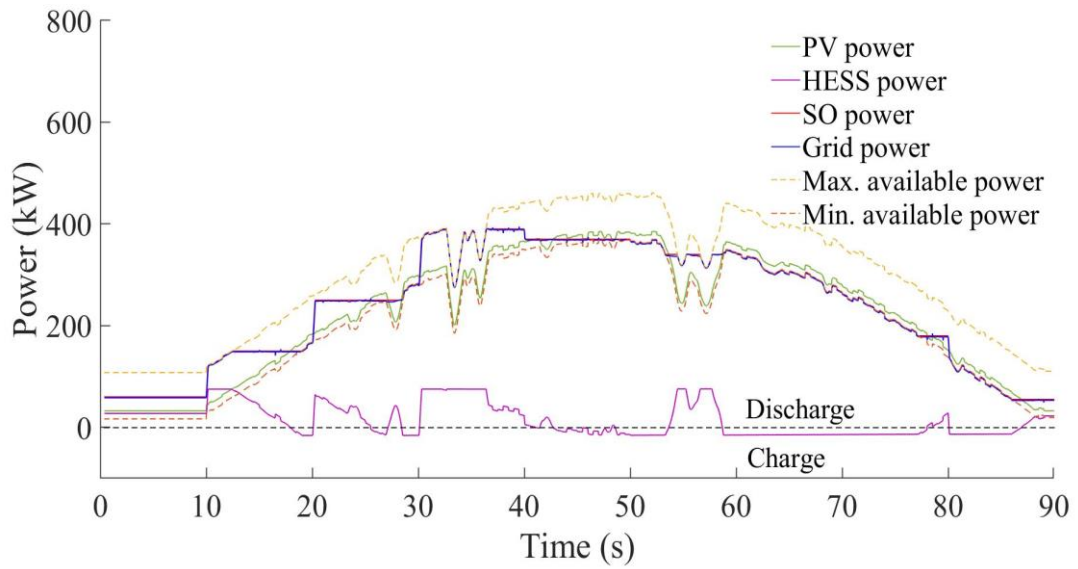


(b)

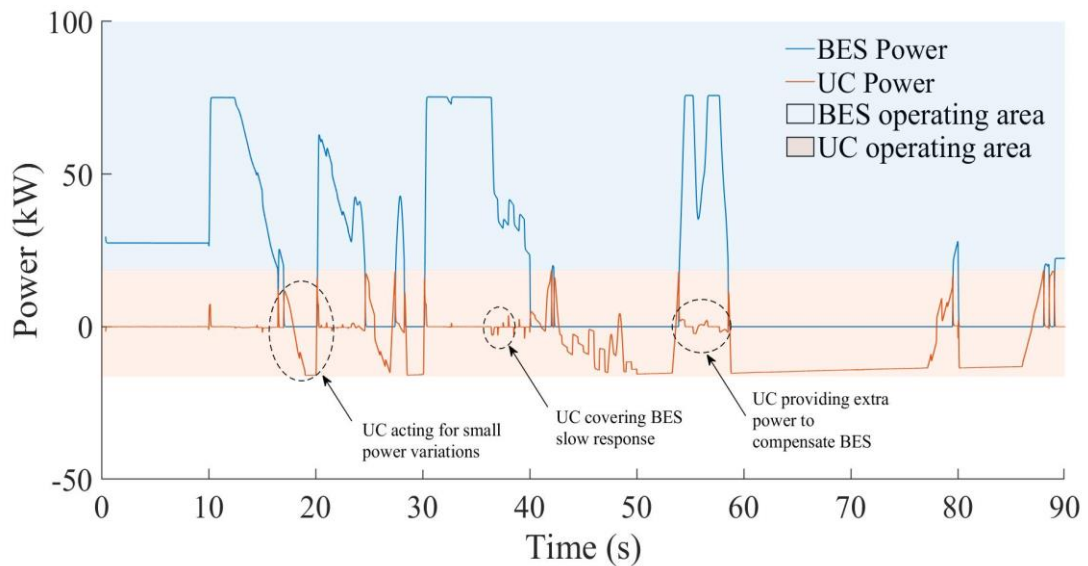
Fig. 8.16. Case 4: Current control (a) BES. (b) UC

To observe the BES reaching its SOC limits in a single simulation, a huge computational effort and time are needed. Thus, the simulation is divided into three parts. In Figs. 8.13 – 8.16, the BES started with a medium initial SOC (50%). In the following figures (Fig. 8.17 and 8.18), the initial BES SOC is set to 92% (above SOC_{max}), and in Figs. 8.19 and 8.20, a low SOC of 31% is represented.

In the case of high SOC, the BES is only allowed to discharge or remain at the same level, which can be observed in Fig. 8.18a. Note that in Fig. 8.18b, the UC SOC varies more intensely due to the fact that the BES is not allowed to charge anymore, thus having the UC to cover the battery more often than with a medium initial BES SOC. In Fig. 8.17a, the power balance can be observed, and in Fig. 8.17b, it is possible to confirm that the BES is not charged anymore because of the absence of the negative operating area. It is also possible to see that the UC is being required for small power variations, providing extra power that the BES is not able to supply, and also for the slow response of the BES, proving the correct functioning of the EMS.

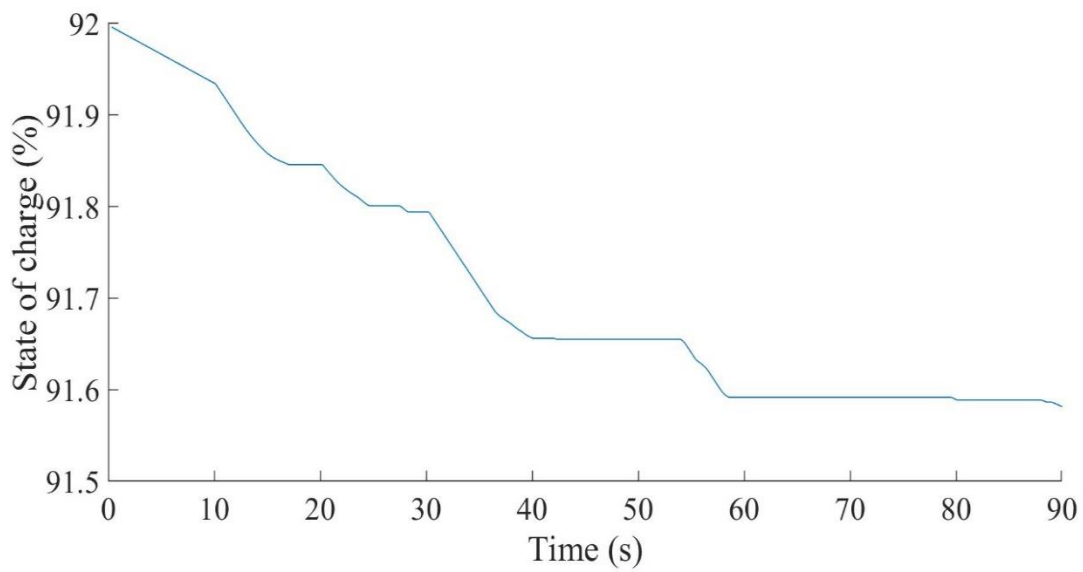


(a)

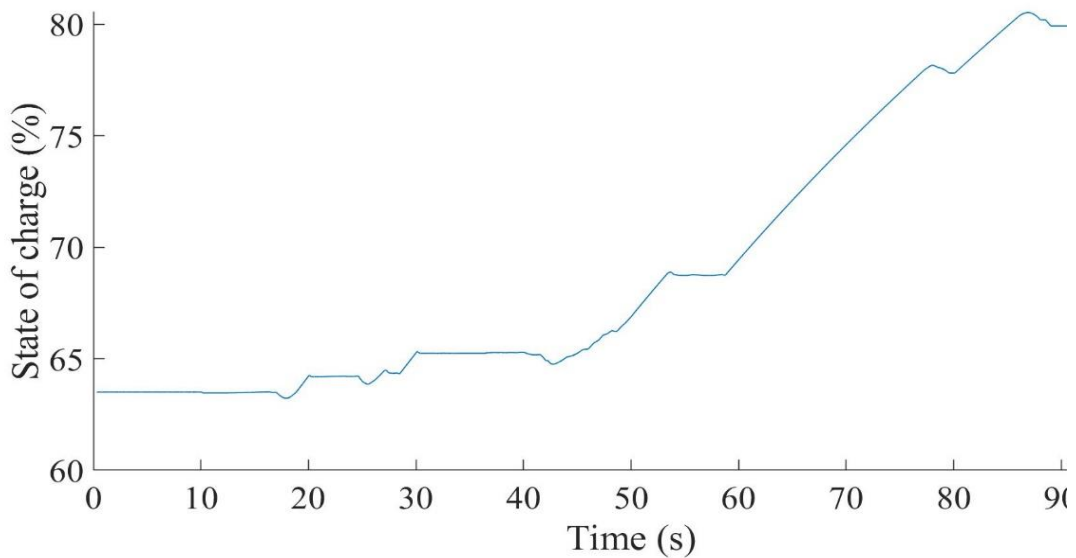


(b)

Fig. 8.17. Case 4: Hybrid system power balance with high initial BES SOC (a) Power balance between PV, HESS, SO, and grid. (b) BES and UC power



(a)

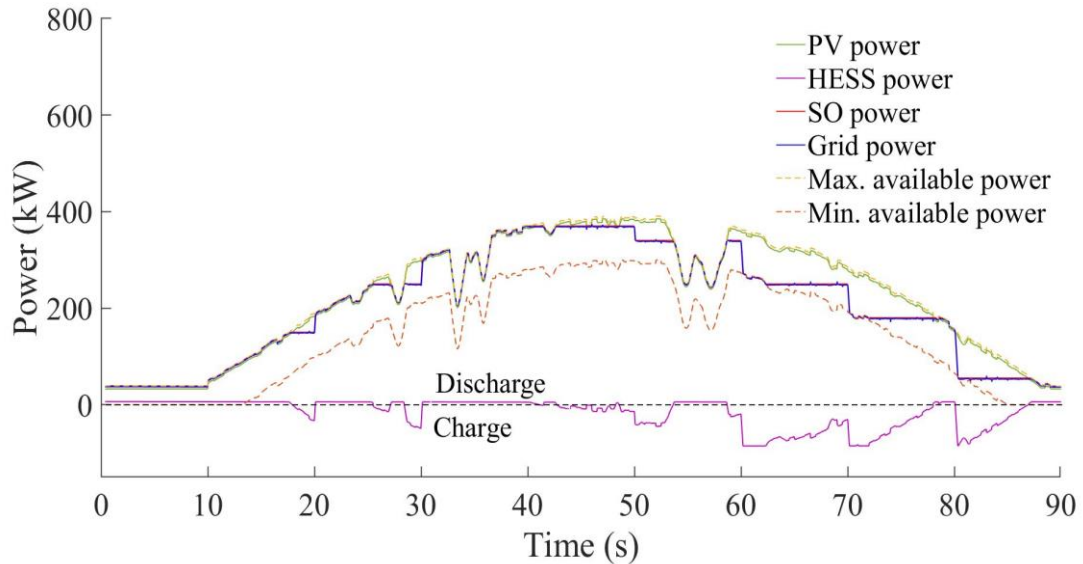


(b)

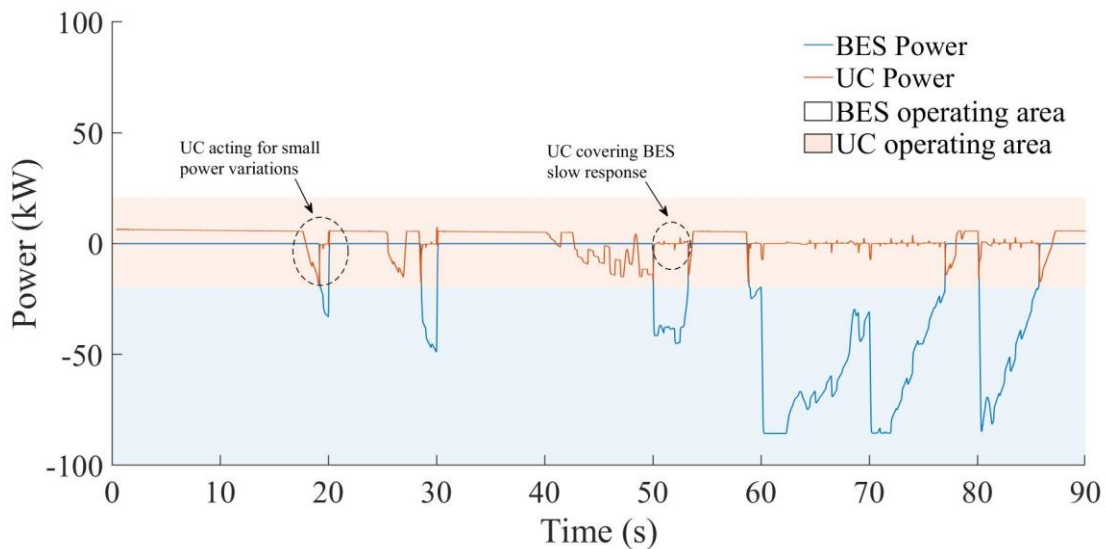
Fig. 8.18. Case 4: State of charge for (a) BES starting with high SOC. (b) UC

The power balance is observed in Fig. 8.19a, where the maximum available power is close to the PV generation, since the BES cannot contribute due to its low SOC and only the UC can be discharged. In Fig. 8.19b, the absence of the positive BES operating area confirms

that the BES is not discharged. The UC is being demanded for small power variations and also for the slow response of the BES.



(a)



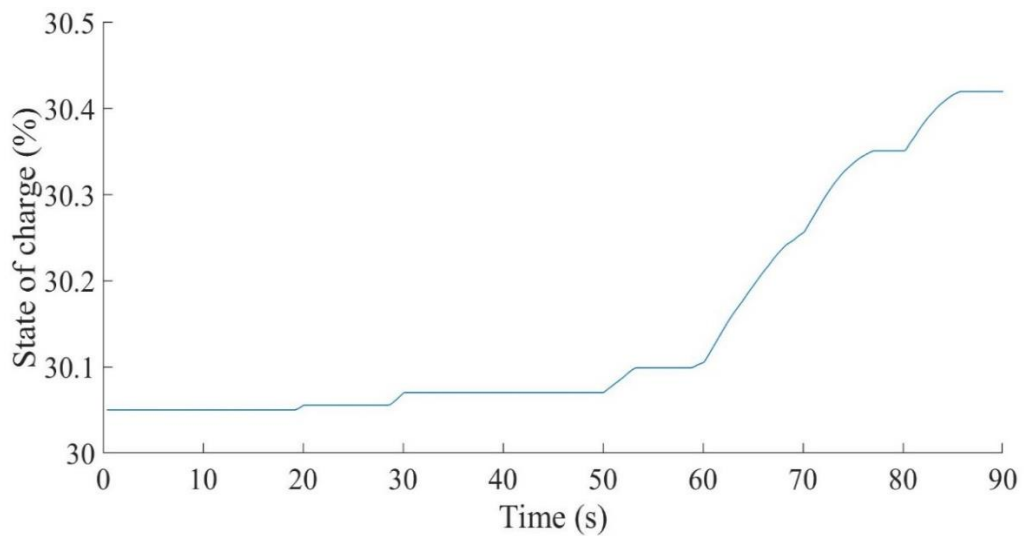
(b)

Fig. 8.19. Case 4: Hybrid system power balance with low initial SOC (a) Power balance between PV, HESS, SO, and grid. (b) BES and UC power for high initial BES SOC

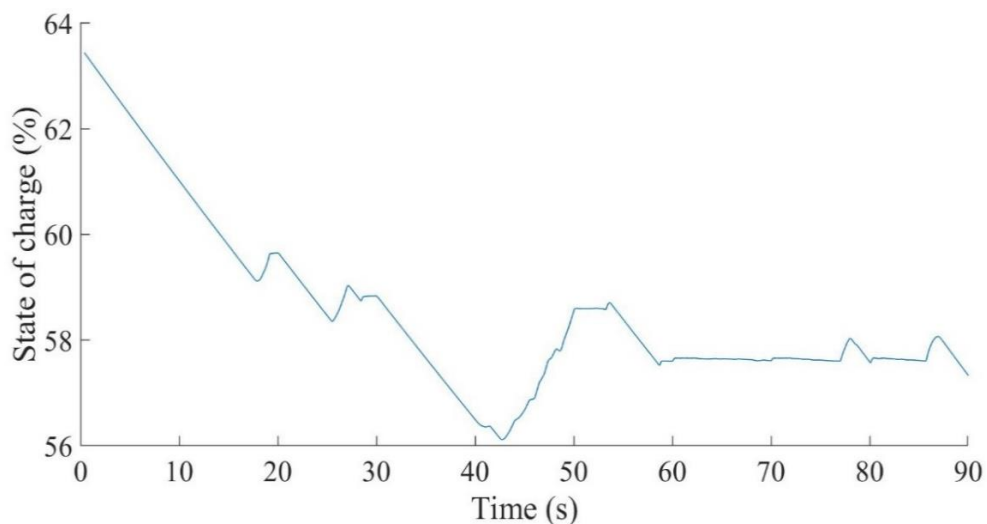
In the case with a 31% initial BES SOC (slightly higher than SOC_{min}), the BES is not allowed to discharge anymore, as previously mentioned. Therefore, the BES can be charged

or maintained at the same level, as shown in Fig. 8.20a. As shown in Fig. 8.20b, the UC has a higher demand (its SOC varies approximately from 63% to 53%), because the BES cannot be discharged. When Fig. 8.20b is compared to Fig. 8.15b, the UC SOC varies less (from 63% to 66%) in the latter, proving that the UC is more demanded when the BES cannot contribute.

Considering the results obtained through simulation for Case 4, it is possible to conclude the correct functioning of the HESS and its respective EMS 3 strategy.



(a)



(b)

Fig. 8.20. Case 4: State of charge for (a) BES starting with low SOC. (b) UC SOC

IV

Future Research and Conclusions

In this section, the main conclusions are drawn from the analyses carried out. The concluding remarks are presented based on the observation of the most important aspects of the study. The evaluation of the hybrid configuration brought the most relevant contributions of this thesis, as presented in this section. Finally, recommendations of future works have the objective to advance in the framework of the current study.

Chapter 9

Conclusions

In this chapter, the conclusions of the thesis and the main contributions of the study are presented.

In summary, the main objective of this thesis was to investigate a large-scale PV power plant and a HESS connected to a type of converter still under development, such as the qZSI. Moreover, the necessary control loops and power dispatch strategies were implemented in all the configurations evaluated. Hence, the challenges of this study involved the topology, the modeling, the dynamic control, and the supervisory energy management system of each configuration.

Part I of the thesis was introductory. From the review of the literature review, it was possible to draw two main conclusions: Efficiency enhancement and integration of storage systems are decisive to promoting the development of intermittent sources. From this part, it was possible to conclude that the most commercialized PV cells technologies are those based on silicon, both mono and poly-crystalline, followed by thin-film cells. As presented, the area required for the power plant is highly dependent on the PV technology, finding that plants of similar powers using thin-film, occupied an area 20% bigger, and three times more PV panels were needed than a plant of similar power which used mono-crystalline panels. Regarding power converters, the configuration most frequently used is based on two stages, a DC/DC and a DC/AC. With regards to the ESS, the trend is a growing installed capacity worldwide, and in the case of batteries, they are considered suitable for PV systems. The technology mostly used today for high power systems is the lithium-ion battery. To meet the requirements for fast response and sufficient power support, it is recommended to combine two or more energy storage systems.

In Part II, the system under study was modeled and the control strategies were presented. This study was crucial, since the efficiency of the plant depends mainly on the operation and control of the converters. The final studied system was composed by PV panels, a qZSI-BES, a DC/DC-ZSC, an UC, and a LCL filter, although in the first simulation

results, the DC/DC-ZSC and UC were not considered. The PV panel technology considered was mono-crystalline, mainly due to its efficiency. For the qZSI-BES, a DM of the system was modeled, and a new SM was proposed, developed, compared, and validated in a HIL system. With this model, it was possible to obtain a substantial time reduction in the simulations, replacing the DM properly for the target simulations of this work. The main limitation of this model is regarding the behavior of the current and voltage harmonics. To connect a HESS, a DC/DC-ZSC converter was needed to control the charge/discharge of the UC. An improved simplified converter model was used in this case. The BES and UC were modeled according to commercially available devices. Moreover, the control loops implemented were described in detail.

The results of the proposed systems were presented and discussed in Part III. Varying irradiation adapted from a real cloudy day was considered to test different operating points. Moreover, grid disturbances were added, as well as a variation on the reactive power reference. Simulation results proved the effectiveness of the proposed hybrid renewable energy system under variable conditions. The system showed a satisfactory performance under grid disturbances and load variations. The SM, when compared to the DM, obtained similar responses for dynamic events, proving the validity of the proposed SM. Only slight differences appeared in the transitory recovery after the grid fault, but these differences were small enough to be neglected in the target simulations of the SM. This new model replaced the DM satisfactorily in long-term simulations, large-scale electric power systems, control design, and dynamic analysis purposes. The HESS presented interesting complementary characteristics that supported the PV generation through the EMS to comply with the grid power requirements. BES and UC lifetime was preserved, since the SOC was maintained between safe levels, and overcharging/overdischarging were avoided. The UC had three main functions: (i) responding to small PV power variations, such as partial shading from clouds; (ii) complementing the BES slow response; and (iii) supplying the additional power demanded that the BES was not able to provide. The control system applied allowed a good model stabilization. The SVM technique was adapted to the qZSI to obtain an appropriate response. A satisfactory regulation of the PV power generation was achieved through the MPPT algorithm and the active power control loop. Furthermore, an adequate variable reference tracking was demonstrated for the reactive power. The three new EMS strategies presented good results and an appropriate power balance.

The main contributions of this thesis were:

- From the review of the literature review, the main features of the PV panels, converters, and energy storage systems were analyzed. Moreover, applications of these systems were presented, based on the available literature. An interesting comparison of the PV panels and ESS technologies highlighted which of the storage/PV materials options are more suitable, according to the intended application.
- It was not possible to find any work in the literature implementing the same configuration as the one presented in this thesis, i.e.: PV system with SM of the qZSI-BES plus SM of DC/DC-ZSC with a UC, connected to grid. Indeed, papers related to qZSI-BES and DC/DC-ZSC can be found, but not in the same system. Most of the qZSI-BES use the DM, and the configurations employed have different elements other than the PV, BES, and/or UC. This new configuration can be mentioned as one important contribution.
- The new SM of qZSI-BES presented an outstanding reduction in the simulation time, precisely 85%, in comparison to the DM. This fact is particularly important for long-term simulations. Moreover, this achievement allowed the application of fuzzy logic, which needs a large computational effort, to perform the energy management between the elements in the power plant.
- The design of the new SM was implemented, assessed, and validated experimentally in laboratory through a TYPHOON HIL system and a dSPACE MicroLabBox control board. This test proved the suitability of this new model to replace the DM in long-term simulations, large-scale electric power systems, control design, and dynamic analysis purposes.
- The control strategy applied to the hybrid system was tested considering fluctuating solar radiation and grid disturbances, and, even with the presence of these disturbances, a proper response was obtained, confirming a satisfactory control operation.
- Three EMS were presented. The first two did not consider the UC, and this element was added in the third one. These strategies allowed the HESS to operate between safe limits. The SO demand was attended, and for one of the

strategies, it was possible to make a profit from the energy price. Moreover, in the configuration with UC, it contributed as a secondary storage source, covering the slow response of the battery, improving the BES lifetime, and acting in small power variations. Fuzzy logic was applied in two of the EMS.

Chapter 10

Future Works

In this chapter, future research areas are indicated as an extension of the work performed in this thesis:

- The use of other storage technologies with different characteristics can be added to the configuration presented herein, comparing which option is more interesting from the technical and economical point of view. Research in storage devices combined with fluctuating renewable energy generation, such as PV or wind, is increasing and needed.
- Other storage units, such as electric vehicles and hydrogen systems could also be added to the same configuration presented, similarly to the UC connected through a DC/DC-ZSC. The use of hydrogen and electric vehicles is also a current trend, with great perspectives for the future, and further research is needed. Moreover, the hydrogen system can be at the same time a storage and generation source.
- Other renewable generation sources, different from PV, and the addition of loads can be considered in this topology. In addition, different converter types and associations could embrace different generation units, in unique or various sharing points.
- Other EMS strategies, adding optimized systems, can generate interesting results.
- The application of model predictive control to the solar radiation can anticipate information for the hybrid plant, and therefore, optimize its operation.
- Advanced control techniques can be relevant to regulate the power delivered to the grid while ensuring a stable and satisfactory operation.
- The same study presented in this thesis can be performed considering the variable cost of energy to obtain more profitable systems.

- The EMS proposed in this thesis did not study the energy market in depth. Considering a real behavior of the electricity market could improve the results to coincide more reliable with the actual market performance.

Bibliography

- [1] Z. Cabrane, M. Ouassaid, and M. Maaroufi, “Analysis and evaluation of battery-supercapacitor hybrid energy storage system for photovoltaic installation,” *Int. J. Hydrogen Energy*, vol. 41, no. 45, pp. 20897–20907, 2016, doi: 10.1016/j.ijhydene.2016.06.141.
- [2] R. Rajesh and M. C. Mabel, “A comprehensive review of photovoltaic systems,” *Renew. Sustain. Energy Rev.*, vol. 51, pp. 231–248, 2015, doi: 10.1016/j.rser.2015.06.006.
- [3] A. Luque and S. Hegedus, *Handbook of Photovoltaic Science*. 2003.
- [4] V. V. Tyagi, N. A. A. Rahim, N. A. Rahim, and J. A. L. Selvaraj, “Progress in solar PV technology: Research and achievement,” *Renew. Sustain. Energy Rev.*, vol. 20, pp. 443–461, 2013, doi: 10.1016/j.rser.2012.09.028.
- [5] S. Kijima and T. Nakada, “High-temperature degradation mechanism of Cu(In,Ga)Se₂-based thin film solar cells,” *Appl. Phys. Express*, vol. 1, no. 7, pp. 0750021–0750023, 2008, doi: 10.1143/APEX.1.075002.
- [6] T. Ameri, G. Dennler, C. Lungenschmied, and C. J. Brabec, “Organic tandem solar cells: A review,” *Energy Environ. Sci.*, vol. 2, no. 4, pp. 347–363, 2009, doi: 10.1039/b817952b.
- [7] A. Review, “The Applications of Polymers in Solar Cells :,” no. 3, pp. 1–46, 2019.
- [8] M. Jørgensen, K. Norrman, and F. C. Krebs, “Stability/degradation of polymer solar cells,” *Sol. Energy Mater. Sol. Cells*, vol. 92, no. 7, pp. 686–714, 2008, doi: 10.1016/j.solmat.2008.01.005.
- [9] M. Itoh, H. Takahashi, T. Fujii, H. Takakura, Y. Hamakawa, and Y. Matsumoto, “Evaluation of electric energy performance by democratic module PV system field test,” *Sol. Energy Mater. Sol. Cells*, vol. 67, no. 1–4, pp. 435–440, Mar. 2001, doi: 10.1016/S0927-0248(00)00312-3.

- [10] L. Wu, W. Tian, and X. Jiang, “Silicon-based solar cell system with a hybrid PV module,” *Sol. Energy Mater. Sol. Cells*, vol. 87, no. 1–4, pp. 637–645, May 2005, doi: 10.1016/j.solmat.2004.09.018.
- [11] M.-E. Yeoh and K.-Y. Chan, “Recent advances in photo-anode for dye-sensitized solar cells: a review,” *Int. J. Energy Res.*, vol. 41, no. 15, pp. 2446–2467, Dec. 2017, doi: 10.1002/er.3764.
- [12] Z. Zhao, H. Xiao, and Y. Yang, “Improved coordinated control strategy of hybrid energy storages in PV Power Smoothing,” *Energy Procedia*, vol. 145, pp. 151–156, 2018, doi: 10.1016/j.egypro.2018.04.026.
- [13] Fraunhofer Institute for Solar Energy Systems, “Photovoltaics Report,” Freiburg, 2021. [Online]. Available: www.ise.fraunhofer.de.
- [14] NREL, “PV modules and cell efficiencies,” Golden, 2021. [Online]. Available: www.nrel.gov.
- [15] A. Goodrich, T. James, and M. Woodhouse, “Residential, commercial, and utilityscale photovoltaic (PV) System prices in the United States: Current drivers and cost-reduction opportunities,” 2012.
- [16] V. Benda and L. Černá, “PV cells and modules – State of the art, limits and trends,” *Heliyon*, vol. 6, no. 12, 2020, doi: 10.1016/j.heliyon.2020.e05666.
- [17] S. Energy, “Photovoltaics report,” no. August, 2018.
- [18] A. Cabrera, E. Bullich, M. Aragués, and O. Gomis-Bellmunt, “Topologies for large scale photovoltaic power plants,” *Renew. Sustain. energy Rev.*, vol. 59, pp. 309–319, 2016, doi: 10.1016/j.rser.2015.12.362.
- [19] P. Frankl, E. Menichetti, M. Raugei, S. Lombardelli, and G. Prennushi, “New Energy Externalities Developments for Sustainability ‘ Final report on technical data , costs and life cycle inventories of PV applications ,” pp. 1–81, 2006.
- [20] T. M. Razykov, C. S. Ferekides, D. Morel, E. Stefanakos, H. S. Ullal, and H. M. Upadhyaya, “Solar photovoltaic electricity: Current status and future prospects,” *Sol. Energy*, vol. 85, no. 8, pp. 1580–1608, 2011, doi: 10.1016/j.solener.2010.12.002.

- [21] I. Hadjipaschalis, A. Poullikkas, and V. Efthimiou, “Overview of current and future energy storage technologies for electric power applications,” *Renew. Sustain. Energy Rev.*, vol. 13, no. 6–7, pp. 1513–1522, 2009, doi: 10.1016/j.rser.2008.09.028.
- [22] European Commission, “Energy storage – the role of electricity,” Brussels, 2017. [Online]. Available: https://ec.europa.eu/energy/sites/ener/files/documents/swd2017_61_document_travail_service_part1_v6.pdf.
- [23] M. E. Amiryar and K. R. Pullen, “A review of flywheel energy storage system technologies and their applications,” *Appl. Sci.*, vol. 7, no. 3, 2017, doi: 10.3390/app7030286.
- [24] A. G. Olabi, T. Wilberforce, M. A. Abdelkareem, and M. Ramadan, “Critical review of flywheel energy storage system,” *Energies*, vol. 14, no. 8, pp. 1–33, 2021, doi: 10.3390/en14082159.
- [25] H. IBRAHIM, A. ILINCA, and J. PERRON, “Energy storage systems—Characteristics and comparisons,” *Renew. Sustain. Energy Rev.*, vol. 12, no. 5, pp. 1221–1250, Jun. 2008, doi: 10.1016/j.rser.2007.01.023.
- [26] H. Chen, T. N. Cong, W. Yang, C. Tan, Y. Li, and Y. Ding, “Progress in electrical energy storage system: A critical review,” *Prog. Nat. Sci.*, vol. 19, no. 3, pp. 291–312, 2009, doi: 10.1016/j.pnsc.2008.07.014.
- [27] A. P. Karpinski, B. Makovetski, S. J. Russell, J. R. Serenyi, and D. C. Williams, “Silver – zinc : status of technology and applications,” no. February, 1999.
- [28] P. P. Lopes and V. R. Stamenkovic, “Past, present, and future of lead–acid batteries,” *Science (80-.)*, vol. 369, no. 6506, pp. 923–924, Aug. 2020, doi: 10.1126/science.abd3352.
- [29] N. Omar *et al.*, *Analysis of Nickel-Based Battery Technologies for Hybrid and Electric Vehicles*. Elsevier Inc., 2014.
- [30] D. Deng, “Li-ion batteries: Basics, progress, and challenges,” *Energy Sci. Eng.*, vol. 3, no. 5, pp. 385–418, 2015, doi: 10.1002/ese3.95.
- [31] O. M. Toledo, D. Oliveira Filho, and A. S. A. C. Diniz, “Distributed photovoltaic

- generation and energy storage systems: A review,” *Renew. Sustain. Energy Rev.*, vol. 14, no. 1, pp. 506–511, 2010, doi: 10.1016/j.rser.2009.08.007.
- [32] H. Akbari *et al.*, “Efficient energy storage technologies for photovoltaic systems,” *Sol. Energy*, no. March, pp. 1–25, 2018, doi: 10.1016/j.solener.2018.03.052.
- [33] IEC, “Electrical Energy Storage - White Paper,” *Int. Electrotech. Comm.*, pp. 1–78, 2011, doi: 10.1002/bse.3280020501.
- [34] A. Berrueta, A. Ursua, I. S. Martin, A. Eftekhari, and P. Sanchis, “Supercapacitors: Electrical Characteristics, Modeling, Applications, and Future Trends,” *IEEE Access*, vol. 7, pp. 50869–50896, 2019, doi: 10.1109/ACCESS.2019.2908558.
- [35] “ESA - Energy Storage Association.” <http://energystorage.org/> (accessed Aug. 28, 2018).
- [36] IRENA, *Hydrogen From Renewable Power: Technology outlook for the energy transition*, no. September. 2018.
- [37] H. S. H. Chung, H. Wang, F. Blaabjerg, and M. Pecht, *Reliability of power electronic converter systems*. 2016.
- [38] S. Piasecki, J. Zaleski, M. Jasinski, S. Bachman, and M. Turzyński, “Analysis of AC/DC/DC Converter Modules for Direct Current Fast-Charging Applications,” *Energies*, vol. 14, no. 19, p. 6369, Oct. 2021, doi: 10.3390/en14196369.
- [39] M. M. Canteli, “Regulación, control y protección de Máquinas Eléctricas,” pp. 1–52, 2010.
- [40] A. Cabrera-Tobar, E. Bullich-Massagué, M. Aragüés-Peñalba, and O. Gomis-Bellmunt, “Topologies for large scale photovoltaic power plants,” *Renew. Sustain. Energy Rev.*, vol. 59, pp. 309–319, 2016, doi: 10.1016/j.rser.2015.12.362.
- [41] S. Sheik Mohammed, D. Devaraj, and T. P. Imthias Ahamed, “A novel hybrid Maximum Power Point Tracking Technique using Perturb & Observe algorithm and Learning Automata for solar PV system,” *Energy*, vol. 112, pp. 1096–1106, 2016, doi: 10.1016/j.energy.2016.07.024.
- [42] M. Mao, L. Zhang, P. Duan, Q. Duan, and M. Yang, “Grid-connected modular PV-

- Converter system with shuffled frog leaping algorithm based DMPPT controller,” *Energy*, vol. 143, pp. 181–190, 2018, doi: 10.1016/j.energy.2017.10.099.
- [43] L. Barelli *et al.*, “Comparative analysis of AC and DC bus configurations for flywheel-battery HESS integration in residential micro-grids,” *Energy*, vol. 204, 2020, doi: 10.1016/j.energy.2020.117939.
- [44] Y. Liu, H. Abu-Rub, B. Ge, F. Blaabjerg, O. Ellabban, and P. C. Loh, *Impedance Source Power Electronic Converters*. Wiley, 2016.
- [45] V. F. Pires, E. Romero-cadaval, D. Vinnikov, I. Roasto, and J. F. Martins, “Power converter interfaces for electrochemical energy storage systems – A review,” *Energy Convers. Manag.*, vol. 86, pp. 453–475, 2014, doi: <http://dx.doi.org/10.1016/j.enconman.2014.05.003>.
- [46] Fang Zheng Peng, “Z-source inverter,” *IEEE Trans. Ind. Appl.*, vol. 39, no. 2, pp. 504–510, 2003, doi: 10.1109/TIA.2003.808920.
- [47] M. Shen, A. Joseph, J. Wang, F. Z. Peng, and D. J. Adams, “Comparison of traditional inverters and Z-source inverter for fuel cell vehicles,” *IEEE Trans. Power Electron.*, vol. 22, no. 4, pp. 1453–1463, 2007, doi: 10.1109/TPEL.2007.900505.
- [48] J. Anderson and F. Z. Peng, “A Class of Quasi-Z-Source Inverters,” in *IEEE Industry Applications Society Annual Meeting*, 2008, pp. 1–7.
- [49] O. Ellabban and H. Abu-rub, “An overview for the Z-Source Converter in motor drive applications,” *Renew. Sustain. Energy Rev.*, vol. 61, pp. 537–555, 2016.
- [50] G. Zhang, Z. Li, B. Zhang, and W. A. Halang, “Power electronics converters : Past , present and future,” *Renew. Sustain. Energy Rev.*, vol. 81, no. May 2016, pp. 2028–2044, 2018, doi: 10.1016/j.rser.2017.05.290.
- [51] D. Vinnikov, I. Roasto, R. Strzelecki, and M. Adamowicz, “Step-up DC/DC converters with cascaded quasi-Z-source network,” *IEEE Trans. Ind. Electron.*, vol. 59, no. 10, pp. 3727–3736, 2012, doi: 10.1109/TIE.2011.2178211.
- [52] B. Poorali, “Improved High Step-Up Z -Source DC – DC Converter,” *IEEE Trans. Power Electron.*, vol. 33, no. 11, pp. 9647–9655, 2018.

- [53] M. Ortega, M. V. Ortega, F. Jurado, J. Carpio, and D. Vera, "Bidirectional DC–DC converter with high gain based on impedance source," *IET Power Electron.*, vol. 12, no. 8, pp. 2069–2078, 2019, doi: 10.1049/iet-pel.2018.5385.
- [54] Y. Li, F. Z. Peng, J. G. Cintron-rivera, and S. Jiang, "Controller Design for Quasi-Z-Source Inverter in Photovoltaic Systems," *2010 IEEE Energy Convers. Congr. Expo.*, pp. 3187–3194, 2010, doi: 10.1109/ECCE.2010.5618288.
- [55] Y. Li, S. Jiang, S. Member, J. G. Cintron-rivera, S. Member, and A. T. Z-source, "Modeling and Control of Quasi-Z-Source Inverter for Distributed Generation Applications," *IEEE Trans. Ind. Electron.*, vol. 60, no. 4, pp. 1532–1541, 2013, doi: 10.1109/TIE.2012.2213551.
- [56] M. Mosa, H. Abu-Rub, and J. Rodriguez, "High performance predictive control applied to three phase grid connected Quasi-Z-Source Inverter," *IECON Proc. (Industrial Electron. Conf.)*, vol. 1, no. c, pp. 5812–5817, 2013, doi: 10.1109/IECON.2013.6700087.
- [57] S. Bloomfield, C. Roberts, and M. Cotterell, "Batteries and Solar Power: Guidance for domestic and small commercial consumers," *Build. Res. Establ.*, 2016, [Online]. Available: www.bre.co.uk.
- [58] A. Mariaud, S. Acha, N. Ekins-Daukes, and N. Shah, "Integrated Optimisation of PV and Battery Storage Systems for UK Non- Domestic buildings," *ASHRAE Annu. Conf. Proceedings, June 24 - June 28*, vol. 199, pp. 1–8, 2017.
- [59] I. Grgi, M. Basic, and D. Vukadinovic, "Optimization of electricity production in a grid-tied solar power system with a three-phase quasi-Z-source inverter," *J. Clean. Prod.*, vol. 221, pp. 656–666, 2019, doi: <https://doi.org/10.1016/j.jclepro.2019.02.245>.
- [60] D. Ghaderi, S. Padmanaban, P. K. Maroti, B. Papari, and J. B. Holm-nielsen, "Design and implementation of an improved sinusoidal controller for a two-phase enhanced impedance source boost," *Comput. Electr. Eng.*, vol. 83, no. 106575, 2020, doi: <https://doi.org/10.1016/j.compeleceng.2020.106575>.
- [61] Y. Liu, B. Ge, H. Abu-Rub, and F. Z. Peng, "Overview of space vector modulations

- for three-phase Z-Source/quasi-z- source inverters,” *IEEE Trans. Power Electron.*, vol. 29, no. 4, pp. 2098–2108, 2014.
- [62] A. R. Yilmaz and B. Erkmén, “FPGA-Based Space Vector PWM and Closed Loop Controllers Design for the Z Source Inverter,” *IEEE Access*, vol. 7, pp. 130865–130873, 2019, doi: 10.1109/ACCESS.2019.2940670.
- [63] M. Mosa, R. S. Balog, and H. Abu-Rub, “High-performance predictive control of quasi-impedance source inverter,” *IEEE Trans. Power Electron.*, vol. 32, no. 4, pp. 3251–3262, 2017, doi: 10.1109/TPEL.2016.2531989.
- [64] D. Sun, B. Ge, D. Bi, and F. Z. Peng, “Analysis and control of quasi-Z source inverter with battery for grid-connected PV system q,” *Int. J. Electr. Power Energy Syst.*, vol. 46, no. 2009, pp. 234–240, 2013, doi: 10.1016/j.ijepes.2012.10.008.
- [65] B. Ge *et al.*, “An energy-stored quasi-Z-source inverter for application to photovoltaic power system,” *IEEE Trans. Ind. Electron.*, vol. 60, no. 10, pp. 4468–4481, 2013, doi: 10.1109/TIE.2012.2217711.
- [66] D. Sun, B. Ge, W. Liang, H. Abu-Rub, and F. Z. Peng, “An energy stored Quasi-Z-Source cascade multilevel inverter-based photovoltaic power generation system,” *IEEE Trans. Ind. Electron.*, vol. 62, no. 9, pp. 5458–5467, 2015, doi: 10.1109/TIE.2015.2407853.
- [67] Y. Liu, B. Ge, H. Abu-Rub, and F. Z. Peng, “Modelling and controller design of quasi-Z-source inverter with battery-based photovoltaic power system,” *IET Power Electron.*, vol. 7, no. 7, pp. 1665–1674, 2014, doi: 10.1049/iet-pel.2013.0389.
- [68] A. Guichi, A. Talha, E. Madjid, and S. Mekhilef, “Energy management and performance evaluation of grid connected PV- battery hybrid system with inherent control scheme,” *Sustain. Cities Soc.*, vol. 41, no. May, pp. 490–504, 2018, doi: 10.1016/j.scs.2018.05.026.
- [69] C. Sing, Y. Jia, L. Lei, Z. Xu, M. D. McCulloch, and K. Po, “A comprehensive review on large-scale photovoltaic system with applications of electrical energy storage,” *Renew. Sustain. Energy Rev.*, vol. 78, no. November 2016, pp. 439–451, 2017, doi: 10.1016/j.rser.2017.04.078.

- [70] C. S. Lai, Y. Jia, L. L. Lai, Z. Xu, M. D. McCulloch, and K. P. Wong, “A comprehensive review on large-scale photovoltaic system with applications of electrical energy storage,” *Renew. Sustain. Energy Rev.*, vol. 78, no. November 2016, pp. 439–451, 2017, doi: 10.1016/j.rser.2017.04.078.
- [71] P. Denholm, J. Eichman, and R. Margolis, “Evaluating the Technical and Economic Performance of PV Plus Storage Power Plants : Report Summary,” 2017.
- [72] V. Viju Nair *et al.*, “Large Scale Grid Integration of Photovoltaic and Energy Storage Systems Using Triple Port Dual Active Bridge Converter Modules,” *IEEE Power Energy Soc. Gen. Meet.*, vol. 2018-Augus, 2018, doi: 10.1109/PESGM.2018.8586158.
- [73] M. Periyamayagam, V. Suresh Kumar, B. Chokkalingam, S. Padmanaban, L. Mihet-Popa, and Y. Adedayo, “A modified high voltage gain quasi-impedance source coupled inductor multilevel inverter for photovoltaic application,” *Energies*, vol. 13, no. 4, 2020, doi: 10.3390/en13040874.
- [74] J. Yuan, Y. Yang, and F. Blaabjerg, “A switched quasi-Z-source inverter with continuous input currents,” *Energies*, vol. 16, no. 3, 2020, doi: 10.3390/en13061390.
- [75] D. Sun, B. Ge, W. Liang, H. Abu-rub, and S. Member, “An Energy Stored Quasi-Z-Source Cascade Multilevel Inverter-Based Photovoltaic,” vol. 62, no. 9, pp. 5458–5467, 2015.
- [76] A. Reimuth, V. Locherer, M. Danner, and W. Mauser, “How do changes in climate and consumption loads affect residential PV coupled battery energy systems?,” *Energy*, vol. 198, p. 117339, 2020, doi: 10.1016/j.energy.2020.117339.
- [77] R. van Haaren, M. Morjaria, and V. Fthenakis, “An energy storage algorithm for ramp rate control of utility scale PV (photovoltaics) plants,” *Energy*, vol. 91, pp. 894–902, 2015, doi: 10.1016/j.energy.2015.08.081.
- [78] V. Kamala Devi, K. Premkumar, and A. Bisharathu Beevi, “Energy management using battery intervention power supply integrated with single phase solar roof top installations,” *Energy*, vol. 163, pp. 229–244, 2018, doi: 10.1016/j.energy.2018.08.085.

- [79] G. Angenendt, S. Zurmühlen, J. Figgner, K. P. Kairies, and D. U. Sauer, “Providing frequency control reserve with photovoltaic battery energy storage systems and power-to-heat coupling,” *Energy*, vol. 194, p. 116923, 2020, doi: 10.1016/j.energy.2020.116923.
- [80] N. Chettibi and A. Mellit, “Intelligent control strategy for a grid connected PV/SOFC/BESS energy generation system,” *Energy*, vol. 147, pp. 239–262, 2018, doi: 10.1016/j.energy.2018.01.030.
- [81] J. Khajesalehi, M. Hamzeh, K. Sheshyekani, and E. Afjei, “Modeling and control of quasi Z-source inverters for parallel operation of battery energy storage systems: Application to microgrids,” *Electr. Power Syst. Res.*, vol. 125, pp. 164–173, 2015, doi: 10.1016/j.epsr.2015.04.004.
- [82] J. Khajesalehi, K. Sheshyekani, M. Hamzeh, and E. Afjei, “High-performance hybrid photovoltaic -battery system based on quasi-Z-source inverter: Application in microgrids,” *IET Gener. Transm. Distrib.*, vol. 9, no. 10, pp. 895–902, 2015, doi: 10.1049/iet-gtd.2014.0336.
- [83] S. Rahman *et al.*, “Design and Implementation of Cascaded Multilevel qZSI Powered Single-Phase Induction Motor for Isolated Grid Water Pump Application,” *IEEE Trans. Ind. Appl.*, vol. 56, no. 2, pp. 1907–1917, 2020, doi: 10.1109/TIA.2019.2959734.
- [84] M. Moslehi, H. Madadi, and M. Ali, “Control of a new stand-alone wind turbine-based variable speed permanent magnet synchronous generator using quasi-Z-source inverter,” *Electr. Power Syst. Res.*, vol. 177, no. March, p. 106010, 2019, doi: 10.1016/j.epsr.2019.106010.
- [85] S. Hu, Z. Liang, D. Fan, and X. He, “Hybrid Ultracapacitor-Battery Energy Storage System Based on Quasi-Z-source Topology and Enhanced Frequency Dividing Coordinated Control for EV,” *IEEE Trans. Power Electron.*, vol. 31, no. 11, pp. 7598–7610, 2016, doi: 10.1109/TPEL.2016.2518749.
- [86] M. Farrokhadi *et al.*, “Microgrid Stability Definitions, Analysis, and Examples,” *IEEE Trans. Power Syst.*, vol. 35, no. 1, pp. 13–29, Jan. 2020, doi: 10.1109/TPWRS.2019.2925703.

- [87] X. Li, L. Yao, and D. Hui, “Optimal control and management of a large-scale battery energy storage system to mitigate fluctuation and intermittence of renewable generations,” *J. Mod. Power Syst. Clean Energy*, vol. 4, no. 4, pp. 593–603, 2016, doi: 10.1007/s40565-016-0247-y.
- [88] A. A. Solomon, D. Faiman, and G. Meron, “Appropriate storage for high-penetration grid-connected photovoltaic plants,” *Energy Policy*, vol. 40, no. 1, pp. 335–344, 2012, doi: 10.1016/j.enpol.2011.10.019.
- [89] G. Zini, “Hydrogen Systems for Large-Scale PV plants: Simulation with real forecast and production data,” *8th Int. Renew. Energy Storage Conf. Exhib. (IRES 2013)*, vol. 9, no. november, pp. 1–25, 2013.
- [90] S. Dahbi, A. Aziz, A. Messaoudi, I. Mazozi, K. Kassmi, and N. Benazzi, “Management of excess energy in a photovoltaic/grid system by production of clean hydrogen,” *Int. J. Hydrogen Energy*, vol. 43, no. 10, pp. 5283–5299, 2018, doi: 10.1016/j.ijhydene.2017.11.022.
- [91] G. S. Georgiou, P. Christodoulides, and S. A. Kalogirou, “Optimizing the energy storage schedule of a battery in a PV grid-connected nZEB using linear programming,” *Energy*, vol. 208, p. 118177, 2020, doi: 10.1016/j.energy.2020.118177.
- [92] A. Youssef, M. El-Telbany, and A. Zekry, “The role of artificial intelligence in photovoltaic systems design and control: A review,” *Renew. Sustain. Energy Rev.*, vol. 78, no. April 2016, pp. 72–79, 2017, doi: 10.1016/j.rser.2017.04.046.
- [93] A. Mellit and S. A. Kalogirou, “Artificial intelligence techniques for photovoltaic applications: A review,” *Prog. Energy Combust. Sci.*, vol. 34, no. 5, pp. 574–632, 2008, doi: 10.1016/j.peccs.2008.01.001.
- [94] P. K. Gayen and A. Jana, “An ANFIS based improved control action for single phase utility or micro-grid connected battery energy storage system,” *J. Clean. Prod.*, vol. 164, pp. 1034–1049, 2017, doi: 10.1016/j.jclepro.2017.07.007.
- [95] T. Wang, H. Kamath, and S. Willard, “Control and Optimization of Grid-Tied Photovoltaic Storage Systems Using Model Predictive Control,” vol. 5, no. 2, pp.

1010–1017, 2014.

- [96] D. Q. Oliveira, A. C. Zambroni de Souza, M. V. Santos, A. B. Almeida, B. I. L. Lopes, and O. R. Saavedra, “A fuzzy-based approach for microgrids islanded operation,” *Electr. Power Syst. Res.*, vol. 149, pp. 178–189, 2017, doi: 10.1016/j.epsr.2017.04.019.
- [97] S. Tamalouzt, N. Benyahia, T. Rekioua, D. Rekioua, and R. Abdessemed, “Performances analysis of WT-DFIG with PV and fuel cell hybrid power sources system associated with hydrogen storage hybrid energy system,” *International Journal of Hydrogen Energy*, vol. 41, no. 45, pp. 21006–21021, 2016, doi: 10.1016/j.ijhydene.2016.06.163.
- [98] S. Dadfar, K. Wakil, M. Khaksar, A. Rezvani, M. R. Miveh, and M. Gandomkar, “Enhanced control strategies for a hybrid battery/photovoltaic system using FGS-PID in grid-connected mode,” *Int. J. Hydrogen Energy*, vol. 44, no. 29, pp. 14642–14660, Jun. 2019, doi: 10.1016/j.ijhydene.2019.04.174.
- [99] E. I. Batzelis, S. A. Papathanassiou, S. Member, and B. C. Pal, “PV System Control to Provide Active Power Reserves Under Partial Shading Conditions,” *IEEE Trans. Power Electron.*, vol. 33, no. 11, pp. 9163–9175, 2018, doi: 10.1109/TPEL.2018.2823426.
- [100] A. Raj and R. P. Praveen, “Highly efficient DC-DC boost converter implemented with improved MPPT algorithm for utility level photovoltaic applications,” *Ain Shams Eng. J.*, no. xxxx, 2021, doi: 10.1016/j.asej.2021.10.012.
- [101] Z. Xie and Z. Wu, “A flexible power point tracking algorithm for photovoltaic system under partial shading condition,” *Sustain. Energy Technol. Assessments*, vol. 49, no. November 2021, p. 101747, 2022, doi: 10.1016/j.seta.2021.101747.
- [102] M. Technologies, “160V 8F Ultracapacitor Datasheet.” pp. 1–7, 2021, [Online]. Available: <https://maxwell.com/products/ultracapacitors/downloads/>.
- [103] Y. Liu, H. Abu-Rub, B. Ge, F. Blaabjerg, O. Ellabban, and P. C. Loh, *Impedance Source Power Electronic Converters*. Wiley-IEEE Press, 2016.
- [104] Y. Liu, H. Abu-Rub, B. Ge, F. Blaabjerg, O. Ellabban, and P. C. Loh, *Impedance*

source power electronic converters. 2016.

- [105] L. de Oliveira-Assis *et al.*, “Simplified model of battery energy-stored quasi-Z-source inverter-based photovoltaic power plant with Twofold energy management system,” *Energy*, no. xxxx, p. 122563, 2021, doi: 10.1016/j.energy.2021.122563.
- [106] T. M. SimPowerSystems, “Reference, Hydro-Québec and the MathWorks,” *Inc., Natick, MA*, 2015.
- [107] R. Dufo-López, T. Cortés-Arcos, J. S. Artal-Sevil, and J. L. Bernal-Agustín, “Comparison of lead-acid and li-ion batteries lifetime prediction models in stand-alone photovoltaic systems,” *Appl. Sci.*, vol. 11, no. 3, pp. 1–16, 2021, doi: 10.3390/app11031099.
- [108] M. Beaudin, H. Zareipour, A. Schellenberglabe, and W. Rosehart, “Energy storage for mitigating the variability of renewable electricity sources: An updated review,” *Energy Sustain. Dev.*, vol. 14, no. 4, pp. 302–314, 2010, doi: 10.1016/j.esd.2010.09.007.
- [109] W.-P. Hong, “A Matlab/Simulink-Based PV array-Supercapacitor Model Employing SimPowerSystem and Stateflow Tool Box,” *J. Korean Inst. Illum. Electr. Install. Eng.*, vol. 28, no. 12, pp. 18–29, 2014, doi: 10.5207/jieie.2014.28.12.018.
- [110] R. Sarrias-Mena, L. M. Fernández-Ramírez, C. A. García-Vázquez, and F. Jurado, “Fuzzy logic based power management strategy of a multi-MW doubly-fed induction generator wind turbine with battery and ultracapacitor,” *Energy*, vol. 70, pp. 561–576, 2014, doi: 10.1016/j.energy.2014.04.049.
- [111] S. Shah and I. Pels, “Step-by-step Design of an LCL Filter for Three-phase Grid Interactive Converter,” no. August, 2015, doi: 10.13140/RG.2.1.3883.6964.
- [112] M. Liserre, F. Blaabjerg, and S. Hansen, “Design and control of an LCL-filter-based three-phase active rectifier,” *IEEE Trans. Ind. Appl.*, vol. 41, no. 5, pp. 1281–1291, 2005, doi: 10.1109/TIA.2005.853373.
- [113] D. Krug and S. Bernet, “Design and Comparison of Medium Voltage Multi-Level Converters for Industry Applications,” *Conf. Rec. 2004 IEEE Ind. Appl. Conf. 2004. 39th IAS Annu. Meet.*, vol. 2, pp. 781–790 vol.2, 2004, doi:

10.1109/IAS.2004.1348503.

- [114] M. T. E. Kahn, “A pattern for LCL filter design for renewable power,” in *ISERD International Conference*, 2018, no. March, pp. 5–10.
- [115] F. Z. Peng, “Z-Source Inverter,” vol. 39, no. 2, pp. 504–510, 2003.
- [116] F. Z. Peng, M. Shen, S. Member, Z. Qian, and S. Member, “Maximum Boost Control of the Z-Source Inverter,” vol. 20, no. 4, pp. 833–838, 2005.
- [117] M. Shen, J. Wang, A. Joseph, F. Z. Peng, L. M. Tolbert, and D. J. Adams, “Maximum Constant Boost Control of the Z-Source Inverter,” *Conf. Rec. 2004 IEEE Ind. Appl. Conf. 2004. 39th IAS Annu. Meet.*, vol. 1, pp. 142–147, 2004, doi: 10.1109/IAS.2004.1348400.
- [118] Texas Instruments, “Field Orientated Control of 3-Phase AC-Motors,” *Control*, no. February, p. 20, 1998.
- [119] Y. Liu, B. Ge, H. Abu-Rub, and F. Z. Peng, “Overview of space vector modulations for three-phase Z-Source/quasi-z- source inverters,” *IEEE Trans. Power Electron.*, vol. 29, no. 4, pp. 2098–2108, 2014, doi: 10.1109/TPEL.2013.2269539.
- [120] A. Yazdani and R. Iravani, *Voltage-sourced converters in power systems: modeling, control, and applications*. John Wiley & Sons, 2010.
- [121] P. García, J. P. Torreglosa, L. M. Fernández, and F. Jurado, “Improving long-term operation of power sources in off-grid hybrid systems based on renewable energy, hydrogen and battery,” *J. Power Sources*, vol. 265, pp. 149–159, Nov. 2014, doi: 10.1016/j.jpowsour.2014.04.118.
- [122] Z. Roumila, D. Rekioua, and T. Rekioua, “Energy management based fuzzy logic controller of hybrid system wind/photovoltaic/diesel with storage battery,” *Int. J. Hydrogen Energy*, vol. 42, no. 30, pp. 19525–19535, 2017, doi: 10.1016/j.ijhydene.2017.06.006.
- [123] Omie, “Day-ahead hourly price,” 2021. <https://www.omie.es/en/market-results/daily/daily-market/daily-hourly-price?scope=daily&date=2021-04-20> (accessed Apr. 20, 2021).

- [124] M. Verij Kazemi, M. Moradi, and R. Verij Kazemi, "Minimization of powers ripple of direct power controlled DFIG by fuzzy controller and improved discrete space vector modulation," *Electr. Power Syst. Res.*, vol. 89, pp. 23–30, 2012, doi: 10.1016/j.epsr.2012.02.008.
- [125] G. Capizzi and G. Tina, "Long-term operation optimization of integrated generation systems by fuzzy logic-based management," *Energy*, vol. 32, no. 7, pp. 1047–1054, 2007, doi: 10.1016/j.energy.2006.07.020.

List of publications

Publications in journals indexed in JCR-SCIE:

1. de Oliveira-Assis, L., Garcia-Triviño, P., Soares-Ramos, E. P. P., Sarrias-Mena, R., Garcia-Vazquez, C. A., Ugalde-Loo, C. E., Fernandez-Ramirez, L. M. “Optimal energy management system using biogeography based optimization for grid-connected MVDC microgrid with photovoltaic, hydrogen system, electric vehicles and Z-source converters”. *Energy Conversion and Management*. v.248, p.114808, 2021.
DOI: <https://doi.org/10.1016/j.enconman.2021.114808>
JCR: 9.709 (Q1)
2. de Oliveira-Assis, L., Soares-Ramos, E.P.P., Sarrias-Mena, R., García-Triviño, P., González-Rivera, E., Sánchez-Sainz, H., Llorens-Iborra, F., Fernández-Ramírez, L.M. “Simplified Model of Battery Energy-Stored Quasi-Z-Source Inverter-Based Photovoltaic Power Plant with Twofold Energy Management System”. *Energy* 2021.
DOI: <https://doi.org/10.1016/j.energy.2021.122563>
JCR: 7.147 (Q1)
3. Soares-Ramos, E. P. P., de Oliveira-Assis, L., Sarrias-Mena, R., Garcia-Triviño, P., Garcia-Vazquez, C. A., Fernandez-Ramirez, Luis M. “Averaged Dynamic Modelling and Control of a Quasi-Z-Source Inverter for Wind Power Applications”. *IEEEAccess*. v.9, p.1 - 1, 2021.
DOI: [10.1109/ACCESS.2021.3104797](https://doi.org/10.1109/ACCESS.2021.3104797)
JCR: 3.367 (Q1)
4. Soares-Ramos, E. P. P., de Oliveira-Assis, L., Sarrias-Mena, R., Fernandez-Ramirez, L. M. “Current status and future trends of offshore wind power in Europe”. *Energy*, v.202, p.117787- ,2020.
DOI: <https://doi.org/10.1016/j.energy.2020.117787>
JCR: 7.147 (Q1)
5. H. Abouobaida, Y. Abouelmahjoub, de Oliveira-Assis, L. “New open circuit fault detection in a DC-DC converter,” *Int. Trans. Electr. Energy Syst.*, vol. 31, no. 11, pp. 1–12, 2021,
DOI: <https://doi.org/10.1002/2050-7038.13094>
SJR: 0.428 (Q2)

Communications in international congresses with peer review:

1. de Oliveira-Assis, L., Soares-Ramos, E. P. P., Sarrias-Mena, R., García-Triviño, P., Fernandez-Ramirez, L. M. “Large-Scale Grid Connected Quasi-Z-Source Inverter-Based PV Power Plant” In: *2020 IEEE International Conference on Environment and Electrical Engineering and 2020 IEEE Industrial and Commercial Power Systems Europe (EEEIC / I&CPS Europe)*, 2020, Madrid.
DOI: [10.1109/EEEIC/ICPSEurope49358.2020.9160529](https://doi.org/10.1109/EEEIC/ICPSEurope49358.2020.9160529)
2. de Oliveira-Assis, L., Soares-Ramos, E. P. P., García-Triviño, P., Sarrias-Mena, R., Garcia-Vazquez, C. A., Fernandez-Ramirez, L. M. “Fuzzy-based Energy Management System for a MVDC PV Power Plant with Battery Stored Quasi-Z-Source Inverter”. In: *2021 IEEE International Conference on Environment and Electrical Engineering and 2020 IEEE Industrial and Commercial Power Systems Europe (EEEIC / I&CPS Europe)*, 2021, Bari.
DOI: [10.1109/EEEIC/ICPSEurope51590.2021.9584829](https://doi.org/10.1109/EEEIC/ICPSEurope51590.2021.9584829)

3. Soares-Ramos, E. P. P., de Oliveira-Assis, L., Sarrias-Mena, R., García-Triviño, P., Garcia-Vazquez, C. A., Fernandez-Ramirez, L. M. “Large-Scale Wind Turbine with Quasi-Z-Source Inverter and Battery” *In: 2021 22nd IEEE International Conference on Industrial Technology (ICIT), 2021, Valencia.*
DOI: [10.1109/ICIT46573.2021.9453537](https://doi.org/10.1109/ICIT46573.2021.9453537)
4. Soares-Ramos, E. P. P., de Oliveira-Assis, L., Sarrias-Mena, R., García-Triviño, P., Garcia-Vazquez, C. A., Fernandez-Ramirez, L. M. “Control of a Grid-connected Wind Turbine with Quasi-Z-Source Inverter” *In: 2020 9th International Conference on Renewable Energy Research and Application (ICRERA), 2020, Glasgow. IEEE, 2020.*
DOI: [10.1109/ICRERA49962.2020.9242843](https://doi.org/10.1109/ICRERA49962.2020.9242843)
5. Garcia-Triviño, P., de Oliveira-Assis, L., Soares-Ramos, E. P. P., Sarrias-Mena, R., Garcia-Vazquez, C. A., Fernandez-Ramirez, L. M. “Configuration and Control of a MVDC Hybrid Charging Station of Electric Vehicles with PV / Battery / Hydrogen System” *In: 2021 IEEE International Conference on Environment and Electrical Engineering and 2020 IEEE Industrial and Commercial Power Systems Europe (EEEIC / I&CPS Europe), 2021, Bari.*
DOI: [10.1109/EEEIC/ICPSEurope51590.2021.9584795](https://doi.org/10.1109/EEEIC/ICPSEurope51590.2021.9584795)

Curriculum Vitae

Laís de Oliveira Assis
PhD scholarship holder in Spain, of CNPq

PhD student in Energy and Sustainable Engineering at the Universidad de Cádiz, Spain. Master in Renewable Energy and Energy Efficiency by the University of Cádiz (2018). Holds a degree in Energy Engineering from Pontifical Catholic University of Minas Gerais (2017), with partial period in Arizona State University, EE.UU. (2015)

Address to access this CV:
<http://lattes.cnpq.br/2517540564634994>

Personal Information

Name Laís de Oliveira Assis

Bibliographic Citation Lais de Oliveira-Assis.

Formal Education/Degree

2018 Ph.D. in progress in Ingeniería Energética y Sostenible .
Universidad de Cádiz, UCA, Spain. *Advisors:* Luis M. Fernández Ramírez and Raúl Sarrias Mena.
Grantee of: Conselho Nacional de Desenvolvimento Científico e Tecnológico ,CNPq ,Brasil

2017 - 2018 Master´s in Energías Renovables y Eficiencia Energética .
Universidad de Cádiz, UCA, Spain. *Year of degree:* 2018.
Advisors: Luis M. Fernández Ramírez and Raúl Sarrias Mena.

2011 - 2017 Graduation in Engenharia de Energia .
Pontifícia Universidade Católica de Minas Gerais, PUC Minas, Brasil.
Grantee of: PROUNI, Brasil .

Languages

Portuguese Native

English English as a Second Language. Advanced level. (Credit Hours: 336h). Arizona State University, ASU, EE. UU. (2014)

Spanish Universidad de Cádiz. B1 level. (2018)

French Escuela Oficial de Idiomas, Algeciras, Espanha. B1 level (2019).

Professional Experience

- **Scholarship / Doctorate**
National Council for Scientific and Technological Development (CNPq), (2020 – actual).
- **Scholarship / Science without borders**
Coordination of Superior Level Staff Improvement (CAPES), Arizona State University, EE. UU., 2014-2015.
- **Research Assistant**
Photovoltaic Reliability Laboratory, Arizona State University, EE. UU., 2014-2015.
- **Scholarship / Teaching assistant in Science and technology of materials**
Pontifical Catholic University of Minas Gerais, 2014, 2016.
- **Scholarship / Undergraduate scientific research**
Fundação de Amparo à Pesquisa do Estado de Minas Gerais (FAPEMIG), 2012-2013

Awards

- 2015** Dean's List - Outstanding Academic Achievement (Spring), Arizona State University.
- 2015** Dean's List - Outstanding Academic Achievement (Fall), Arizona State University.
- 2009** Outstanding student, SENAI - MG.

Articles in Scientific Journals

1. SOARES-RAMOS, EMANUEL P. P. ; DE OLIVEIRA-ASSIS, LAIS ; SARRIAS-MENA, RAUL ; GARCIA-TRIVINO, PABLO ; Garcia-Vazquez, Carlos Andres ; FERNANDEZ-RAMIREZ, LUIS M. . Averaged Dynamic Modelling and Control of a Quasi-Z-Source Inverter for Wind Power Applications. IEEE Access, v. 9, p. 1-1, 2021.
2. DE OLIVEIRA-ASSIS, LAIS ; GARCÍA-TRIVIÑO, PABLO ; SOARES-RAMOS, EMANUEL P.P. ; SARRIAS-MENA, RAÚL ; GARCÍA-VÁZQUEZ, CARLOS ANDRÉS ; UGALDE-LOO, CARLOS ERNESTO ; FERNÁNDEZ-RAMÍREZ, LUIS M. . Optimal energy management system using biogeography based optimization for grid-connected MVDC microgrid with photovoltaic, hydrogen system, electric vehicles and Z-source converters. ENERGY CONVERSION AND MANAGEMENT, v. 248, p. 114808, 2021.
3. DE OLIVEIRA-ASSIS, LAIS ; SOARES-RAMOS, EMANUEL P.P. ; SARRIAS-MENA, RAÚL ; GARCÍA-TRIVIÑO, PABLO ; GONZÁLEZ-RIVERA, ENRIQUE ; SÁNCHEZ-SAINZ, HIGINIO ; Llorens-Iborra, Francisco ; FERNÁNDEZ-RAMÍREZ, LUIS M. . Simplified model of battery energy-stored quasi-Z-source inverter-based photovoltaic power plant with Twofold energy management system. ENERGY, v. xxx, p. 122563, 2021.
4. ABOUBAIDA, HASSAN ; ABOUELMAHJOUR, YOUNES ; OLIVEIRA'ASSIS, LAIS . New open circuit fault detection in a converter. International Transactions on Electrical Energy Systems, v. e13094, p. n/a, 2021.
5. SOARES-RAMOS, EMANUEL P.P. ; DE OLIVEIRA-ASSIS, LAIS ; SARRIAS-MENA, RAÚL ; FERNÁNDEZ-RAMÍREZ, LUIS M. . Current status and future trends of offshore wind power in Europe. ENERGY, v. 202, p. 117787, 2020.

6. RAMOS, E. P. P. S. ; SILVA, A. V. ; PIRES, I. A. ; ASSIS, L. O. . Comportamento do Gerador Eólico Duplamente Alimentado Submetido Distúrbios na rede Elétrica e à Variação da Velocidade do Vento. Revista Brasileira de Energia, v. 20, p. 129-157, 2014.

Complete works published in conference proceedings

1. DE OLIVEIRA-ASSIS, LAIS ; SOARES-RAMOS, EMANUEL P. P. ; GARCIA-TRIVINO, PABLO ; SARRIAS-MENA, RAUL ; Garcia-Vazquez, Carlos Andres ; FERNANDEZ-RAMIREZ, LUIS M. . Fuzzy-based Energy Management System for a MVDC PV Power Plant with Battery Stored Quasi-Z-Source Inverter, 2021, Bari. 2021 IEEE International Conference on Environment and Electrical Engineering and 2021 IEEE Industrial and Commercial Power Systems Europe (EEEIC / I&CPS Europe), 2021. p. 1.
2. GARCIA-TRIVINO, PABLO ; OLIVEIRA-ASSIS, LAIS DE ; SOARES-RAMOS, EMANUEL P. P. ; SARRIAS-MENA, RAUL ; Garcia-Vazquez, Carlos Andres ; FERNANDEZ-RAMIREZ, LUIS M. . Configuration and Control of a MVDC Hybrid Charging Station of Electric Vehicles with PV/Battery/Hydrogen System, 2021, Bari. 2021 IEEE International Conference on Environment and Electrical Engineering and 2021 IEEE Industrial and Commercial Power Systems Europe (EEEIC / I&CPS Europe), 2021. p. 1.
3. SOARES-RAMOS, EMANUEL P. P. ; DE OLIVEIRA-ASSIS, LAIS ; SARRIAS-MENA, RAUL ; GARCIA-TRIVINO, PABLO ; GARCIA-VAZQUEZ, CARLOS A. ; FERNANDEZ-RAMIREZ, LUIS M. . Large-Scale Wind Turbine With Quasi-Z-Source Inverter and Battery, 2021, Valencia. 2021 22nd IEEE International Conference on Industrial Technology (ICIT), 2021. p. 403.
4. DE OLIVEIRA-ASSIS, LAIS ; SOARES-RAMOS, EMANUEL P. P. ; SARRIAS-MENA, RAUL ; GARCIA-TRIVINO, PABLO ; FERNANDEZ-RAMIREZ, LUIS M. . Large-Scale Grid Connected Quasi-Z-Source Inverter-Based PV Power Plant, 2020, Madrid. 2020 IEEE International Conference on Environment and Electrical Engineering and 2020 IEEE Industrial and Commercial Power Systems Europe (EEEIC / I&CPS Europe), 2020. p. 1-6.
5. SOARES-RAMOS, EMANUEL P. P. ; DE OLIVEIRA-ASSIS, LAIS ; SARRIAS-MENA, RAUL ; GARCIA-TRIVINO, PABLO ; GARCIA-VAZQUEZ, CARLOS A. ; FERNANDEZ-RAMIREZ, LUIS M. . Control of a Grid-connected Wind Turbine with Quasi-Z-Source Inverter, 2020, Glasgow. 2020 9th International Conference on Renewable Energy Research and Application (ICRERA), 2020. p. 309.